Non-equilibrium Quantum Dynamics
of Condensed Matter Models

—————————————————————————

by

Sashwin Sewran

—————————————————————————

Submitted in fulfilment of the

requirements for the degree of

Master of Science

in the

School of Chemistry and Physics

University of KwaZulu-Natal

Pietermaritzburg

November 2013

As the candidate's supervisor I have approved this dissertation for submission.

Signed:...   Name: Dr. A. Sergi   Date:..........................

Abstract

In this dissertation, we studied the generation of squeezed states induced by a time-dependent interaction and the influence of temperature on the strength of the squeezing in a condensed matter model. The model studied comprised two quantum harmonic oscillators, with a time-dependent, non-linear coupling between them. The influence of the thermal bath on the non-equilibrium dynamics of the model was represented in terms of non-Hamiltonian thermostats and a collection of independent harmonic oscillators with Ohmic spectral density. The equations of motion were studied in the Wigner representation, which introduces a phase space description for the model. The representation of the system in quantum phase space allowed us to investigate the difference between purely classical evolution and the relative importance of quantum corrections with respect to the dynamics. The dynamics was studied by means of computer simulation techniques. The numerical simulation of the non-equilibrium statistical mechanics of both time-dependent and non-linear interactions allowed us to investigate conditions beyond those in recent literature [1, 2].

Preface

The computational work described in this dissertation was carried out in the School of Chemistry and Physics, University of KwaZulu-Natal, Pietermaritzburg, from January 2012 to November 2013, under the supervision of Doctor Alessandro Sergi.

These studies represent original work by the author and have not otherwise been submitted in any form for any degree or diploma to any tertiary institution. Where use has been made of the work of others it is duly acknowledged in the text.

Declaration 1 - Plagiarism

I, ... declare that

- The research reported in this thesis, except where otherwise indicated, is my original research.

- This thesis has not been submitted for any degree or examination at any other university.

- This thesis does not contain other persons data, pictures, graphs or other information, unless specifically acknowledged as being sourced from other persons.

- This thesis does not contain other persons' writing, unless specifically acknowledged as being sourced from other researchers. Where other written sources have been quoted, then:

  a. Their words have been re-written but the general information attributed to them has been referenced

  b. Where their exact words have been used, then their writing has been placed in italics and inside quotation marks, and referenced.

- This thesis does not contain text, graphics or tables copied and pasted from the Internet, unless specifically acknowledged, and the source being detailed in the thesis and in the Bibliography.

Signed: ....

Contents

List of Figures

Acknowledgements

Firstly, I would like to express my sincere gratitude to my supervisor, Dr. Alessandro Sergi, for his guidance, patience and motivation throughout this work. His vast knowledge of this field was a source of inspiration to me. I am also thankful to him for allowing me opportunities to attend conferences and encouraging me to present my research.

I am extremely grateful to the members of my research group for their constant input, and making the past two years an enjoyable experience. I would like to thank Kostya for his assistance in helping me understand certain technical aspects. Also, I would like to thank Daniel for his assistance on a daily basis. Not forgetting Nkosinathi, whose generosity of his time has no bounds. I would like to thank him for reading this dissertation and providing constructive feedback with helpful suggestions. His encouragement helped me get through some stressful periods.

A very special thank you is extended to my parents, grandparents and sister who have all supported me throughout the completion of this dissertation. They allowed me to give me full attention to my work and always encouraged me to strive for the best.

Chapter 1

Introduction

Computational physics is the study of physics which forms a bridge between experimental and theoretical physics. We can construct a model which represents processes which occur in nature. The model does not mimic the entire process, however the essential features of the system are captured. The dynamics of the model are then simulated under conditions which are similar to those of the natural system. Following this, we can compare the numerical results with theoretical predictions, derived from approximated theories. Of equal importance is the comparison with experimental results. If these results are in agreement, then we can extend the model to study the behaviour of a system under conditions which are not feasible to recreate in the laboratory [3]. Also, the model can be used to gain further insights into how processes evolve at a molecular level, which is impossible to do in an experiment. A schematic representation of the relationship between theoretical, experimental and computational physics is shown in fig. 1.1.

In condensed matter physics, we construct models of natural systems which are studied on a microscopic scale. Through the calculation of statistical averages, it is then possible to make inferences about the system on a macroscopic scale. These models can be used to improve our understanding of the behaviour of natural systems, and the parameter ranges under which they exhibit interesting behaviour. Quantum mechanics is the fundamentally accepted theory used to describe condensed matter physics. It is generally thought that quantum features are strong in a low temperature environment, and are wiped out, due to decoherence and dissipation, in a high temperature environment. However, recent experiments on biological systems, which have exhibited certain inherently quantum characteristics, have called for the reassessment of the importance of quantum
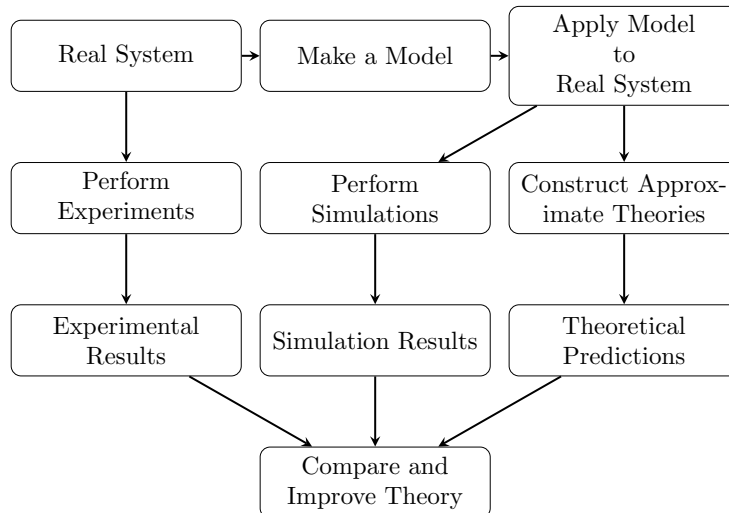
Figure 1.1: Schematic representation of the relationship between theoretical, experimental and computational physics.

coherence in non-equilibrium systems [4, 5]. The physical problem which we want to investigate is the role of time-dependent processes in nature, by studying systems which are in a condensed phase at non-equilibrium. Some of these important time-dependent processes include charge transfer, transfer of energy in light harvesting complexes, transport in quantum systems, protein modeling, driven systems and generation of squeezed states [6, 7, 8, 9, 10, 11, 12]. By studying time-dependent processes in our model, we may get further insight of quantum coherence in non-equilibrium systems. The work presented in this dissertation will focus on how a time-dependent interaction can be used a source of generating a squeezed state, a subset of time-dependent processes. The influence of temperature on the amount of squeezing we can generate, will also be investigated.

The usefulness of squeezing in condensed matter models, is best understood by considering the speculative molecular mechanism of the motion of a proton passing through an ion channel. Figure 1.2 provides an illustration of this process. It is possible that the proton requires an accurate position, in order to pass through the channel. The accuracy of the position of the proton can be improved, if its position is squeezed. By generating a squeezed state, we can limit the fluctuations in the values of the proton's position. However, this effect of squeezing the position, is performed at the expense of increasing the fluctuations of the proton's momentum. In this mechanism, the speed at which the proton moves through the channel is not of high importance. It may even aid in the rate

Coherent State

Squeezed State

Ion Channel

Ion Channel

Membrane

Membrane
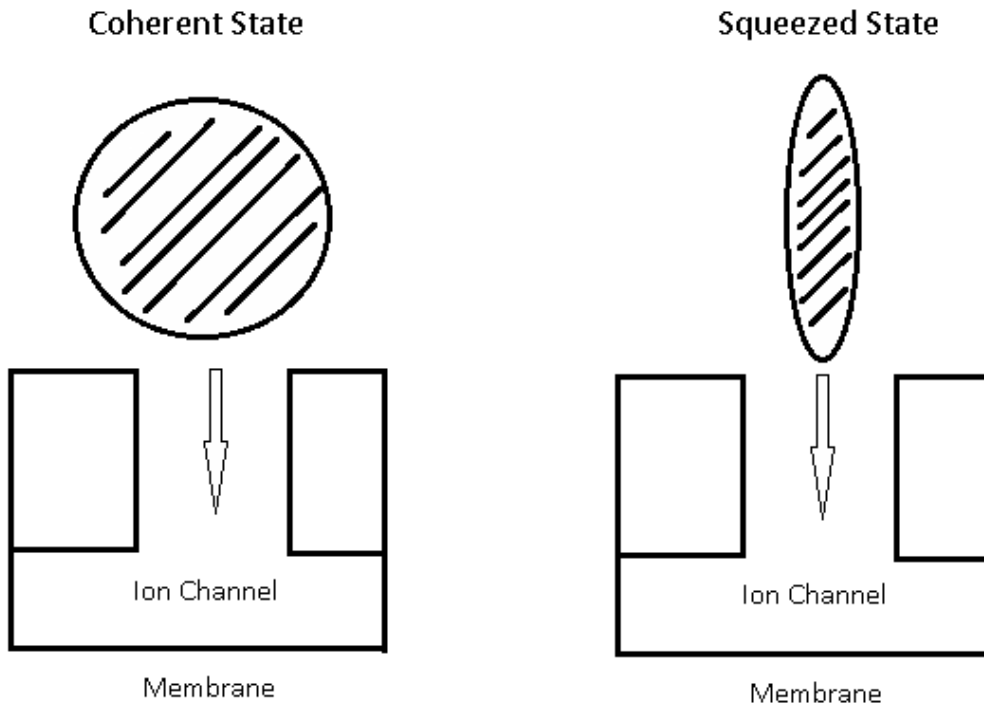
Figure 1.2: Schematic representation of the motion of a proton as it passes through an ion channel.

of the reaction. It is possible that a state in which the position of the proton is squeezed, can be generated by introducing a time-dependent interaction between the proton and the channel, with non-linear effects. Another example where squeezing may be useful in condensed matter is in molecular recognition, where reactions take place based on the lock and key model [13]. It should be noted that the examples discussed here are preliminary, and are presented to demonstrate the importance of squeezed states in condensed matter models. Squeezed states have widespread applications, especially in experiments which are limited by quantum noise. The control of quantum fluctuations can be used to limit the sensitivity of quantum experiments. Some of these applications can be found in condensed matter [14, 15, 16], spectroscopy [17], quantum information [18] and gravitational wave detection [19].

The formal definition of a squeezed state arises from the Heisenberg uncertainty principle. In 1927 Heisenberg developed the indeterminacy principle, where he related the uncertainties of the position and momentum of a free particle [20]. He presented the idea that there is a limit to the accuracy with which we can know both the particle's position and

momentum, simultaneously. The more accurately the position of the particle is known, the less accurately the momentum of the particle is known, and vice versa. Thus, the operators can not be specified with unlimited accuracy. This relation provided a physical interpretation of quantum mechanics and became an integral part in the development of quantum theory [21]. The measurement of the particle's position changes its momentum by an unknown amount. Therefore, the information we gain from the measurement is limited by the uncertainty relation.

In classical mechanics, if the exact position and momentum of a particle is known then it is possible to accurately predict the future position and momentum of the particle, provided the forces acting on the particle are known. However, when the system is given a quantum treatment, it is impossible to make this prediction. Instead of accurate values for the future coordinates, the coordinates can take on a range of values with a certain probability. Conjugate variables are subject to the Heisenberg uncertainty principle and have fluctuations associated with them. Consider two operators, $\hat{A}$ and $\hat{B}$, which satisfy the commutation relation

$$\left[\hat{A}, \hat{B}\right] = i\hat{C} .$$ (1.1)

From the Heisenberg uncertainty relation, which governs the product of the variances of these operators and limits the measurement of both variables in the same state, we obtain

$$\left\langle \left(\Delta\hat{A}\right)^2\right\rangle \left\langle \left(\Delta\hat{B}\right)^2\right\rangle \geq \frac{1}{4}\left|\left\langle\hat{C}\right\rangle\right|^2 .$$ (1.2)

If $\hat{A}$ and $\hat{B}$ have an equal amount of uncertainty and the product of their uncertainties is at a minimum the system is said to be in a coherent state or minimum uncertainty state [22]. A consequence of eqn. (1.2) is that the variance of both operators can not be less than $\frac{1}{2}\left|\left\langle\hat{C}\right\rangle\right|$ simultaneously. However, it is possible to reduce the fluctuations in one of the variables,

$$\left\langle \left(\Delta\hat{A}\right)^2\right\rangle < \frac{1}{2}\left|\left\langle\hat{C}\right\rangle\right| \quad \text{or} \quad \left\langle \left(\Delta\hat{B}\right)^2\right\rangle < \frac{1}{2}\left|\left\langle\hat{C}\right\rangle\right| .$$ (1.3)

When this occurs, the system is said to be in a squeezed state [23]. A consequence of a squeezed state is that one of the operators will have less fluctuations than it would in a

coherent state. To ensure that the uncertainty relation is not violated, the fluctuations in the conjugate variable must be increased.

The study presented in this dissertation uses a model comprising two quantum harmonic oscillators with a time-dependent, non-linear interaction between them. This model does not have an analytical solution. The influence of the thermal bath on the non-equilibrium dynamics of the model was represented in terms of non-Hamiltonian thermostats and a collection of independent harmonic oscillators with Ohmic spectral density. Initially, the system of oscillators are in a thermal state. After time $t = 0$, the time-dependent interaction is switched on. This drives the oscillators into a non-equilibrium state.

The equations of motion are solved using the Wigner-Heisenberg representation of quantum mechanics by means of computer simulation. This formalism allows us to avoid complex matrix calculations, since we represent operators of the Hilbert space as functions of phase space. In this representation, the quantum dynamics of harmonic systems reduces to purely classical evolution. We consider the canonical ensemble, since we want to control the temperature at which the simulation is performed. It is easier to control the temperature of the system, in an experiment, rather than its energy. In the canonical ensemble, we can derive the analytical form of the Wigner function in the initial thermal state. The quantum initial conditions are sampled from this distribution function. To simulate the dynamics of the coupled oscillators in contact with a thermal bath, we can use the partial Wigner transform over the bath degrees of freedom. This will allow us to treat the bath classically while the coupled oscillators are given a full quantum treatment.

Our objective is then to solve the quantum non-equilibrium statistical mechanics of the model. To simulate the dynamics of the Wigner function, we map the Wigner function as a cloud of points. We can propagate these points as trajectories and calculate the averages of an observable over the time evolved Wigner function. The dynamics of the system can be numerically integrated by using the symmetric Trotter factorization of the Liouville operator. Having outlined the procedure to calculate the dynamics, we first verify that the time-dependent interaction generates of a squeezed state. Since we are interested in condensed matter physics, the sensitivity of temperature to the amount of squeezing which can be generated will be investigated. The influence of temperature is given importance,

since it is the most convenient control parameter in experimental studies. The temperature of the environment acts as a source of energy when it interacts with the system, depending on whether the reaction taking place is endothermic or exothermic.

This dissertation is organized as follows. In Chapter 2, the Wigner formulation of quantum mechanics is introduced. This is followed by a discussion on how the quantum dynamics of a system of N harmonic oscillators can be reduced to classical evolution, within the Wigner formalism. Next, a brief discussion on Hamiltonian and non-Hamiltonian theory is provided. Using non-Hamiltonian theory, it is then shown how it is possible to simulate an environment with only a few degrees of freedom. Extended system dynamics are then introduced along with a procedure for calculating the quantum corrections of such systems in Wigner quantum dynamics. Chapter 3 encompasses how a computer simulation of the Wigner function is performed. It is then shown how the initial conditions are sampled using normal mode coordinates. Finally, the numerical evolution of the Wigner function is discussed. In Chapter 4, the results of the study are shown. Using the calculated variances and marginal distribution of the normal modes, it is shown how squeezed states are generated by using a time-dependent interaction. The temperature dependence on the strength of squeezing is also shown. In Chapter 5, a summary of the work performed in this dissertation is provided. Conclusions and perspectives are elucidated, with a brief discussion on possible future work. The Appendices contain the derivation of the Wigner function in the initial thermal state, an explanation as to why there is no analytical solution to the equations of motion, the transformation from Cartesian to normal mode coordinates and the derivation of the time-reversible numerical algorithms.

Chapter 2

Wigner formulation of quantum mechanics

In this chapter, a discussion on the form of the Wigner function, its derivation from the Weyl function and its interpretation as a quasiprobability distribution function will be provided. Through the use of the Wigner function, it will be shown how we can treat the quantum dynamics of N decoupled quantum harmonic oscillators by classical means. Non-hamiltonian theory and extended system dynamics will be introduced as a method of controlling the temperature of a system in the Wigner formulation. Lastly, quantum correction terms of thermostat schemes will be calculated.

In classical mechanics, the Hamiltonian equations of motion show a correlation between the position and momentum of a particle

$$\dot{q} = \frac{\partial}{\partial p} H(q, p, t) \tag{2.1}$$

$$\dot{p} = -\frac{\partial}{\partial q} H(q, p, t) . \tag{2.2}$$

The description of the particle in phase space requires the use of a joint probability distribution function, $f(q, p)$. In order for a complete classical description to emerge from the quantum case, it is necessary to have a quantum description of the particle in phase space [24]. In providing this phase space representation of a quantum system, we must ensure that Heisenberg's uncertainty principle is not violated.

2.1 Quantum mechanics in phase space

Prior to the formulation of quantum mechanics in phase space, quantum mechanics had been treated in the formalism of wave functions or operators. In 1932, Eugene Wigner was amongst the first to provide a formulation of quantum mechanics in phase space, equivalent to the Heisenberg and Shrödinger formulations [25]. In his formulation, he made use of a quasiprobability distribution function, known as the Wigner function. This quasiprobability distribution function does not hold all of the properties of a probability distribution function, however its usefulness lies in the way the quantum average of an observable is calculated in phase space. We can gain a deeper understanding of the relationship between classical and quantum mechanics by comparing the methods in calculating observable averages.

For a complete description of the Wigner function, it is necessary to begin by defining the Weyl transform of an operator. The Weyl transform of an arbitrary operator, $\hat{\chi}$, in the position basis is defined as [26]

$$\tilde{\chi}(x,p) \;=\; \int_{-\infty}^{+\infty} e^{-\frac{ipy}{\hbar}} \left\langle x + \frac{y}{2} \,\middle|\, \hat{\chi} \,\middle|\, x - \frac{y}{2} \right\rangle dy \;. \tag{2.3}$$

In the momentum basis, it is given by

$$\tilde{\chi}(x,p) \;=\; \int_{-\infty}^{+\infty} e^{-\frac{ixz}{\hbar}} \left\langle p + \frac{z}{2} \,\middle|\, \hat{\chi} \,\middle|\, p - \frac{z}{2} \right\rangle dz \;. \tag{2.4}$$

A tilde is used to denote the Weyl transform. The transform allows us to interpret an operator of the Hilbert space as a function of phase space. The representation is useful in constructing and implementing numerical algorithms to simulate the dynamics of a quantum system. We avoid complex matrix calculations and complications with commutator brackets.

One of the properties of the Weyl transform required in future calculations, is the Weyl transform of the identity matrix

$$
\begin{aligned}
\tilde{1} &= \int_{-\infty}^{+\infty} e^{-\frac{ipy}{\hbar}} \left\langle x + \frac{y}{2} \,\middle|\, \hat{1} \,\middle|\, x - \frac{y}{2} \right\rangle dy \\
&= \int_{-\infty}^{+\infty} e^{-\frac{ipy}{\hbar}} \delta(y) dy \quad = 1 \;.
\end{aligned}
\tag{2.5}
$$

Another property of the Weyl transform, to be used later on, is that the trace of two operators, $\hat{A}$ and $\hat{B}$, is equivalent to the integral over phase space of the product of the Weyl transforms of both operators [27]

$$Tr\left[\hat{A}, \hat{B}\right] = \frac{1}{h} \int_{-\infty}^{+\infty} \int_{-\infty}^{+\infty} \tilde{A}(x,p)\tilde{B}(x,p)dxdp . \tag{2.6}$$

Having defined the Weyl transform, we now introduce the Wigner function. It is defined as the Weyl transform of the density matrix divided by Planck's constant [26]

$$W(x,p) = \frac{\tilde{\rho}}{h} . \tag{2.7}$$

Like the Weyl transform, the Wigner function may be expressed in both the position and momentum basis

$$W(x,p) = \frac{1}{h} \int_{-\infty}^{+\infty} e^{-\frac{ipy}{\hbar}} \left\langle x + \frac{y}{2} \left| \hat{\rho} \right| x - \frac{y}{2} \right\rangle dy \tag{2.8}$$

$$= \frac{1}{h} \int_{-\infty}^{+\infty} e^{-\frac{ixz}{\hbar}} \left\langle p + \frac{z}{2} \left| \hat{\rho} \right| p - \frac{z}{2} \right\rangle dz . \tag{2.9}$$

The state of a system is described by the density matrix, $\hat{\rho}$. Quantum statistical averages may be calculated through use of this operator as

$$\langle \chi \rangle = Tr\left(\hat{\rho}\hat{\chi}\right) . \tag{2.10}$$

Equation (2.6) allows us to rewrite the right hand side in terms of phase space functions

$$\langle \chi \rangle = \frac{1}{h} \int_{-\infty}^{+\infty} \int_{-\infty}^{+\infty} \tilde{\rho}(x,p)\tilde{\chi}(x,p)dxdp \tag{2.11}$$

$$= \int_{-\infty}^{+\infty} \int_{-\infty}^{+\infty} W(x,p)\tilde{\chi}(x,p)dxdp \tag{2.12}$$

where we have used the definition of the Wigner function. This result can be interpreted by making a comparison to the calculation of statistical averages in classical mechanics [28]. Equation (2.12) has the form of the average of a quantity $\tilde{\chi}(x,p)$ in phase space,

where the Wigner function is the probability distribution function.

For a function to be characterized as a probability function, it needs to be normalized and non-negative. To check that the Wigner function is normalized, we calculate the trace of the density matrix using eqn. (2.6)

$$
\begin{aligned}
Tr\left(\hat{\rho}\hat{1}\right) &= \frac{1}{h}\int_{-\infty}^{+\infty}\int_{-\infty}^{+\infty}\tilde{\rho}(x,p)\tilde{1}dxdp \\
&= \int_{-\infty}^{+\infty}\int_{-\infty}^{+\infty}W(x,p)dxdp \quad = 1 \; .
\end{aligned} \tag{2.13}
$$

From eqn. (2.13), we see that the Wigner function is normalized. We now proceed to check that it is non-negative. To perform this check, consider two orthogonal states of a system, $|\phi_1\rangle$ and $|\phi_2\rangle$. Each state has a density matrix associated to it, $\hat{\rho}_1$ and $\hat{\rho}_2$ respectively. Using eqns. (2.6) and (2.7), the trace of the density matrices is given by

$$
\begin{aligned}
Tr\left[\hat{\rho}_1,\hat{\rho}_2\right] &= \int_{-\infty}^{+\infty}\int_{-\infty}^{+\infty}W_1(x,p)W_2(x,p)dxdp \; . \\
&= \frac{1}{h}\left\langle \phi_1 \,|\, \phi_2 \right\rangle \; .
\end{aligned} \tag{2.14}
$$

However, for orthogonal states we have $\langle \phi_1 \,|\, \phi_2 \rangle = 0$, which implies that

$$
\int_{-\infty}^{+\infty}\int_{-\infty}^{+\infty}W_1(x,p)W_2(x,p)dxdp = 0 \; . \tag{2.15}
$$

This is only possible if either $W_1(x,p)$, $W_2(x,p)$ or both, have negative values for some region of space. The violation of positiveness is caused by quantum interference [29]. As such, we can not call the Wigner function a probability function. Instead, we interpret it as a quasiprobability distribution function [24].

A useful property of the Wigner function, required for future calculations, is the Wigner transform of the product of two arbitrary operators, $\hat{A}$ and $\hat{B}$. It is defined as [30]

$$
\begin{aligned}
\left(\hat{A}\hat{B}\right)_W &= A_W(R,P)e^{\frac{i\hbar}{2}\overleftarrow{\partial}_j\mathcal{B}_{jk}\overrightarrow{\partial}_k}B_W(R,P) \tag{2.16} \\
&= B_W(R,P)e^{-\frac{i\hbar}{2}\overleftarrow{\partial}_j\mathcal{B}_{jk}\overrightarrow{\partial}_k}A_W(R,P) \; , \tag{2.17}
\end{aligned}
$$

where we have introduced the antisymmetric matrix $\mathcal{B}$ [31], which is defined in a different

way depending on the type of dynamics we want to generate. In the notation used, W is a subscript to denote the Wigner transform and we have used a double summation to sum over elements of $\mathcal{B}$. Written explicitly, in canonical coordinates, the exponent is the Poisson bracket

$$\overleftarrow{\partial}_j \mathcal{B}_{jk} \overrightarrow{\partial}_k \;\; = \;\; \sum_{i=1}^{N} \left(\frac{\overleftarrow{\partial}}{\partial R_i} \frac{\overrightarrow{\partial}}{\partial P_i} - \frac{\overleftarrow{\partial}}{\partial P_i} \frac{\overrightarrow{\partial}}{\partial R_i} \right) \tag{2.18}$$

where the gradient is the derivative in phase space. The arrows above the derivatives indicate the direction in which the derivative acts.

Partial Wigner representation

The partial Wigner representation is a widely used tool in molecular dynamics simulations [32, 33, 34]. It is a powerful technique, in particular, for treating quantum systems in contact with an environment. If a system is placed in contact with a thermal bath, an infinte number of degrees of freedom is required to model the bath in a fully quantum way. However, it is possible to use an approximation technique to simulate the evolution of the total system, called the quantum-classical (QC) approximation. In the QC approximation, the system of interest is given a full quantum treatment while the bath degrees of freedom are treated classically. This approximation allows us to simulate a thermal bath with a finite number of degrees of freedom, and is generally used when the bath particles are much heavier than the system.

The partial Wigner transform involves taking the Weyl transform over only the bath degrees of freedom. We then have a Hamiltonian which contains both operators of the Hilbert space as well as functions of phase space,

$$\hat{H}\left(\hat{q}, \hat{R}, \hat{p}, \hat{P}\right) \;\; \rightarrow \;\; H_W\left(\hat{q}, R, \hat{p}, P\right) \;,$$

where the subscript W now denotes a partial Wigner transform. Coordinates $(\hat{q}, \hat{p})$ are that of the quantum system of interest, while (R, P) are the coordinates of the bath.

For a bath of N degrees of freedom, the partial Wigner transform of the density matrix is

defined as [30]

$$\rho_W(R, P) \;=\; \frac{1}{(2\pi\hbar)^{3N}} \int dz\, e^{\frac{iPz}{\hbar}} \left\langle R - \frac{z}{2} \,\middle|\, \hat{\rho} \,\middle|\, R + \frac{z}{2} \right\rangle . \tag{2.19}$$

Since we are considering the motion of particles in 3 dimensions, the vectors have dimensions $3N$. Also, the factor $\frac{1}{(2\pi\hbar)}$ becomes $\frac{1}{(2\pi\hbar)^{3N}}$.

For an arbitrary operator, $\hat{\chi}$, the partial Wigner transform is

$$\chi_W(R, P) \;=\; \int dz\, e^{\frac{iPz}{\hbar}} \left\langle R - \frac{z}{2} \,\middle|\, \hat{\chi} \,\middle|\, R + \frac{z}{2} \right\rangle . \tag{2.20}$$

This transform is used when implementing the QC approximation.

2.2 Quantum dynamics of harmonic systems

In this section, we will consider the evolution in time of decoupled harmonic oscillators. In order to get the form of the Hamiltonian such that the oscillators are decoupled, we use normal mode coordinates instead of Cartesian coordinates. The derivation of the equations used to perform the transformation between normal mode and Cartesian coordinates may be found in Appendix B.

Consider now a Hamiltonian operator comprising N harmonic, decoupled oscillators, expressed in normal mode coordinates,

$$\hat{H} = \sum_{n=1}^{N} \left(\frac{1}{2m} \hat{P}_n^2 + \frac{1}{2} m\omega_n^2 \hat{R}_n^2 \right) . \tag{2.21}$$

Here $\hat{P}_n$, $\hat{R}_n$ and ω_n are the momentum, position and frequency of mode n respectively. Without loss of generality, all normal modes are given equal mass m. We are interested in calculating the statistical average of an arbitrary observable, χ. The evolution of an operator $\hat{\chi}$, corresponding to the observable χ, is given by the Heisenberg equation of motion

$$\frac{\partial \hat{\chi}}{\partial t} \;=\; \frac{i}{\hbar} \left[\hat{H}, \hat{\chi} \right] . \tag{2.22}$$

We now introduce the Wigner function which will allow us express quantum mechanical expectation values as averages over phase space. In doing so, we avoid complex matrix algebra, which is computationally demanding, in calculating the dynamics of the system. Using eqn. (2.17), we take the Wigner transform of eqn. (2.22) to get the equation of motion of χ_W

$$
\begin{aligned}
\frac{\partial \chi_W}{\partial t} &= \frac{i}{\hbar}\left(H_W e^{\frac{i\hbar}{2}\overleftarrow{\partial}_j \mathcal{B}_{jk}\overrightarrow{\partial}_k}\chi_W - \chi_W e^{\frac{i\hbar}{2}\overleftarrow{\partial}_j \mathcal{B}_{jk}\overrightarrow{\partial}_k}H_W\right) \\
&= \frac{i}{\hbar}\left(H_W e^{\frac{i\hbar}{2}\overleftarrow{\partial}_j \mathcal{B}_{jk}\overrightarrow{\partial}_k}\chi_W - H_W e^{-\frac{i\hbar}{2}\overleftarrow{\partial}_j \mathcal{B}_{jk}\overrightarrow{\partial}_k}\chi_W\right) \\
&= \frac{i}{\hbar}H_W\left(e^{\frac{i\hbar}{2}\overleftarrow{\partial}_j \mathcal{B}_{jk}\overrightarrow{\partial}_k} - e^{-\frac{i\hbar}{2}\overleftarrow{\partial}_j \mathcal{B}_{jk}\overrightarrow{\partial}_k}\right)\chi_W \\
&= \frac{2i\times i}{\hbar}H_W\frac{\left(e^{\frac{i\hbar}{2}\overleftarrow{\partial}_j \mathcal{B}_{jk}\overrightarrow{\partial}_k} - e^{-\frac{i\hbar}{2}\overleftarrow{\partial}_j \mathcal{B}_{jk}\overrightarrow{\partial}_k}\right)}{2i}\chi_W \\
\frac{\partial \chi_W}{\partial t} &= \frac{2}{\hbar}H_W \sin\left(\frac{\hbar}{2}\overleftarrow{\partial}_j \mathcal{B}_{jk}\overrightarrow{\partial}_k\right)\chi_W \quad,
\end{aligned}
\tag{2.23}
$$

where we have introduced the canonical antisymmetric matrix, $\mathcal{B}$ [31] and used Einstein notation to sum over repeated indices. Using the Moyal bracket [35], eqn. (2.23) is shown to be equivalent to Heisenberg's equation of motion. It is the equation of motion for the Wigner transformed operator. The difference in formulation can be seen in the evolution of the observable. Equation (2.23) expresses the evolution of an observable in terms functions of phase space while Heisenberg's equation expresses the evolution in terms of operators of the Hilbert space.

To simplify eqn. (2.23), the sine term is expressed in the form of a Maclaurin series.

$$
\begin{aligned}
\sin\left(\frac{\hbar}{2}\overleftarrow{\partial}_j \mathcal{B}_{jk}\overrightarrow{\partial}_k\right) &= \frac{\hbar}{2}\overleftarrow{\partial}_j \mathcal{B}_{jk}\overrightarrow{\partial}_k - \frac{\left(\frac{\hbar}{2}\overleftarrow{\partial}_j \mathcal{B}_{jk}\overrightarrow{\partial}_k\right)^3}{3!} + \cdots \\
&= \frac{\hbar}{2}\overleftarrow{\partial}_j \mathcal{B}_{jk}\overrightarrow{\partial}_k - \frac{\hbar^3}{48}\left(\overleftarrow{\partial}_j \mathcal{B}_{jk}\overrightarrow{\partial}_k\right)^3 + \cdots
\end{aligned}
\tag{2.24}
$$

Since the Hamiltonian only contains quadratic terms in both position and momentum, and none of the terms contain both position and momentum, third order or higher terms of $\hbar$ have no effect on the Hamiltonian. Thus we can ignore higher order terms, which means

$$
\sin\left(\frac{\hbar}{2}\overleftarrow{\partial}_j \mathcal{B}_{jk}\overrightarrow{\partial}_k\right) = \frac{\hbar}{2}\overleftarrow{\partial}_j \mathcal{B}_{jk}\overrightarrow{\partial}_k \,.
\tag{2.25}
$$

The evolution of an observable in the Wigner picture is then given by

$$
\begin{aligned}
\frac{\partial \chi_W}{\partial t} &= H_W \left(\overleftarrow{\partial}_j \mathcal{B}_{jk} \overrightarrow{\partial}_k \right) \chi_W \\
&= H_W \left[\sum_{i=1}^{N} \left(\frac{\overleftarrow{\partial}}{\partial R_i} \frac{\overrightarrow{\partial}}{\partial P_i} - \frac{\overleftarrow{\partial}}{\partial P_i} \frac{\overrightarrow{\partial}}{\partial R_i} \right) \right] \chi_W \; .
\end{aligned}
\tag{2.26}
$$

where we observe that the time evolution of an observable of an arbitrary operator reduces to classical propagation [28]. Thus, without any approximations, the quantum dynamics of harmonic systems look purely classical to first order of $\hbar$.

The importance of this result lies in the fact that it allows us to simulate the quantum dynamics of a harmonic system via classical methods. This simplifies our numerical task while allowing us to investigate quantum phenomena. We will be able to distinguish between classical and quantum behaviour by our choice of initial conditions. Since the dynamics of the system looks classical, all quantum effects are in the initial conditions. It is therefore imperative that we study the distribution functions used to generate both classical and quantum initial conditions, and interpret their differences. A detailed discussion on this topic can be found in the next chapter.

2.3   Temperature control in the Wigner formulation

The Hamiltonian formalism is the fundamentally accepted theory used in molecular dynamics simulations [36, 3]. In what follows, the properties constituting a Hamiltonian theory are discussed. Non-Hamiltonian theory is then introduced together with explanations of why this formalism is preferred over Hamiltonian theory. Finally, a description of extended system dynamics, in the canonical ensemble, which follows non-Hamiltonian theory, is provided.

Changing the way molecular dynamics trajectory samples phase space dynamically, allows us to choose an ensemble which allows the greatest insight into the behaviour of condensed matter systems for various thermodynamic constraints [37]. Non-Hamiltonian dynamics generates various statistical ensembles under which experiments are performed,

such as canonical (NVT) and isothermal-isobaric (NPT) ensembles. These ensembles are generated by using extended systems. Within the extended system framework, there is an exchange of energy between the system and its environment. One of the ways we can create an extended system is by using non-Hamiltonian dynamics.

2.3.1   Non-Hamiltonian dynamics and extended systems

A theory is considered to be Hamiltonian if its bracket algebra constitutes a Lie algebra [28]. Consider the following elements of a mathematical space $\{\alpha, \beta, \gamma\}$, and a complex number c. The mathematical space then constitutes a Lie algebra, if the following axioms are satisfied

$$(\alpha, \beta) = -(\beta, \alpha) \tag{2.27}$$

$$c(\alpha, \beta) = (c\alpha, \beta) = (\alpha, c\beta) \tag{2.28}$$

$$(\alpha + \beta, \gamma) = (\alpha, \gamma) + (\beta, \gamma)\,, \tag{2.29}$$

as well as the Jacobi relation,

$$\mathcal{J} = ((\alpha, \beta), \gamma) + ((\gamma, \alpha), \beta) + ((\beta, \gamma), \alpha) = 0\,. \tag{2.30}$$

In the properties above, a generic bracket, $(..,..)$, has been used. In classical mechanics the bracket would be Poissonian whereas in quantum mechanics it would be commutative. Equation (2.27) shows the anti-commutative nature of the elements and is crucial in defining time evolution. Linearity between elements of the mathematical space and complex number, c, is evident in equations (2.28) and (2.29). The Jacobi relation, $\mathcal{J} = 0$, ensures invariance of the algebra under time translation [38].

A theory becomes non-Hamiltonian when the Jacobi relation is no longer fulfilled, i.e. $\mathcal{J} \neq 0$, while eqns. (2.27) to (2.29) are satisfied. Thus, the algebra of non-Hamiltonian theory is not left invariant under time translation. This problem is overcome by the advantages of using the non-Hamiltonian formalism to represent an environment around our system [37]. In order to simulate an environment in Hamiltonian theory, one requires an infinite number of degrees of freedom. From a computational perspective, this method is

very demanding due to restrictions in the amount of memory which can be stored during a simulation and the time spent to perform the simulation. However, if one makes use of non-Hamiltonian theory, an environment can be simulated with a few degrees of freedom. In this regard, non-Hamiltonian theory is favoured to Hamiltonian theory.

A key feature in solving problems theoretically or numerically is being able to compare results with those calculated experimentally. It is thus of utmost importance to be able to control certain thermodynamic properties of a system while simulating its dynamics. Experimentally, it is easier to control properties such as temperature and pressure, instead of the energy of a given system. To this end, we need to chose the correct ensembles which gives us this control. Using extended system thermostat schemes allows us to control the temperature of the system while still being able to simulate an environment with a few degrees of freedom. A discussion of such schemes follows.

Nosé-Hoover thermostat

The Nosé-Hoover (NH) thermostat was first introduced in [39] to simulate an environment in contact with a system of interest, using few degrees of freedom. The method of simulating an environment through thermostats works by forming an extended system through the introduction of fictitious variables. This extended system is formed in the canonical ensemble, thus allowing us to control the temperature of the system by mimicking an infinite bath.

The Hamiltonian of the NH extended system is

$$H^{NH} \;\; = \;\; \frac{P^2}{2M} + V(R) + \frac{P_\eta^2}{2m_\eta} + gk_BT_{ext}\eta \tag{2.31}$$

where P and R are the phase space variables of particle M, and $V(R)$ its potential. Here η is the fictitious Nosé variable with associated conjugate momentum P_η and mass m_η . g is the number of degrees of freedom in the system to which the thermostat is attached, k_B is the Boltzmann constant and T_{ext} is the temperature of the environment. The Hamiltonian is a conserved quantity and we can calculate it to verify that the numerical integration of the equations of motion is accurate.

The phase space point of the extended system is defined as

$$x = (R, \eta, P, P_\eta) \ . \tag{2.32}$$

We can use the antisymmetric matrix, $\mathcal{B}^{NH}$, to express the equations of motion as [31]

$$\begin{aligned} \dot{x} &= \{x, H^{NH}\} \\ &= \frac{\partial x}{\partial x_j} \mathcal{B}^{NH}_{jk} \frac{\partial H^{NH}}{\partial x_k} \ . \end{aligned} \tag{2.33}$$

The antisymmetric matrix for this extended system is

$$\mathcal{B}^{\mathbf{NH}} = \begin{bmatrix} 0 & 0 & 1 & 0 \\ 0 & 0 & 0 & 1 \\ -1 & 0 & 0 & -P \\ 0 & -1 & P & 0 \end{bmatrix} \ . \tag{2.34}$$

Written explicitly, the equations of motion are

$$\dot{R} = \frac{P}{M} \tag{2.35}$$

$$\dot{P} = -\frac{\partial V(R)}{\partial R} - \frac{P_\eta}{m_\eta} P \tag{2.36}$$

$$\dot{\eta} = \frac{P_\eta}{m_\eta} \tag{2.37}$$

$$\dot{P}_\eta = \left(\frac{P^2}{M} - g k_B T_{ext} \right) \ , \tag{2.38}$$

and the NH Liouville operator is

$$\begin{aligned} iL^{NH} &= \mathcal{B}^{NH}_{jk} \frac{\partial H^{NH}}{\partial x_j} \frac{\partial}{\partial x_k} \\ &= \frac{P}{M} \frac{\partial}{\partial R} + \frac{P_\eta}{m_\eta} \frac{\partial}{\partial \eta} + \left(-\frac{\partial V(R)}{\partial R} - \frac{P_\eta}{m_\eta} P \right) \frac{\partial}{\partial P} + \left(\frac{P^2}{M} - g k_B T_{ext} \right) \frac{\partial}{\partial P_\eta} \end{aligned} \tag{2.39}$$

It is impossible to see the form of the coupling between the system of interest and the thermostats from the Hamiltonian. However, from eqn. (2.38) we can see that the thermostat acts as a feedback mechanism between the kinetic energy of the system it is attached to and the external temperature, such that the temperature of the system tends toward the

temperature of the bath [40].

In order to produce canonically distributed positions and momenta, the NH thermostat assumes that the dynamics of the system is ergodic. However, this assumption does not hold for all systems. We can overcome this by using a chain of thermostats, called the Nosé-Hoover Chain thermostat [41].

Nosé-Hoover Chain thermostat

The Nosé-Hoover Chain (NHC) thermostat was first introduced as an extension of the already established NH thermostat [41]. Like the NH thermostat, this method of simulating an environment works by forming an extended system through the introduction of fictitious variables. The NHC is preferred to the NH thermostat since it allows us to generate a canonical distribution without imposing constraints on the ergodicity of the system. However, in order to maintain accuracy in the numerical integration of the NHC equations of motion, a higher order algorithm is required [42].

The NHC can consist of multiple thermostats. For the purposes of this work, will consider a chain comprised of two thermostats. The Hamiltonian of the NHC extended system is then

$$H^{NHC} \;\; = \;\; \frac{P^2}{2M} + V(R) + \frac{P_{\eta_1}^2}{2m_{\eta_1}} + \frac{P_{\eta_2}^2}{2m_{\eta_2}} + gk_B T_{ext}\eta_1 + k_B T_{ext}\eta_2 \qquad (2.40)$$

where P and R are the phase space variables of particle M, and $V(R)$ is it is potential. Here η_1 and η_2 are the fictitious variables with associated conjugate momentum P_{η_1} and P_{η_2}, and masses m_{η_1} and m_{η_2} respectively. g is the number of degrees of freedom in the system to which the thermostats are attached, k_B is the Boltzmann constant and T_{ext} is the temperature of the bath. The Hamiltonian is a conserved quantity and we can calculate it to verify that the numerical integration of the equations of motion is accurate.

The phase space point of the extended system is defined as

$$x \;\; = \;\; (R, \eta_1, \eta_2, P, P_{\eta_1}, P_{\eta_2}) \; . \qquad (2.41)$$

We can use the antisymmetric matrix [37], $\mathcal{B}^{NHC}$, to express the equations of motion as

$$
\begin{aligned}
\dot{x} &= \{x, H^{NHC}\} \\
&= \frac{\partial x}{\partial x_j} \mathcal{B}_{jk}^{NHC} \frac{\partial H^{NHC}}{\partial x_k} \; .
\end{aligned}
\tag{2.42}
$$

The antisymmetric matrix for this extended system is

$$
\mathcal{B}^{\mathbf{NHC}} = \begin{bmatrix}
0 & 0 & 0 & 1 & 0 & 0 \\
0 & 0 & 0 & 0 & 1 & 0 \\
0 & 0 & 0 & 0 & 0 & 1 \\
-1 & 0 & 0 & 0 & -P & 0 \\
0 & -1 & 0 & P & 0 & -P_{\eta_1} \\
0 & 0 & -1 & 0 & P_{\eta_1} & 0
\end{bmatrix} \; .
\tag{2.43}
$$

Written explicitly, the equations of motion are

$$
\dot{R} = \frac{P}{M}
\tag{2.44}
$$

$$
\dot{P} = -\frac{\partial V(R)}{\partial R} - \frac{P_{\eta_1}}{m_{\eta_1}} P
\tag{2.45}
$$

$$
\dot{\eta}_1 = \frac{P_{\eta_1}}{m_{\eta_1}}
\tag{2.46}
$$

$$
\dot{\eta}_2 = \frac{P_{\eta_2}}{m_{\eta_2}}
\tag{2.47}
$$

$$
\dot{P}_{\eta_1} = \left(\frac{P^2}{M} - g k_B T_{ext} \right) - P_{\eta_1} \frac{P_{\eta_2}}{m_{\eta_2}}
\tag{2.48}
$$

$$
\dot{P}_{\eta_2} = \frac{P_{\eta_1}^2}{m_{\eta_1}} - k_B T_{ext} \; .
\tag{2.49}
$$

and the NHC Liouville operator is

$$
\begin{aligned}
iL^{NHC} &= \mathcal{B}_{jk} \frac{\partial H^{NHC}}{\partial x_j} \frac{\partial}{\partial x_k} \\
&= \frac{P}{M} \frac{\partial}{\partial R} + \frac{P_{\eta_1}}{m_{\eta_1}} \frac{\partial}{\partial \eta_1} + \frac{P_{\eta_2}}{m_{\eta_2}} \frac{\partial}{\partial \eta_2} + \left(-\frac{\partial V(R)}{\partial R} - \frac{P_{\eta_1}}{m_{\eta_1}} P \right) \frac{\partial}{\partial P} \\
&\quad + \left(\frac{P^2}{M} - g k_B T_{ext} \right) \frac{\partial}{\partial P_{\eta_1}} - P_{\eta_1} \frac{P_{\eta_2}}{m_{\eta_2}} \frac{\partial}{\partial P_{\eta_1}} \\
&\quad + \left(\frac{P_{\eta_1}^2}{m_{\eta_1}} - k_B T_{ext} \right) \frac{\partial}{\partial P_{\eta_2}}
\end{aligned}
\tag{2.50}
$$
$$
\tag{2.51}
$$

It is impossible to see the form of the coupling between the system of interest and the NHC

from the Hamiltonian. However, from eqns. (2.48) and (2.49) we can see that thermostat one acts as a feedback mechanism between the kinetic energy of the system it is attached to and the temperature of the bath. The function of thermostat two is to control the fluctuations of thermostat one [41].

Both the NH and NHC thermostat schemes can be extended to the quantum case. It will be shown in the next section, only for the NH extended system. However an explanation of how we can generalize these calculations for NHC dynamics, will be provided

2.3.2 Nosé-Hoover in Wigner quantum dynamics

To describe a thermostat scheme in Wigner quantum dynamics, we need to calculate the quantum corrections arising in the new equations of motion. This calculation is not original work and is outlined in [40]. It is performed in this study for completeness of the theory.

We begin by introducing the Moyal operator, as defined in [40],

$$
\begin{aligned}
\overrightarrow{\mathcal{M}} \quad = \quad & H_W \exp\left[\frac{i\hbar}{2}\left(\overleftarrow{\partial_j}\mathcal{B}_{jk}^{NH}\overrightarrow{\partial_k}\right) + \overleftarrow{\partial_j}(\partial_k\mathcal{B}_{jk}^{NH})\right] \\
& -H_W \exp\left[\frac{-i\hbar}{2}\left(\overleftarrow{\partial_j}\mathcal{B}_{jk}^{NH}\overrightarrow{\partial_k}\right) + \overleftarrow{\partial_j}(\partial_k\mathcal{B}_{jk}^{NH})\right] .
\end{aligned}
\tag{2.52}
$$

Using eqn. (2.52), we can write down the equation of motion of the Wigner function in Wigner quantum dynamics

$$
\frac{\partial f_W}{\partial t} \quad = \quad -\frac{i}{\hbar}\overrightarrow{\mathcal{M}}f_W .
\tag{2.53}
$$

From this equation of motion, we will calculate the quantum corrections.
Consider now the Hamiltonian of the NH extended quantum system

$$
H_W^{NH} \quad = \quad \hat{H}^{NH}
\tag{2.54}
$$

where we have taken the Wigner transform to represent the system in phase space.
Now by substituting the antisymmetric matrix, defined in eqn. (2.34), into the Moyal

operator, the equation of motion reduces to

$$\frac{\partial f_W}{\partial t} = -\frac{i}{\hbar}\overrightarrow{\mathcal{M}}f_W \tag{2.55}$$

$$= -\frac{i}{\hbar}\left\{H_W^{NH}\exp\left[\frac{i\hbar}{2}\left(\overleftarrow{\partial_j}\mathcal{B}_{jk}^{NH}\overrightarrow{\partial_k}\right) + \overleftarrow{\partial_j}(\partial_k\mathcal{B}_{jk}^{NH})\right]\right.$$
$$\left. -H_W^{NH}\exp\left[\frac{-i\hbar}{2}\left(\overleftarrow{\partial_j}\mathcal{B}_{jk}^{NH}\overrightarrow{\partial_k}\right) + \overleftarrow{\partial_j}(\partial_k\mathcal{B}_{jk}^{NH})\right]\right\}f_W \tag{2.56}$$

$$= \frac{2}{\hbar}H_W^{NH}\sin\left[\frac{\hbar}{2}\left(\overleftarrow{\partial_j}\mathcal{B}_{jk}^{NH}\overrightarrow{\partial_k}\right) + \overleftarrow{\partial_j}(\partial_k\mathcal{B}_{jk}^{NH})\right]f_W\ . \tag{2.57}$$

A Taylor series expansion is now used to expand the sine term

$$\frac{\partial f_W}{\partial t} = H_W^{NH}\overleftarrow{\partial_j}\mathcal{B}_{jk}^{NH}\overrightarrow{\partial_k}f_W + H_W^{NH}\overleftarrow{\partial_j}(\partial_k\mathcal{B}_{jk}^{NH})f_W$$
$$+ \sum_{n=3,5,7,\ldots}\frac{1}{n!}\left(\frac{i\hbar}{2}\right)^{n-1}H_W^{NH}\left[\left(\overleftarrow{\partial_j}\mathcal{B}_{jk}^{NH}\overrightarrow{\partial_k}\right) + \overleftarrow{\partial_j}(\partial_k\mathcal{B}_{jk}^{NH})\right]^n f_W\ . \tag{2.58}$$

By using the antisymmetric property of $\mathcal{B}^{NH}$, defining the phase space compressibility as

$$\kappa = \left(\partial_k\mathcal{B}_{kj}^{NH}\right)\partial_j H_W^{NH} \tag{2.59}$$

and using the definition of the Nosé-Hoover Liouville operator, defined in eqn. (2.39), the equations of motion can be rewritten as

$$\frac{\partial f_W}{\partial t} = -iL_{NH}f_W - \kappa f_W + \sum_{n=3,5,7,\ldots}\frac{1}{n!}\left(\frac{i\hbar}{2}\right)^{n-1}H_W^{NH}\left[\left(\overleftarrow{\partial_j}\mathcal{B}_{jk}^{NH}\overrightarrow{\partial_k}\right) + \overleftarrow{\partial_k}(\partial_j\mathcal{B}_{jk}^{NH})\right]^n f_W\ . \tag{2.60}$$

If we only consider zero order terms of order of $\hbar$, the equations of motion represents classical evolution. Thus, all quantum correction terms can be found from evaluating

$$H_W^{NH}\left[\left(\overleftarrow{\partial_j}\mathcal{B}_{jk}^{NH}\overrightarrow{\partial_k}\right) + \overleftarrow{\partial_k}\left(\partial_j\mathcal{B}_{jk}^{NH}\right)\right]f_W\quad . \tag{2.61}$$

However, recalling that the only terms in $\mathcal{B}^{NH}$ containing elements of the extended phase

space point are $\mathcal{B}_{34}^{NH}$ and $\mathcal{B}_{43}^{NH}$, results in

$$\frac{\partial \mathcal{B}^{NH}}{\partial x_1} = \frac{\partial \mathcal{B}^{NH}}{\partial R} = 0 \qquad (2.62)$$

$$\frac{\partial \mathcal{B}^{NH}}{\partial x_2} = \frac{\partial \mathcal{B}^{NH}}{\partial \eta} = 0 \qquad (2.63)$$

$$\frac{\partial \mathcal{B}^{NH}}{\partial x_4} = \frac{\partial \mathcal{B}^{NH}}{\partial P_\eta} = 0 \qquad (2.64)$$

while

$$\frac{\partial \mathcal{B}_{34}^{NH}}{\partial x_3} = \frac{\partial (-P)}{\partial P} = -1 \qquad (2.65)$$

$$\frac{\partial \mathcal{B}_{43}^{NH}}{\partial x_3} = \frac{\partial P}{\partial P} = 1 \ . \qquad (2.66)$$

This allows us to simplify $\overleftarrow{\partial_j} \left(\partial_k \mathcal{B}_{jk}^{NH} \right)$

$$\overleftarrow{\partial_j}(\partial_k \mathcal{B}_{jk}^{NH}) = \overleftarrow{\partial x_4} \left(\frac{\partial \mathcal{B}_{43}^{NH}}{\partial x_3} \right) = \frac{\overleftarrow{\partial}}{\partial P_\eta} \ . \qquad (2.67)$$

Considering only non zero elements of $\mathcal{B}^{NH}$, allows us to simplify $\overleftarrow{\partial_j} \mathcal{B}_{jk}^{NH} \overrightarrow{\partial_k}$

$$\overleftarrow{\partial_j} \mathcal{B}_{jk}^{NH} \overrightarrow{\partial_k} = \frac{\overleftarrow{\partial}}{\partial R} \frac{\overrightarrow{\partial}}{\partial P} + \frac{\overleftarrow{\partial}}{\partial \eta} \frac{\overrightarrow{\partial}}{\partial P_\eta} - \frac{\overleftarrow{\partial}}{\partial P} \frac{\overrightarrow{\partial}}{\partial R} - \frac{\overleftarrow{\partial}}{\partial P} P \frac{\overrightarrow{\partial}}{\partial P_\eta} - \frac{\overleftarrow{\partial}}{\partial P_\eta} \frac{\overrightarrow{\partial}}{\partial \eta} + \frac{\overleftarrow{\partial}}{\partial P_\eta} P \frac{\overrightarrow{\partial}}{\partial P} \qquad (2.68)$$

Substituting the results of eqns. (2.67) and (2.68) into eqn. (2.61), the quantum correction terms are given by

$$\sum_{n=3,5,7,\dots} \frac{1}{n!} \left(\frac{i\hbar}{2} \right)^{n-1} H_W^{NH} \left[\frac{\overleftarrow{\partial}}{\partial R} \frac{\overrightarrow{\partial}}{\partial P} + \frac{\overleftarrow{\partial}}{\partial \eta} \frac{\overrightarrow{\partial}}{\partial P_\eta} - \frac{\overleftarrow{\partial}}{\partial P} \frac{\overrightarrow{\partial}}{\partial R} - \frac{\overleftarrow{\partial}}{\partial P} P \frac{\overrightarrow{\partial}}{\partial P_\eta} - \frac{\overleftarrow{\partial}}{\partial P_\eta} \frac{\overrightarrow{\partial}}{\partial \eta} + \frac{\overleftarrow{\partial}}{\partial P_\eta} P \frac{\overrightarrow{\partial}}{\partial P} \right]^n f_W \ . \qquad (2.69)$$

By analysing the form of H_W^{NH}, it becomes possible to find the quantum correction terms

which are not equal to zero. These terms are

$$H_W^{NH} \frac{\overleftarrow{\partial^n}}{\partial x_j^n} \frac{\overrightarrow{\partial^n}}{\partial x_k^n} f_W \;=\; V(r) \frac{\overleftarrow{\partial^n}}{\partial R^n} \frac{\overrightarrow{\partial^n}}{\partial P^n} f_W \tag{2.70}$$

$$H_W^{NH} \left(-\frac{\overleftarrow{\partial}}{\partial P} P \frac{\overrightarrow{\partial}}{\partial P_\eta} \right)^n f_W \;\neq\; 0 \tag{2.71}$$

$$H_W^{NH} \left(\frac{\overleftarrow{\partial}}{\partial P_\eta} P \frac{\overrightarrow{\partial}}{\partial P} \right) \left(-\frac{\overleftarrow{\partial}}{\partial P} P \frac{\overrightarrow{\partial}}{\partial P_\eta} \right)^{n-1} f_W \;\neq\; 0 \tag{2.72}$$

$$H_W^{NH} \left(\frac{\overleftarrow{\partial}}{\partial P_\eta} P \frac{\overrightarrow{\partial}}{\partial P} \right)^2 \left(-\frac{\overleftarrow{\partial}}{\partial P} P \frac{\overrightarrow{\partial}}{\partial P_\eta} \right)^{n-2} f_W \;\neq\; 0 \tag{2.73}$$

$$H_W^{NH} \left(-\frac{\overleftarrow{\partial}}{\partial P} \frac{\overrightarrow{\partial}}{\partial R} \right)^2 \left(-\frac{\overleftarrow{\partial}}{\partial P} P \frac{\overrightarrow{\partial}}{\partial P_\eta} \right)^{n-1} f_W \;\neq\; 0 \tag{2.74}$$

$$H_W^{NH} \left(-\frac{\overleftarrow{\partial}}{\partial P} P \frac{\overrightarrow{\partial}}{\partial R} \right)^2 \left(-\frac{\overleftarrow{\partial}}{\partial P} P \frac{\overrightarrow{\partial}}{\partial P_\eta} \right)^{n-2} f_W \;\neq\; 0 \,. \tag{2.75}$$

Thus, all quantum correction terms can be calculated by evaluating

$$\sum_{n=3,5,7,\ldots} \frac{1}{n!} \left(\frac{i\hbar}{2} \right)^{n-1} H_W^{NH} \left\{ \frac{\overleftarrow{\partial^n}}{\partial R^n} \frac{\overrightarrow{\partial^n}}{\partial P^n} + \left[-\frac{\overleftarrow{\partial}}{\partial P} \left(\frac{\overrightarrow{\partial}}{\partial R} - P \frac{\overrightarrow{\partial}}{\partial P_\eta} \right) + \frac{\overleftarrow{\partial}}{\partial P_\eta} \left(-\frac{\overrightarrow{\partial}}{\partial \eta} + P \frac{\overrightarrow{\partial}}{\partial P} \right) \right]^n \right\} f_W \,. \tag{2.76}$$

While the extension of the NHC in quantum dynamics is not shown, the quantum correction terms can also be calculated for the NHC, by substituting the antisymmetric matrix $\mathcal{B}^{NHC}$ instead of $\mathcal{B}^{NH}$ in eqn. (2.57) and following the procedure outlined here.

Chapter 3

Computer simulation of the dynamics of the Wigner function

This chapter contains the procedure to derive a general time reversible algorithm using the symmetric Trotter factorization of the Liouville operator. The various condensed matter models, used to study the generation of squeezed states and the influence of temperature on the amount of squeezing, are introduced. An explanation of how the initial conditions of the system are sampled, is provided. The treatment of the numerical evolution of the Wigner function is discussed.

3.1 Time reversible algorithms and the Liouville-Trotter factorization

In the discussion of non-Hamiltonian theory, it was shown that the Jacobian relation, eqn. (2.30), no longer holds. Thus, the algebra of non-Hamiltonian theory is not left invariant under time translation. In deriving a numerical algorithm for the integration of non-Hamiltonian equations of motion, it is then of utmost importance that other laws of symmetry are not violated. One such property is that of time reversibility. An algorithm is time reversible if the equations of motion are left invariant under a change of sign in time. This ensures that the behaviour of microscopic systems is independent of the direction of the flow of time [43, 44].

In [42, 45, 46] it is shown how a time reversible algorithm can be derived, by making

use of the symmetric Trotter factorization of the Liouville propagator. In deriving a time reversible algorithm, we begin by stating the form of the Liouville operator in terms of bracket algebra

$$
\begin{aligned}
iLx &= \{x, H\}_B & (3.1)\\
&= \frac{\partial x}{\partial x_j} \mathcal{B}_{jk} \frac{\partial H}{\partial x_k} \;. & (3.2)
\end{aligned}
$$

where x is the extended phase space point and H is the extended system Hamiltonian. This allows us to write the equations of motion as

$$
\dot{x} = iLx \tag{3.3}
$$

with formal solution

$$
x(t) = \exp\left(iL\Delta t\right) x(0) \tag{3.4}
$$

where Δt is time discretization, $x(0)$ is the initial state of the system and $\exp\left(iL\Delta t\right)$ is the classical propagator which evolves the system forward in time.

The classical propagator may be written as

$$
U(t) = \exp\left(iL\Delta t\right) \;, \tag{3.5}
$$

where $U(t)$ is a unitary operator, i.e. $U(-t) = U^{-1}(t)$.

By using the Hermitian property of the Liouville operator $L^\dagger = L$ [47], we can verify both the unitary property of $U(t)$

$$
\begin{aligned}
U^\dagger(t)U(t) &= \exp\left(-iL^\dagger\Delta t\right)\exp\left(iL\Delta t\right)\\
&= \exp\left(-iL\Delta t\right)\exp\left(iL\Delta t\right)\\
&= 1 \;, & (3.6)
\end{aligned}
$$

and the time reversibility of the equations of motion

$$
\begin{aligned}
x(t) &= U(t)x(0) \\
U(-t)x(t) &= U(-t)U(t)x(0) \\
&= \exp\left(-iL\Delta t\right)\exp\left(iL\Delta t\right)x(0) \\
&= x(0) \, .
\end{aligned}
\tag{3.7}
$$

The solution given by eqn. (3.4) is not useful in solving the equations of motion, since evaluating the right hand side is equivalent to integrating the classical equations of motion. However, the solution is known in a few simple cases. The Liouville operator may be decomposed into n non-commuting operators

$$
\begin{aligned}
iL &= \sum_{j=1}^{n} iL_j \\
&= iL_1 + iL_2 + iL_3 + \cdots + iL_n
\end{aligned}
\tag{3.8}
$$

where n represents the number of elements in the phase space point. Consider now a system which has a 2-dimensional phase space point, $x = (r, p)$. The Liouville operator of this system may thus be written as

$$
iL = iL_1 + iL_2
\tag{3.9}
$$

where $[L_1, L_2] \neq 0$. The non-commutative property of the operators implies that

$$
\begin{aligned}
\exp\left(iL\Delta t\right) &= \exp\left[i\left(L_1 + L_2\right)\Delta t\right] \\
&\neq \exp\left(iL_1\Delta t\right)\exp\left(iL_2\Delta t\right) \, .
\end{aligned}
\tag{3.10}
$$

Thus, to expand the evolution operator it is necessary to use the Trotter factorization [36]. The Trotter theorem is defined as

$$
e^{(A+B)} = \lim_{N \to \infty}\left[e^{A/2N}e^{B/N}e^{A/2N}\right]^{N} \, .
\tag{3.11}
$$

This equation is formally correct for an infinite value of N. However, for sufficiently large

but finite value of N, we can rewrite the theorem as

$$e^{(A+B)} = \left(e^{A/2N}e^{B/N}e^{A/2N}\right)^N e^{\mathcal{O}(1/N^2)} \tag{3.12}$$

This theorem is then applied to the system of interest by identifying

$$\begin{aligned}
\frac{A}{N} &= \frac{iL_2 t}{N} \\
\frac{B}{N} &= \frac{iL_1 t}{N} \,.
\end{aligned} \tag{3.13}$$

Substituting these results back into eqn. (3.12), we obtain

$$e^{(iL_1+iL_2)\frac{t}{N}} \approx \left(e^{iL_2/2}e^{iL_1}e^{iL_2/2}\right)^{\frac{t}{N}} \,. \tag{3.14}$$

We can interpret the above equation as the approximate propagation of the system over a small time interval. Using a time discretization $h = t/N$, we can then write the propagation of the system over the discretization as

$$e^{i(L_1+L_2)h} \approx e^{iL_2 h/2}e^{iL_1 h}e^{iL_2 h/2} \,. \tag{3.15}$$

where we have approximated the result to second order of h

$$e^{iLh} = e^{iL_2 h/2}e^{iL_1 h}e^{iL_2 h/2} + \mathcal{O}(h^3) \,. \tag{3.16}$$

The importance of the above result lies in it is implementation to produce a numerical algorithm. When the evolution operator, e^{iLh}, acts on the system, each individual propagator acts sequentially. First $e^{iL_2 h/2}$, then $e^{iL_1 h}$ and finally $e^{iL_2 h/2}$. This process is known as the direct translation technique [47]. The results of each action of the individual propagator feeds into the next action.

Two mathematical properties which will be needed further on in deriving a time reversible algorithm are

$$\exp\left[c\frac{\partial}{\partial x}\right]f(x) = f(x+c) \tag{3.17}$$

$$\exp\left[cx\frac{\partial}{\partial x}\right]f(x) = f(xe^c) \,. \tag{3.18}$$

3.2 Physical models

In this section, a discussion of different physical models used in our numerical study is provided. The equations of motion of each model are discussed. Liouville operators are constructed which will allow us to apply the symmetric Trotter factorization of the Liouville operators to generate time-reversible algorithms for each model. We begin by discussing a system of two coupled oscillators with a time-dependent interaction between them. Reasons as to why this model can not be solved analytically are discussed. Finally a thermal bath, used to simulate an environment, is attached to the system of coupled oscillators. Two different types of thermal baths are studied. First a bath of N independent harmonic oscillators is used and then we use the Nosé-Hoover Chain thermostat.

3.2.1 Coupled, driven oscillators

We studied numerically a model comprising two quantum harmonic oscillators with an oscillatory, time-dependent, non-linear coupling between them. The Hamiltonian of the driven, coupled oscillators is

$$ H \;=\; \frac{p_1^2}{2m} + \frac{p_2^2}{2m} + \frac{K}{2}q_1^2 + \frac{K}{2}q_2^2 + \frac{m\omega^2(t)}{2}\left(q_2 - q_1\right)^2 \qquad (3.19) $$

where

$$ \omega(t) \;=\; \omega_0 \sin\left(\omega_d t\right) = \sqrt{\frac{K(t)}{m}} \;. \qquad (3.20) $$

Here p_1 and p_2 are the momenta of the oscillators, m is the mass of both oscillators, q_1 and q_2 are the displacement of the oscillators from their equilibrium positions, K is the spring constant of both oscillators, $\omega(t)$ is the time-dependent frequency used to couple the oscillators, ω_0 is the amplitude of the frequency, ω_d is the driving frequency and $K(t)$ is the coupling function between the oscillators. The general nature of the coupling function used to model the interaction between the oscillators, will make this model easier to generalize to other systems of interest.

Initially the system is at thermal equilibrium before being driven to a non-equilibrium state through a time-dependent interaction. In [1] and [2] analytical solutions to similar

models have been found. However, our system differs in the non-linearity and time depen-
dence of the interaction between the oscillators. In Appendix C, we show that there is no
analytical solution to our system. In trying to solve the equations of motion of the system,
we find a Mathieu differential equation. This equation has no analytical solution in terms
of known functions, only in terms of infinite series with recurring coefficients, because
of the time-dependent frequency used to couple the oscillators. Floquet theory can be
used to establish certain properties of the differential equation, however some numerical
approximation must be taken to find a solution [48].

Having shown that this system can not be solved analytically, we solve the equations of
motion numerically by deriving a time reversible algorithm. To derive the algorithm, we
require the Liouville operators. From the equations of motion, the total Liouville operator
is

$$L \quad = \quad \sum_{i=1}^{2} L_i \tag{3.21}$$

where the individual operators are

$$L_1 \quad = \quad \frac{p_1}{m} \frac{\partial}{\partial q_1} + \frac{p_2}{m} \frac{\partial}{\partial q_2} \tag{3.22}$$

$$L_2 \quad = \quad \left[-Kq_1 + K(t)(q_2 - q_1) \right] \frac{\partial}{\partial p_1} + \left[-Kq_2 - K(t)(q_2 - q_1) \right] \frac{\partial}{\partial p_2} . \tag{3.23}$$

The derivation of the algorithm can be found in Appendix D.1.

3.2.2 Coupled, driven oscillators attached to a harmonic bath

Thus far, the model which we have considered has been an idealized one. In reality the
driven oscillators will interact with their environment. The first type of environment
which we will consider is a thermal bath of N independent harmonic oscillators. The bath
is coupled to the driven oscillators via a bilinear coupling. Since the system is made up of
harmonic oscillators, we can describe the evolution of the system via classical means. The
total Hamiltonian is made up of contributions of the Hamiltonians of the driven system
H_S, the bath that is coupled to the subsystem H_B, and the coupling between the system

and bath H_{SB}, and is given by

$$
\begin{aligned}
H_T \quad = \quad & H_S + H_B + H_{SB} && (3.24) \\
= \quad & \frac{p_1^2}{2m} + \frac{p_2^2}{2m} + \frac{K}{2}q_1^2 + \frac{K}{2}q_2^2 + \frac{K(t)}{2}(q_2 - q_1)^2 \\
& + \sum_{j=1}^{N} \left(\frac{P_j^2}{2m_j} + \frac{1}{2}m_j\omega_j^2 R_j^2 \right) - \sum_{\alpha=1}^{2}\sum_{j=1}^{N} q_\alpha c_j R_j \ , && (3.25)
\end{aligned}
$$

where

$$
\omega_j \quad = \quad -\omega_c ln\left(1 - j\frac{\omega_0}{\omega_c}\right) \tag{3.26}
$$

$$
\omega_0 \quad = \quad \frac{\omega_c}{N}\left[1 - exp\left(-\frac{\omega_{max}}{\omega_c}\right)\right] \tag{3.27}
$$

$$
c_j \quad = \quad \sqrt{\xi\hbar\omega_0 m_j\omega_j} \ . \tag{3.28}
$$

Equation (3.26) shows that each oscillator in the bath has a different frequency. The form of ω_j, ω_0 and c_j allows us to efficiently represent an environment made up of an infinite bath of oscillators with Ohmic spectral density [32]. ξ and ω_c characterize the spectral density of the bath. The Kondo parameter, ξ, is a measure of the strength of the coupling between the subsystem and bath where the coupling between each oscillator in the bath and the subsystem is specified by c_j. The initial values of R_j and P_j are sampled from the distribution function

$$
\rho_W(R_j, P_j, \beta) = \prod_{j=1}^{N} \left\{ \frac{1}{\pi\hbar}\tanh\left(\frac{\hbar\omega_j}{2}\beta\right) \exp\left[-\frac{2}{\hbar\omega_j}\tanh\left(\frac{\hbar\omega_j}{2}\beta\right) \left(\frac{1}{2m_j}P_j^2 + \frac{1}{2}m_j\omega_j^2 R_j^2 \right) \right] \right\}
$$

derived in Appendix A, using the values of ω_j.

The equations of motion, of the total system are

$$\dot{q}_1 \;\; = \;\; \frac{\partial H_T}{\partial p_1} = \frac{p_1}{m} \tag{3.29}$$

$$\dot{q}_2 \;\; = \;\; \frac{\partial H_T}{\partial p_2} = \frac{p_2}{m} \tag{3.30}$$

$$\dot{R}_j \;\; = \;\; \frac{\partial H_T}{\partial P_j} = \frac{P_j}{m_j} \tag{3.31}$$

$$\dot{p}_1 \;\; = \;\; -\frac{\partial H_T}{\partial q_1} = F_1 + F_{SB} \tag{3.32}$$

$$\dot{p}_2 \;\; = \;\; -\frac{\partial H_T}{\partial q_2} = F_2 + F_{SB} \tag{3.33}$$

$$\dot{P}_j \;\; = \;\; -\frac{\partial H_T}{\partial R_j} = F_j \tag{3.34}$$

where we have introduced the forces

$$F_1 \;\; = \;\; -Kq_1 + K(t)(q_2 - q_1) \tag{3.35}$$

$$F_2 \;\; = \;\; -Kq_2 - K(t)(q_2 - q_1) \tag{3.36}$$

$$F_j \;\; = \;\; -m_j\omega_j^2 R_j + c_j \sum_{\alpha=1}^{2} q_\alpha \tag{3.37}$$

$$F_{SB} \;\; = \;\; \sum_{j=1}^{N} c_j R_j \; . \tag{3.38}$$

From the equations of motion we can construct Liouville operators which will allow us to derive a time reversible algorithm. The total Liouville operator is made up of 4 individual operators

$$L \;\; = \;\; \sum_{i=1}^{4} L_i \tag{3.39}$$

where the individual operators are

$$L_1 \;\; = \;\; \sum_{\alpha=1}^{2} \frac{p_\alpha}{m_\alpha} \frac{\partial}{\partial q_\alpha} \tag{3.40}$$

$$L_2 \;\; = \;\; \sum_{\alpha=1}^{2} \left(F_\alpha + F_{SB} \right) \frac{\partial}{\partial p_\alpha} \tag{3.41}$$

$$L_3 \;\; = \;\; \sum_{j=1}^{N} \frac{P_j}{m_j} \frac{\partial}{\partial R_j} \tag{3.42}$$

$$L_4 \;\; = \;\; \sum_{j=1}^{N} F_j \frac{\partial}{\partial P_j} \tag{3.43}$$

The derivation of the algorithm can be found in Appendix D.2.

3.2.3 Coupled, driven oscillators attached to a Nosé-Hoover Chain thermostat

While the harmonic bath of oscillators does accurately represent an environment for the driven system, we would like to be able to represent the environment with a minimal number of degrees of freedom. To this end, we make use of the Nosé-Hoover Chain (NHC) thermostat. The theory and advantages of the NHC thermostat are discussed in detail in section 2.3.

For the purposes of this work, we chose to use a chain consisting of 2 thermostats. This allows to write the explicit form of $\mathcal{B}$ while limiting the tensorial notation [37]. The total Hamiltonian of the system then consists of the driven system, the harmonic bath and the 2 thermostats. Its form is given by

$$\begin{aligned} H^{NHC} \;\; = \;\; & \frac{p_1^2}{2m_1} + \frac{p_2^2}{2m_2} + \frac{K}{2} q_1^2 + \frac{K}{2} q_2^2 + \frac{K(t)}{2} (q_2 - q_1)^2 \\ & + \frac{P_0^2}{2M} + \frac{1}{2} M \omega_0^2 R_0^2 - c_0 R_0 \left(q_1 + q_2 \right) \\ & + \frac{P_{\eta_1}^2}{2m_{\eta_1}} + \frac{P_{\eta_2}^2}{2m_{\eta_2}} + g k_B T_{ext} \eta_1 + k_B T_{ext} \eta_2 \end{aligned} \tag{3.44}$$

P_0 and R_0 are the phase space variables of the bath oscillator having mass M and frequency ω_0. A bilinear interaction is used to model the behaviour between the bath and driven system. η_1 and η_2 are the fictitious Nosé variables with associated conjugate momentum P_{η_1} and P_{η_2}, and masses m_{η_1} and m_{η_2} respectively. The number of degrees of

freedom in the bath to which the thermostats are attached is given by g, k_B is the Boltzmann constant and T_{ext} is the temperature of the bath.

To derive the algorithm to include the extended system, we begin by writing the equations of motion using matrix notion [37]

$$\dot{x} = \sum_{i,j} \mathcal{B}_{ij}^{NHC} \frac{\partial H^{NHC}}{\partial x_j} \qquad (3.45)$$

where the phase space vector is

$$x = (q_1, q_2, R_0, \eta_1, \eta_2, p_1, p_2, P_0, P_{\eta_1}, P_{\eta_2}) \ . \qquad (3.46)$$

Written explicitly, the antisymmetric matrix is

$$\mathcal{B}^{NHC} = \begin{bmatrix} 0 & 0 & 0 & 0 & 0 & 1 & 0 & 0 & 0 & 0 \\ 0 & 0 & 0 & 0 & 0 & 0 & 1 & 0 & 0 & 0 \\ 0 & 0 & 0 & 0 & 0 & 0 & 0 & 1 & 0 & 0 \\ 0 & 0 & 0 & 0 & 0 & 0 & 0 & 0 & 1 & 0 \\ 0 & 0 & 0 & 0 & 0 & 0 & 0 & 0 & 0 & 1 \\ -1 & 0 & 0 & 0 & 0 & 0 & 0 & 0 & 0 & 0 \\ 0 & -1 & 0 & 0 & 0 & 0 & 0 & 0 & 0 & 0 \\ 0 & 0 & -1 & 0 & 0 & 0 & 0 & 0 & -P_0 & 0 \\ 0 & 0 & 0 & -1 & 0 & 0 & 0 & P_0 & 0 & -P_{\eta_1} \\ 0 & 0 & 0 & 0 & -1 & 0 & 0 & 0 & P_{\eta_1} & 0 \end{bmatrix} \ . \qquad (3.47)$$

Performing the multiplication, the equations of motion may be explicitly written as

$$\dot{q}_1 = \frac{\partial H_T}{\partial p_1} = \frac{p_1}{m_1} \tag{3.48}$$

$$\dot{q}_2 = \frac{\partial H_T}{\partial p_2} = \frac{p_2}{m_2} \tag{3.49}$$

$$\dot{R}_0 = \frac{\partial H_T}{\partial P_0} = \frac{P_0}{M} \tag{3.50}$$

$$\dot{\eta}_1 = \frac{\partial H_T}{\partial P_{\eta_1}} = \frac{P_{\eta_1}}{m_{\eta_1}} \tag{3.51}$$

$$\dot{\eta}_2 = \frac{\partial H_T}{\partial P_{\eta_2}} = \frac{P_{\eta_2}}{m_{\eta_2}} \tag{3.52}$$

$$\dot{p}_1 = -\frac{\partial H_T}{\partial q_1} = -Kq_1 + K(t)(q_2 - q_1) + c_0 R_0 \tag{3.53}$$

$$\dot{p}_2 = -\frac{\partial H_T}{\partial q_2} = -Kq_2 - K(t)(q_2 - q_1) + c_0 R_0 \tag{3.54}$$

$$\dot{P}_0 = -\frac{\partial H_T}{\partial R_0} - P_0 \frac{P_{\eta_1}}{m_{\eta_1}} = -M\omega_0^2 R_0 + c_0(q_1 + q_2) - P_0 \frac{P_{\eta_1}}{m_{\eta_1}} \tag{3.55}$$

$$\dot{P}_{\eta_1} = \left(\frac{P_0^2}{M} - gk_B T_{ext}\right) - P_{\eta_1}\frac{P_{\eta_2}}{m_{\eta_2}} \tag{3.56}$$

$$\dot{P}_{\eta_2} = \frac{P_{\eta_1}^2}{m_{\eta_1}} - k_B T_{ext} \tag{3.57}$$

In constructing the Liouville operator associated with the equations of motion, terms that involve the driven system $(L_1 + L_2)$ are separated from those that involve the NHC thermostat, L^{NHC}. This allows us to write the total Liouville operator as

$$L = L_1 + L_2 + L^{NHC} \tag{3.58}$$

where

$$L_1 = \frac{p_1}{m_1}\frac{\partial}{\partial q_1} + \frac{p_2}{m_2}\frac{\partial}{\partial q_2} + \frac{P_0}{M_0}\frac{\partial}{\partial R_0} \tag{3.59}$$

$$L_2 = (F_1 + c_0 R_0)\frac{\partial}{\partial p_1} + (F_2 + c_0 R_0)\frac{\partial}{\partial p_2} + F_0\frac{\partial}{\partial P_0} \tag{3.60}$$

and

$$\begin{aligned} L_{NHC} = &-P_0\frac{P_{\eta_1}}{m_{\eta_1}}\frac{\partial}{\partial P_0} + \frac{P_{\eta_1}}{m_{\eta_1}}\frac{\partial}{\partial \eta_1} + \frac{P_{\eta_2}}{m_{\eta_2}}\frac{\partial}{\partial \eta_2} \\ &+ \left(F_{P_{\eta_1}} - P_{\eta_1}\frac{P_{\eta_2}}{m_{\eta_2}}\right)\frac{\partial}{\partial P_{\eta_1}} + F_{P_{\eta_2}}\frac{\partial}{\partial P_{\eta_2}} \, . \end{aligned} \tag{3.61}$$

The following forces have been introduced

$$F_1 = -Kq_1 + K(t)(q_2 - q_1) \tag{3.62}$$

$$F_2 = -Kq_2 - K(t)(q_2 - q_1) \tag{3.63}$$

$$F_0 = -M\omega_0^2 R_0 + c_0(q_1 + q_2) \tag{3.64}$$

$$F_{P_{\eta_1}} = \left(\frac{P_0^2}{M_0} - gk_B T_{ext}\right) \tag{3.65}$$

$$F_{P_{\eta_2}} = \frac{P_{\eta_1}^2}{m_{\eta_1}} - k_B T_{ext} . \tag{3.66}$$

By using a generalization of the Trotter factorization, we can write the evolution of the system as

$$\exp(hL) = \exp\left\{h\left[(L_1 + L_2) + L^{NHC}\right]\right\} \tag{3.67}$$

$$= \exp\left(\frac{h}{2}L^{NHC}\right)\exp\left[h(L_1 + L_2)\right]\exp\left(\frac{h}{2}L^{NHC}\right) . \tag{3.68}$$

Using the Trotter factorization once again on $\exp\left[h(L_1 + L_2)\right]$, we get

$$\exp(hL) = \exp\left(\frac{h}{2}L^{NHC}\right)\exp\left(\frac{h}{2}L_2\right)\exp(hL_1)\exp\left(\frac{h}{2}L_2\right)\exp\left(\frac{h}{2}L^{NHC}\right) . \tag{3.69}$$

We apply $\exp\left(\frac{h}{2}L_{NHC}\right)$ to change the thermostat variables and the momentum of the bath. Then $\exp\left[h(L_1 + L_2)\right]$ implements the velocity-Verlet procedure to change the driven system and bath variables. The output of this step feeds into $\exp\left(\frac{h}{2}L_{NHC}\right)$, which updates the thermostat variables and the momentum of the bath.

In order to improve the accuracy of the numerical trajectories, a higher order algorithm is required. This is achieved by applying of the Yoshida weight scheme and a multiple time step procedure to the NHC part of the propagator [42]. This scheme is defined as

$$exp\left(iL^{NHC}\frac{h}{2}\right) = \prod_{i=1}^{Nc}\left[\prod_{j=1}^{Nys} exp\left(iL^{NHC}\frac{w_j h}{2Nc}\right)\right] . \tag{3.70}$$

Expanding the right hand side of eqn. (3.70), produces

$$
\begin{aligned}
exp\left(iL^{NHC}\frac{w_j h}{2Nc}\right) &= exp\left(\frac{w_j h}{4Nc}F_{P_{\eta_2}}m_{\eta_2}\frac{\partial}{\partial P_{\eta_2}}\right)exp\left(-\frac{w_j h}{8Nc}\frac{P_{\eta_2}}{m_{\eta_2}}P_{\eta_1}\frac{\partial}{\partial P_{\eta_1}}\right)\times \\
&\quad\times exp\left(\frac{w_j h}{4Nc}F_{P_{\eta_1}}m_{\eta_1}\frac{\partial}{\partial P_{\eta_1}}\right)exp\left(-\frac{w_j h}{8Nc}\frac{P_{\eta_2}}{m_{\eta_2}}P_{\eta_1}\frac{\partial}{\partial P_{\eta_1}}\right)\times \\
&\quad\times exp\left(-\frac{w_j h}{2Nc}\left[\frac{P_{\eta_1}}{m_{\eta_1}}P_Q\frac{\partial}{\partial P_Q}\right]\right)\times \\
&\quad\times exp\left(\frac{w_j h}{2Nc}\left[\frac{P_{\eta_1}}{m_{\eta_1}}\frac{\partial}{\partial \eta_1}+\frac{P_{\eta_2}}{m_{\eta_2}}\frac{\partial}{\partial \eta_2}\right]\right)\times \\
&\quad\times exp\left(-\frac{w_j h}{8Nc}\frac{P_{\eta_2}}{m_{\eta_2}}P_{\eta_1}\frac{\partial}{\partial P_{\eta_1}}\right)exp\left(\frac{w_j h}{4Nc}F_{P_{\eta_1}}m_{\eta_1}\frac{\partial}{\partial P_{\eta_1}}\right)\times \\
&\quad\times exp\left(-\frac{w_j h}{8Nc}\frac{P_{\eta_2}}{m_{\eta_2}}P_{\eta_1}\frac{\partial}{\partial P_{\eta_1}}\right) \\
&\quad\times exp\left(\frac{w_j h}{4Nc}F_{P_{\eta_2}}m_{\eta_2}\frac{\partial}{\partial P_{\eta_2}}\right)\ .
\end{aligned}
\tag{3.71}
$$

where N_c is the number of multiple time steps and N_{ys} is the number of Yoshida weights. To avoid a singularity within the algorithm, we follow the prescription detailed in [42], and make use of a higher order Maclaurin series to evaluate the action of P_{η_1}. Applying the direct translation technique to eqn. (3.69), allows us to obtain the pseudo code to implement the numerical integration. Details of this procedure can be found in Appendix D.3.

3.3 Normal modes and sampling initial conditions

In order to calculate the motion of a system in phase space as a superposition of normal modes, we need to diagonlize the Hamiltonian of said system. Once diagonlized, we can view the Hamiltonian as a sum of independent modes. By introducing the concept of normal modes, we can decompose the differential equations which govern the motion of the oscillators. The behaviour of the normal modes is then analogous to that of a simple harmonic oscillator, which becomes simple to solve.

The Hamiltonian of the driven, coupled oscillators is

$$
H = \frac{p_1^2}{2m}+\frac{p_2^2}{2m}+\frac{K}{2}q_1^2+\frac{K}{2}q_2^2+\frac{m\omega^2(t)}{2}\left(q_2-q_1\right)^2\ .
\tag{3.72}
$$

The derivation of the normal mode coordinates and equations used to transform between Cartesian and normal mode coordinates is shown in Appendix B.

The new set of coordinates allows to diagonlize the Hamiltonian, which is now the sum of 2 modes

$$H^N \quad = \quad \sum_{k=1}^{2} H_k^N \tag{3.73}$$

where

$$H_k^N \quad = \quad \left(\frac{P_k^2}{2m} + \frac{1}{2} m \omega_k^2 R_k^2 \right) \tag{3.74}$$

is the Hamiltonian of oscillator k, given in normal mode coordinates. P_k and R_k are the normal mode coordinates and momenta of oscillator k and ω_k its associated normal mode frequency.

In terms of Cartesian coordinates, the normal mode coordinates are defined as

$$R_1 \quad = \quad \frac{1}{\sqrt{2}} \left(q_1 + q_2 \right) \tag{3.75}$$

$$R_2 \quad = \quad \frac{1}{\sqrt{2}} \left(q_1 - q_2 \right) . \tag{3.76}$$

Normal mode 1 is the sum of the motion of the oscillators, which can be interpreted as the motion of the centre of mass of the system. The centre of mass for a two particle system represents the average of the displacement of both particles. Normal mode 1 can be thought of as a single particle having mass 2m with frequency ω_1. Normal mode 2 is the difference between the oscillators, which can be interpreted as their relative displacement. The motion of the relative displacement always leaves the centre of mass unchanged.

It was shown that the normal mode frequencies of each mode are

$$\omega_1 \quad = \quad \sqrt{\frac{K}{m}} \tag{3.77}$$

$$\omega_2 \quad = \quad \sqrt{\frac{K + 2K(t)}{m}} . \tag{3.78}$$

ω_1 and ω_2 are called the eigenfrequncies or characteristic frequencies. For ω_1, the amplitudes of the oscillators are the same and they are in phase with each other. The frequency ω_1 is the frequency of the oscillators if they were not coupled. For ω_2, the amplitudes of the oscillators are the same and they are out of phase with each other. A new frequency has been introduced because of the coupling between the oscillators. It is important to note that the new frequency, ω_2, is always larger than the frequency of the oscillators if they were not coupled, ω_1. From the motion of the coupled oscillators, we have introduced a system where the motion is governed by a set of decoupled linear differential equations. The normal mode corresponding to the sum of the two variables oscillates at the frequency which the particles would oscillate if they were decoupled. We

have another normal mode which oscillates at a higher frequency. Normal mode 2 is a faster mode than normal mode 1.

Now that we have the Hamiltonian in the form of decoupled normal modes, we can calculate the initial conditions of the system. The initial conditions are sampled from the Wigner function in the initial thermal state.

$$\rho_W = \prod_{k=1}^{2} \left\{ \frac{1}{\pi\hbar} \tanh\left(\frac{\hbar\omega_k}{2}\beta\right) \exp\left[-\frac{2}{\hbar\omega_k}\tanh\left(\frac{\hbar\omega_k}{2}\beta\right)H_k^N\right]\right\}. \tag{3.79}$$

The complete derivation of this distribution function is shown in Appendix A. Substituting eqn. (3.74) into eqn. (3.79), eqn. (3.79) becomes

$$\begin{aligned}
\rho_W &= \prod_{k=1}^{2} \left\{ \frac{1}{\pi\hbar} \tanh\left(\frac{\hbar\omega_k}{2}\beta\right) \exp\left[-\frac{2}{\hbar\omega_k}\tanh\left(\frac{\hbar\omega_k}{2}\beta\right)\left(\frac{P_k^2}{2m} + \frac{1}{2}m\omega_k^2 R_k^2\right)\right]\right\} \\
&= \prod_{k=1}^{2} \left\{ \frac{1}{\pi\hbar} \tanh\left(\frac{\hbar\omega_k}{2}\beta\right) \exp\left[-\frac{2}{\hbar\omega_k}\tanh\left(\frac{\hbar\omega_k}{2}\beta\right)\left(\frac{P_k^2}{2m}\right)\right] \right. \\
&\qquad \left. \times \exp\left[-\frac{2}{\hbar\omega_k}\tanh\left(\frac{\hbar\omega_k}{2}\beta\right)\left(\frac{1}{2}m\omega_k^2 R_k^2\right)\right]\right\} \\
&= \prod_{k=1}^{2} \left\{ \frac{1}{\pi\hbar} \tanh\left(\frac{\hbar\omega_k}{2}\beta\right) \exp\left[-\frac{P_k^2}{2}\left(\frac{2}{\hbar\omega_k m}\right)\tanh\left(\frac{\hbar\omega_k}{2}\beta\right)\right] \right. \\
&\qquad \left. \times \exp\left[-\frac{R_k^2}{2}\left(\frac{2m\omega_k}{\hbar}\right)\tanh\left(\frac{\hbar\omega_k}{2}\beta\right)\right]\right\} \\
&= \prod_{k=1}^{2} \left\{ \frac{1}{\pi\hbar} \tanh\left(\frac{\hbar\omega_k}{2}\beta\right) \exp\left[-\frac{P_k^2}{2\sigma_{P_k}^2}\right] \exp\left[-\frac{R_k^2}{2\sigma_{R_k}^2}\right]\right\} \tag{3.80}
\end{aligned}$$

where we have introduced

$$\sigma_{P_k}^2 = \left[\left(\frac{2}{\hbar\omega_k m}\right)\tanh\left(\frac{\hbar\omega_k}{2}\beta\right)\right]^{-1} \tag{3.81}$$

$$\text{and} \quad \sigma_{R_k}^2 = \left[\left(\frac{2m\omega_k}{\hbar}\right)\tanh\left(\frac{\hbar\omega_k}{2}\beta\right)\right]^{-1} \tag{3.82}$$

$$\therefore \sigma_{P_k} = \left[\left(\frac{2}{\hbar\omega_k m}\right)\tanh\left(\frac{\hbar\omega_k}{2}\beta\right)\right]^{-\frac{1}{2}} \tag{3.83}$$

$$\sigma_{R_k} = \left[\left(\frac{2m\omega_k}{\hbar}\right)\tanh\left(\frac{\hbar\omega_k}{2}\beta\right)\right]^{-\frac{1}{2}}. \tag{3.84}$$

Equation (3.80) has the form of the product of two gaussian distribution functions. This allows us to sample the initial conditions from a gaussian distribution function and then normalize them using eqns. (3.83) and (3.84). The initial conditions we obtain from this distribution function describe the initial quantum state of the system. Since we know that the dynamics of our system looks purely classical, these initial conditions characterize the quantum behaviour of the system.

We now consider the high temperature limit, $(T \rightarrow \infty, \beta \rightarrow 0)$. In this limit we can expand $\tanh(x)$ in terms of exponents, to first order,

$$\tanh(x) = \frac{\exp(x) - \exp(-x)}{\exp(x) + \exp(-x)} \tag{3.85}$$

$$\approx \frac{1 + x - (1 - x)}{1 + x + 1 - x} \tag{3.86}$$

$$= x + O(x^2) \tag{3.87}$$

Identifying $x = \frac{\hbar\omega_k}{2}\beta$ and using the limit of high temperature allows us to simplify eqn. (3.79),

$$\rho_W = \prod_{k=1}^{N} \left\{ \frac{1}{\pi\hbar} \left(\frac{\hbar\omega_k}{2}\beta \right) \exp\left[-\frac{2}{\hbar\omega_k} \left(\frac{\hbar\omega_k}{2}\beta \right) \left(\frac{P_k^2}{2m} + \frac{1}{2}m\omega_k^2 R_k^2 \right) \right] \right\}$$

$$= \prod_{k=1}^{N} \left\{ \frac{\beta\omega_k}{2\pi} \exp\left[-\beta \left(\frac{P_k^2}{2m} + \frac{1}{2}m\omega_k^2 R_k^2 \right) \right] \right\} \tag{3.88}$$

This expression is the classical canonical distribution function, which will used to sample the classical initial conditions.

$$\rho_W = \prod_{k=1}^{N} \left\{ \frac{\beta\omega_k}{2\pi} \exp\left[\frac{-\beta P_k^2}{2m} \right] \exp\left[\frac{-\beta}{2}m\omega_k^2 R_k^2 \right] \right\}$$

$$= \prod_{k=1}^{N} \left\{ \frac{\beta\omega_k}{2\pi} \exp\left[-\frac{P_k^2}{2\sigma_{P_k}^2} \right] \exp\left[-\frac{R_k^2}{2\sigma_{R_k}^2} \right] \right\} \tag{3.89}$$

where we have introduced

$$\sigma_{P_k}^2 = \frac{m}{\beta} \tag{3.90}$$

$$\text{and} \quad \sigma_{R_k}^2 = \frac{1}{m\beta\omega_k^2} \tag{3.91}$$

$$\therefore \sigma_{P_k} = \sqrt{mk_BT} \tag{3.92}$$

$$\sigma_{R_k} = \sqrt{\frac{k_BT}{m\omega_k^2}} \tag{3.93}$$

Thus, by changing how we sample the initial conditions of the system, we can study differences between the classical and quantum behaviour of the system.

3.4   Numerical evolution of the Wigner function

Our objective is to solve the non-equilibrium statistical mechanics of the model. This is done by using the Wigner approach to quantum mechanics and Monte-Carlo sampling of the initial conditions [3]. The initial conditions of the system are sampled, in terms of normal mode coordinates,

from the Wigner function in the initial thermal state, given by eqn. (3.79). In the initial state, the oscillators have not started to interact. The coordinates are then transformed from normal mode to Cartesian coordinates, which are propagated as a cloud of points. A schematic representation of the evolution of the Wigner function can be seen in fig. 3.1.
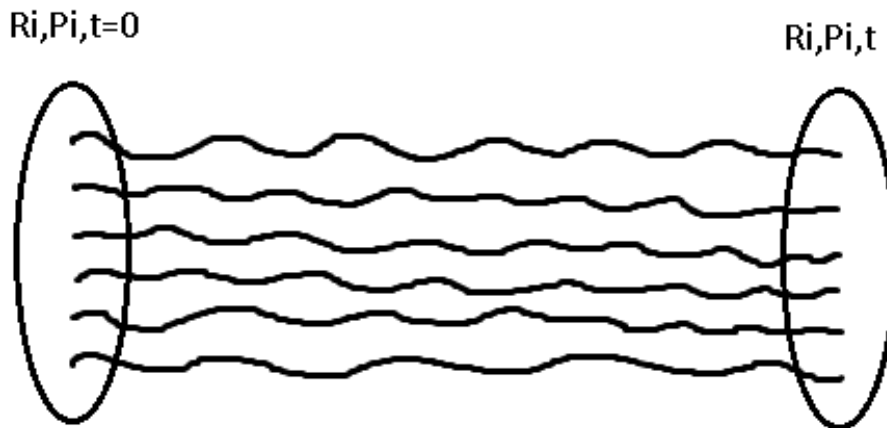
Figure 3.1: Illustration of the numerical evolution of the Wigner function, over a finite time.

After time $t = 0$, we no longer have the analytical form of the density matrix to describe the system. Instead, we have a cloud of points. We numerically simulate the propagation of the Wigner function, using time reversible algorithms. In the Wigner representation, we calculate statistical averages over the time evolved Wigner function. The average of a desired observable, χ, is given by

$$< \hat{\chi} > \quad = \quad \int_\tau d^N R \, d^N P \; \rho_W(R,P,t)\chi_W(R,P) \,. \tag{3.94}$$

Equation 3.94 can be applied to calculate the average of the variance of the normal mode coordinates in the Wigner representation, to verify if our system is squeezed or not. Recall from Chapter 1, that if two operators satisfy the relation $\left[\hat{A}, \hat{B}\right] = i\hat{C}$, then we have a squeezed state if

$$\left\langle \left(\Delta\hat{A}\right)^2 \right\rangle < \frac{1}{2}\left|\left\langle\hat{C}\right\rangle\right| \qquad \text{or} \qquad \left\langle \left(\Delta\hat{B}\right)^2 \right\rangle < \frac{1}{2}\left|\left\langle\hat{C}\right\rangle\right| \,. \tag{3.95}$$

In the case of normal mode coordinates, their commutation relation is $\left[\hat{R}, \hat{P}\right] = i\hbar$. In the case of dimensionless coordinates, $\hbar$ is equal to 1. Thus, we have squeezing in one of the normal modes, if

$$\left\langle \left(\Delta\hat{R}\right)^2 \right\rangle < \frac{1}{2} \qquad \text{or} \qquad \left\langle \left(\Delta\hat{P}\right)^2 \right\rangle < \frac{1}{2} \,. \tag{3.96}$$

Using eqn. (3.94), we can calculate the variance of each normal mode coordinate,

$$
\begin{aligned}
\sigma_\chi^2 &= <\hat{\chi}^2> - <\hat{\chi}>^2 & (3.97) \\
&= \int_\tau d^N q\, d^N p\; \rho_W(q,p,t)\chi_W^2(q,p) - \left[\int_\tau d^N q\, d^N p\; \rho_W(q,p,t)\chi_W(q,p)\right]^2 . & (3.98)
\end{aligned}
$$

We can then compare the calculated variance, given by eqn. (3.98), to the threshold for squeezing, which in this case is given by eqn. (3.96).

We can also use another method to visualize squeezing in our system. Since we evolve the Wigner function as a cloud of points, and consequently do not have an analytical form after time $t = 0$, we can construct the histograms of the marginal distribution functions of each normal mode,

$$
\begin{aligned}
W(R_1, P_1, t) &= \int dR_2\, dP_2\, W(R_1, R_2, P_1, P_2, t) & (3.99) \\
W(R_2, P_2, t) &= \int dR_1\, dP_1\, W(R_1, R_2, P_1, P_2, t) . & (3.100)
\end{aligned}
$$

The histograms will also give us an intuitive idea of how squeezing may be useful. We should be able to clearly visualize squeezing in our system if our system is in a squeezed state.

Chapter 4

Numerical Results

In this chapter, the results of the numerical study are shown together with their interpretation. Firstly, a comparison between classical and quantum sampled initial conditions is made by analysing the different shapes in the distributions of the initial positions and momenta of each normal mode. We then consider the dynamics of the coupled oscillators without an environment. The stability of the numerical algorithm to solve the equations of motion is shown in the form of the conservation of the Hamiltonian in the absence of driving. Next, the generation of a squeezed state is shown by comparing the variance of each normal mode coordinate to the threshold for squeezing. To visualize the squeezing effect, the marginal distribution of each normal mode is plotted at the initial and a later time. Two different types of environments are then added to the coupled oscillators. The results of these simulations are shown, together with an explanation of the influence of temperature and coupling strength on the strength of squeezing.

4.1 Initial conditions

To illustrate the differences between the classical and quantum initial conditions, we plot the sampled initial values of the momentum and position of a normal mode. We show the results of normal mode 1, however the same behaviour is observed in normal mode 2. The classical initial conditions are sampled from the classical canonical distribution function given by eqn. (3.88), while the quantum initial conditions are sampled from the analytical form of the Wigner function in the initial thermal state, given by eqn. (3.79). Figures 4.1a and 4.1b show the classical and quantum initial conditions of normal mode 1, respectively. In each plot, we used the same set of parameters to generate the initial conditions. For the classical case, the initial values were seen to be localised at the origin. However, for the quantum case, we observe a delocalisation where the initial conditions are spread over a wider region.
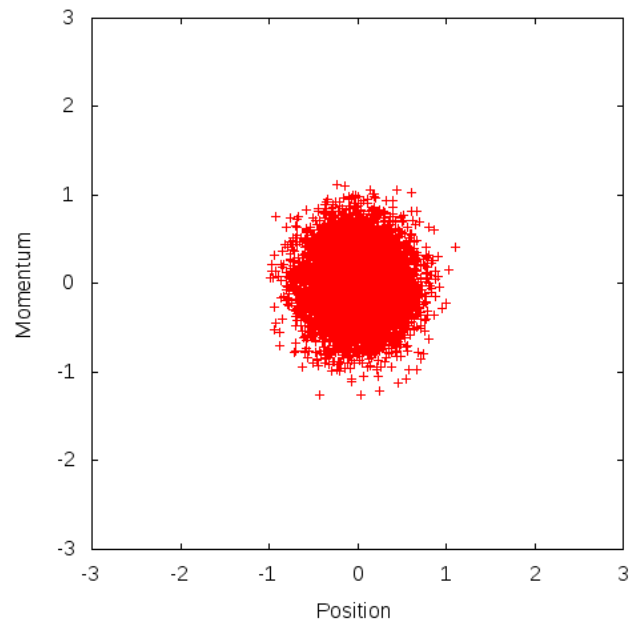
(a) Classical initial conditions of normal mode 1.
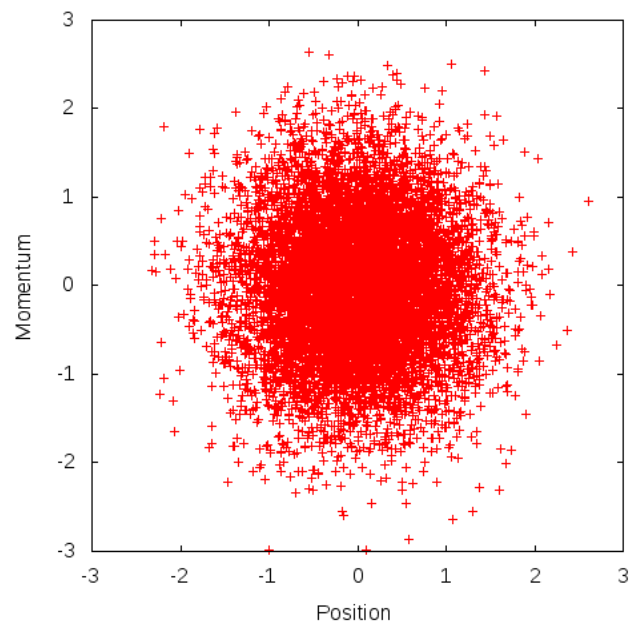
(b) Quantum initial conditions of normal mode 1.

Figure 4.1: Classical and quantum initial values of the position and momentum of normal mode 1. Parameters used in this simulation: $m = 1.0$, $K = 1.25$ and $T_1 = T_2 = 1.0$. 10 000 points were sampled in each case.

4.2   Coupled oscillators

In this section, we present the results of the simulation of the system of coupled, driven oscillators whose Hamiltonian is given by eqn. (3.19). For all further simulations of the dynamics, we used a time-step of 0.01, 25 000 molecular dynamics steps, 10 000 Monte-Carlo steps, dimensionless co-ordinates and scaled units. In order to check that the time-reversible algorithm used is numerically stable, we ensure that the Hamiltonian of the system is conserved, in the absence of driving. See fig. 4.2a. The standard deviation of each point is also calculated to ensure that the results do not depend on the seed used to generate the random numbers. We then look at the Hamiltonian when driving is introduced to the system in fig. 4.2b. As expected, the driving violates the conservation of the Hamiltonian as we observe large fluctuations. The strength of the fluctuations in the Hamiltonian is proportional to the amplitude of the time-dependent frequency, while the period of oscillations depends on the driving frequency.

The variance of each normal mode co-ordinate is shown in fig. 4.3a. The coordinates of normal mode 1 maintain a constant value even when driving is switched on between the oscillators. However, we observe a decrease and increase in the variance of the position and momentum of normal mode 2 respectively. We observe a change in the variance of only normal mode 2 because of the form of the normal mode frequencies, see eqns. (3.77) and (3.78). Only the frequency of normal mode 2 contains a time-dependence, while the frequency of normal mode 1 has a constant value. In fig. 4.3b, the variance of the position of normal mode 2 is shown to be below the threshold for squeezing. As a result of the time-dependent interaction, the system is driven from a thermal state into a squeezed state. The inset in fig. 4.3b showing the short time simulation of the dynamics, indicates that the process of generating a squeezed state is a fast one. However it is not an instantaneous one, as there are initially points lying above the threshold for squeezing, after the time-dependent interaction is switched on at time t=0.

To improve our intuitive understanding of how squeezing occurs in our system, we plotted 2-dimensional surface plots of the marginal distributions at the initial time when the system was in a thermal state, for each normal mode. These plots were then compared to a later time, to verify if we observe squeezing in the normal mode. To study these effects, we used quantum initial conditions to generate the marginal distribution functions. From figs. 4.4a and 4.4b, normal mode 1 was seen to maintain its circular distribution, after the time-dependent interaction had been introduced, indicating that it is not squeezed. However, in figs. 4.5a and 4.5b, we see a change in the distribution for normal mode 2. Starting in a thermal state where the distribution is circular, the distribution becomes elliptical, after the time-dependent interaction is switched on. Figure 4.5b shows squeezing in the position and elongation in the momentum of normal mode 2, which is consistent with the results obtained in fig. 4.3a.
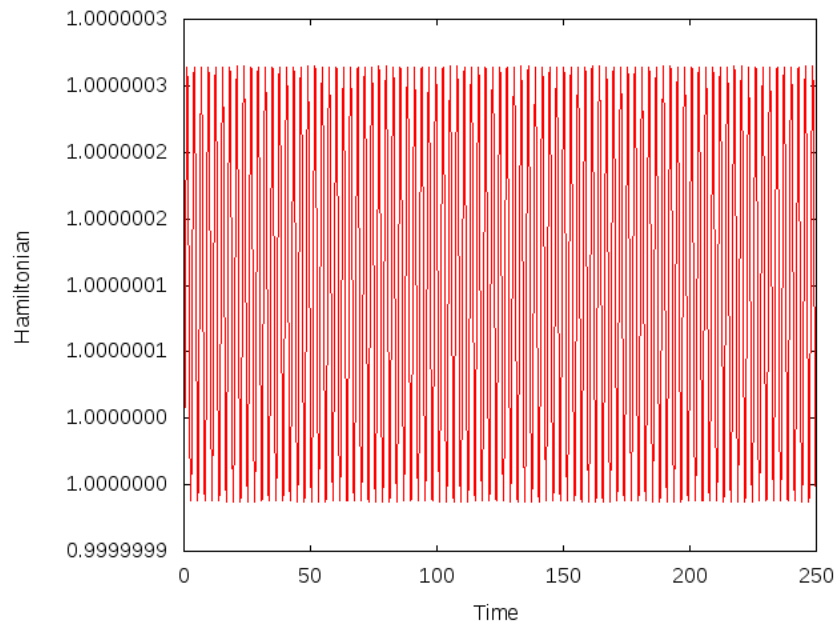
(a) Normalized Hamiltonian without driving between the oscillators.
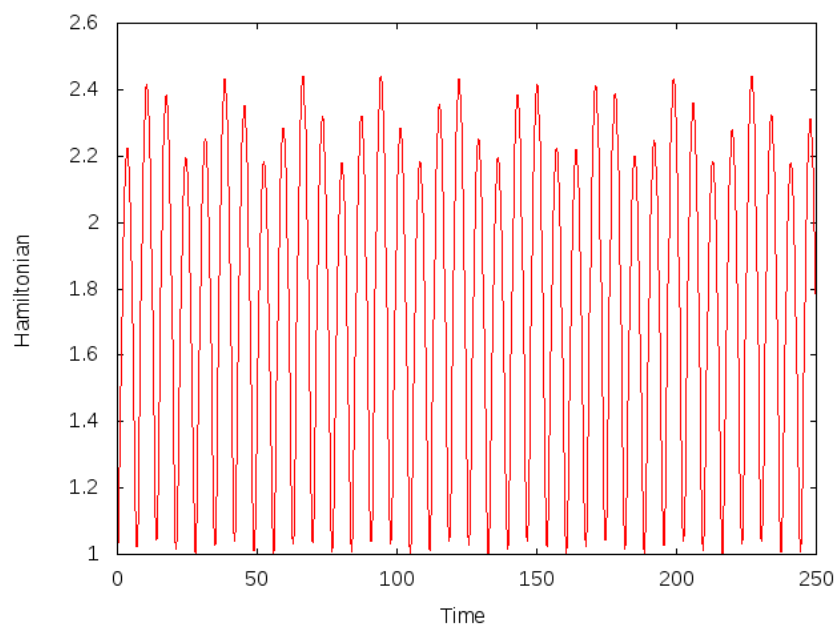
(b) Normalized Hamiltonian with driving between oscillators.

Figure 4.2: Normalized Hamiltonian in the absence of driving (a) and when the driving is introduced to the system (b). Parameters used in this simulation: $m = 1.0$, $K = 1.25$, $T_1 = T_2 = 1.0$, $\omega_0 = 2.50$ and $\omega_d = 0.45$.
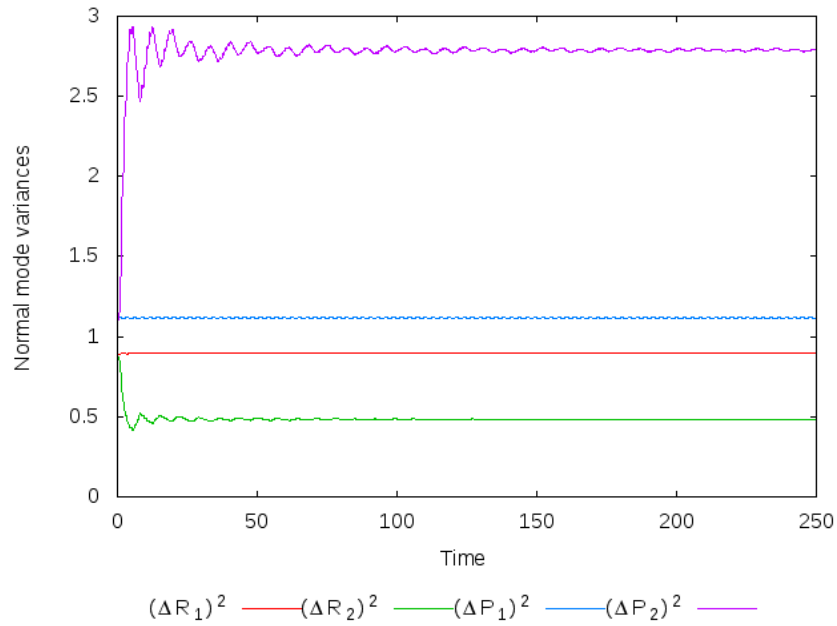
(a) Variance of each normal mode coordinate. The red, green, blue and purple lines represent the variances of R_1, R_2, P_1 and P_2 respectively.
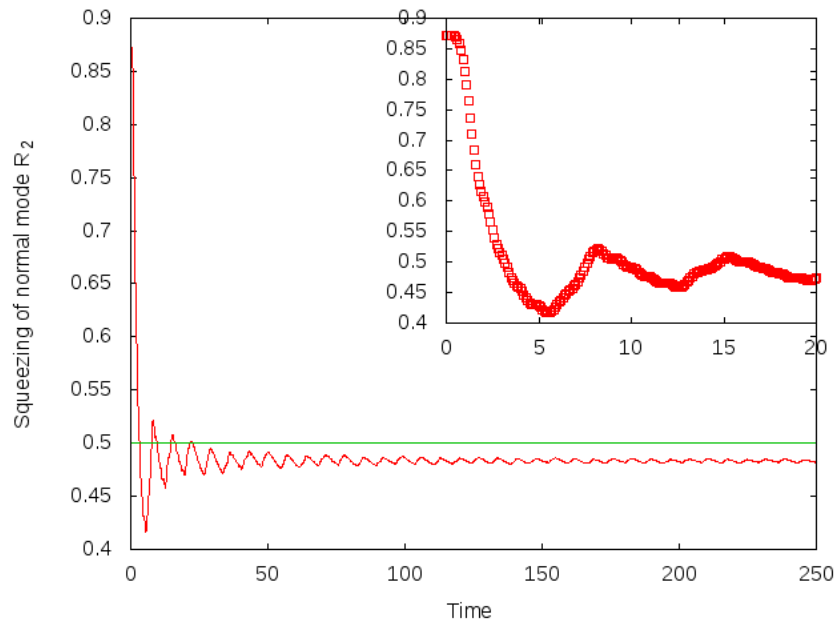
(b) Variance of normal mode coordinate R_2, indicated by the red line, below the threshold for squeezing, indicated by the green line. The inset shows the short time simulation of the variance of R_2, represented by red points.

Figure 4.3: Variance of all normal mode coordinates (a) and variance of R_2 below the threshold for squeezing together with an inset of the short time simulation (b). Parameters used in this simulation: $m = 1.0$, $K = 1.25$, $T_1 = T_2 = 0.1$, $\omega_0 = 2.50$ and $\omega_d = 0.45$.
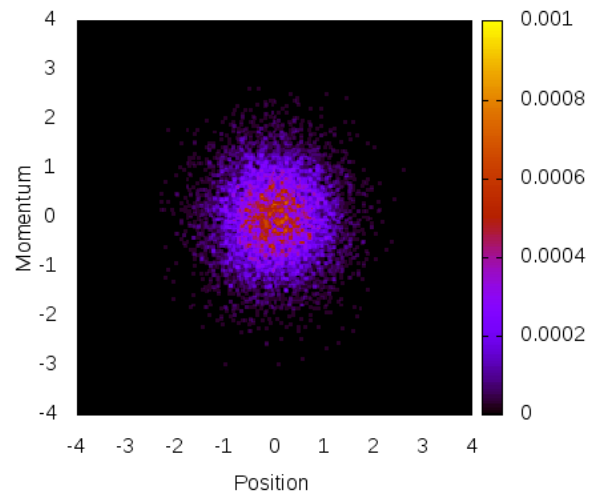
(a) Marginal distribution function of normal mode 1 at t=0.
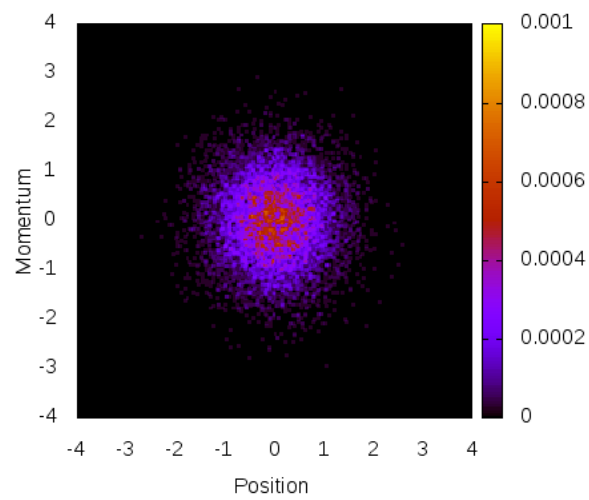
(b) Marginal distribution function of normal mode 1 at t=200.

Figure 4.4: Two-dimensional surface plots of the marginal distribution functions of normal mode 1 at t=0 (a) and t=200 (b). Parameters used in this simulation: $m = 1.0$, $K = 1.25$, $T_1 = T_2 = 0.1$, $\omega_0 = 2.50$ and $\omega_d = 0.45$.
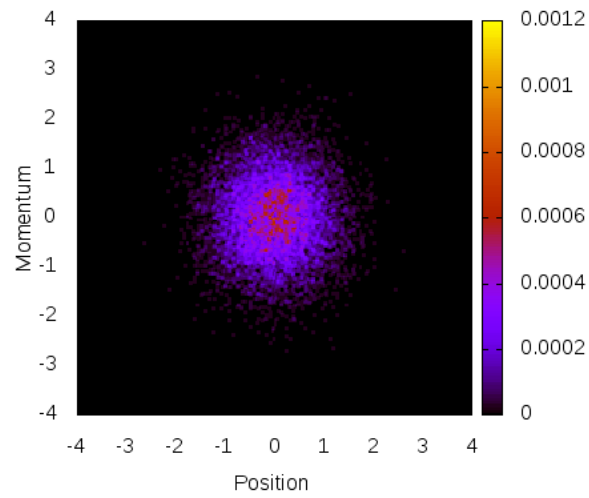
(a) Marginal distribution function of normal mode 2 at t=0.
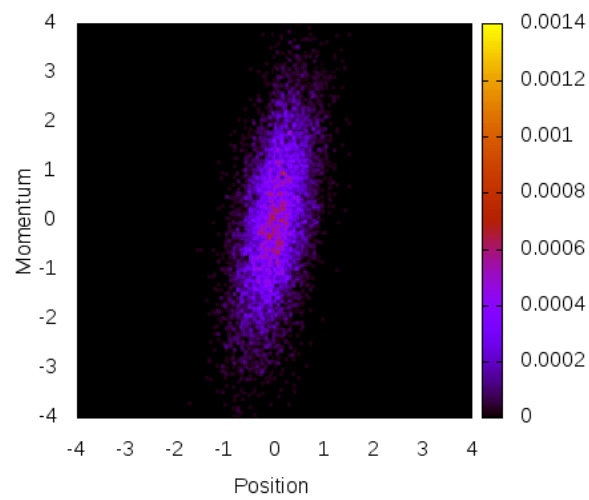
(b) Marginal distribution function of normal mode 2 at t=200.

Figure 4.5: Two-dimensional surface plots of the marginal distribution functions of normal mode 2 at t=0 (a) and t=200 (b). Parameters used in this simulation: $m = 1.0$, $K = 1.25$, $T_1 = T_2 = 0.1$, $\omega_0 = 2.50$ and $\omega_d = 0.45$.

4.3 Coupled oscillators attached to a harmonic bath

We now introduce an environment of a bath of $N = 200$ harmonic oscillators, bi-linearly coupled to the system of coupled, driven oscillators. The Hamiltonian of this system is given by eqn. (3.25). 200 oscillators were used since it corresponds to the minimum number of oscillators that can describe an infinite bath and be in agreement with linear response theory [49, 50]. To check that the numerical algorithm used to solve the system is stable, we calculated the Hamiltonian of the total system in the absence of driving. Figure 4.6 shows that this quantity is conserved which implies that the algorithm is stable. This calculation was performed using weak and strong coupling strength to the bath ($\xi = 0.007, 0.3$), with low, medium and high temperature values of the bath ($T_b = 0.1, 1.0, 10.0$). All sets of parameter values yielded results which were in agreement with each other. For these simulations we set ω_c to 1.0 and ω_{max} to 3.0.
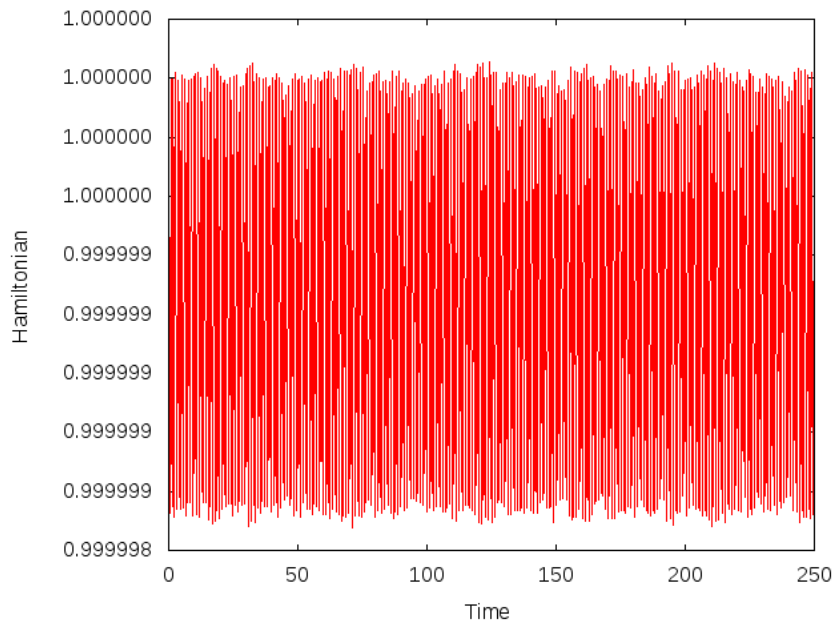
Figure 4.6: Normalized Hamiltonian of coupled oscillators, in the absence of driving, attached to a harmonic bath. Parameters used in this simulation: $m = 1.0$, $K = 1.25$, $T_1 = T_2 = 0.1$ $T_b = 1.0$ and $\xi = 0.007$.

In fig. 4.7a the variance of each normal mode coordinate is shown. We only observe a change in fluctuations of normal mode two, when driving is introduced to the system. The variance of the position decreases at the expense of an increase in the variance of its momentum. This occurs as a result of the time-dependent interaction between the oscillators. In fig. 4.7b, we show that the variance of the position of normal mode two is indeed below the threshold for squeezing which indicates that the system has been driven from a thermal to a squeezed state. The inset in fig. 4.7b shows that even when an environment is attached to the system of coupled oscillators, the time taken for the system to go from a thermal to a squeezed state does not change.

Following this, a study to investigate the influence of temperature on the strength of squeezing was performed. In fig. 4.8, four different temperatures of the bath, which differ by an order of magnitude ($T_b = 0.01, 0.1, 1.0, 2.0$), were used. We found that as we decrease the temperature of the bath, we obtained stronger squeezing. However, there is a limit to which we can squeeze normal mode two. If we use a value of 0.01 for T_b, then we generate exactly the same amount of squeezing as we would using a value of 0.1 for T_b. An increase in temperature, caused weaker squeezing in normal mode two, eventually resulting in not being able to generate a squeezed state.
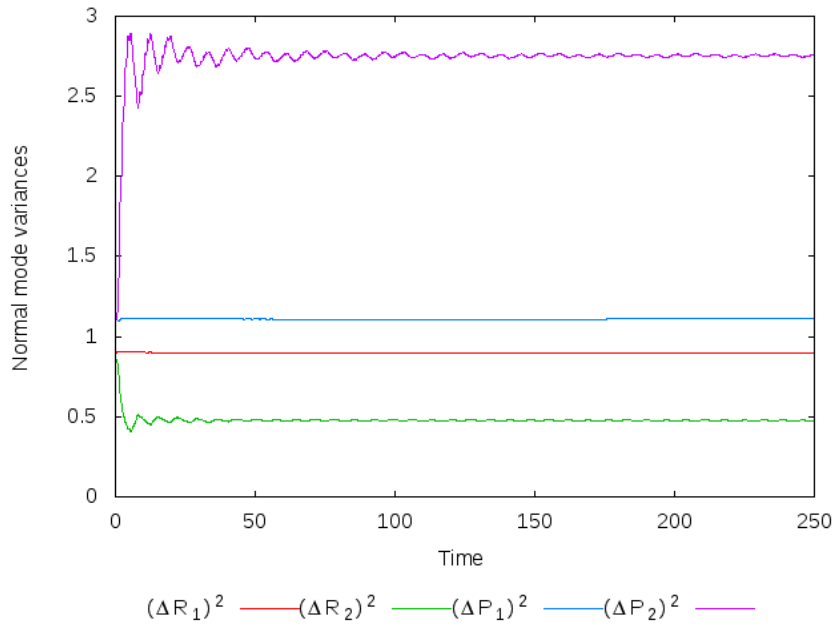
(a) Variance of each normal mode coordinate. The red, green, blue and purple lines represent the variances of R_1, R_2, P_1 and P_2 respectively.
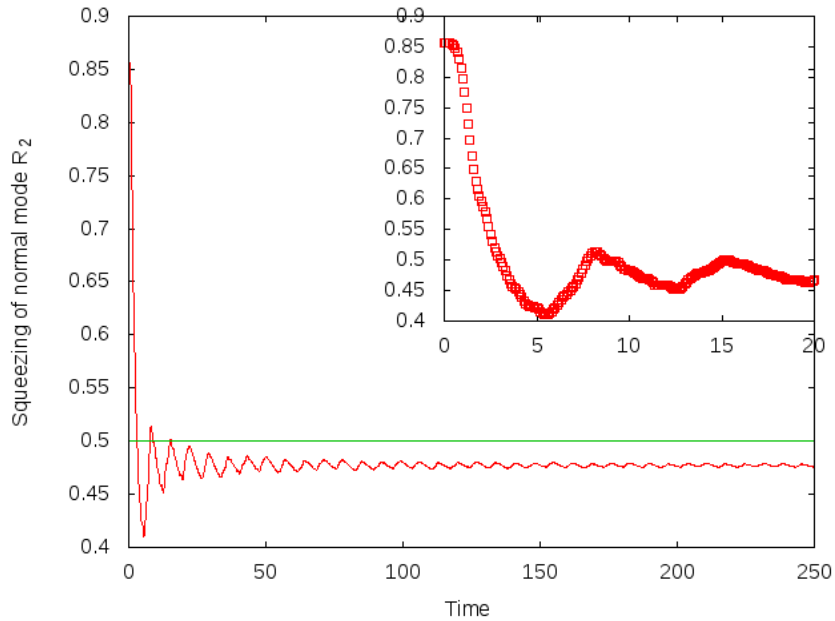
(b) Variance of normal mode coordinate R_2, indicated by the red line, below the threshold for squeezing, indicated by the green line. The inset shows the short time simulation of the variance of R_2, represented by red points.

Figure 4.7: Variance of all normal mode coordinates (a) and variance of R_2 below the threshold for squeezing together with an inset of the short time simulation (b). Parameters used in this simulation: $m = 1.0$, $K = 1.25$, $T_1 = T_2 = 1.0$, $\omega_0 = 2.50$, $\omega_d = 0.45$, $T_b = 1.0$ and $\xi = 0.007$.
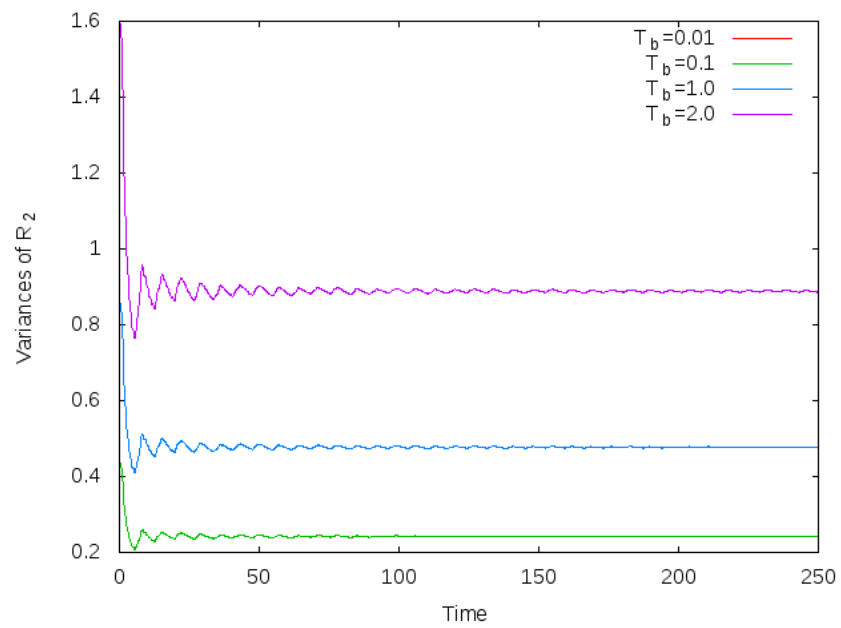
Figure 4.8: Variance of normal mode coordinate R_2, with four different temperatures of the bath. The red, green, blue and purple lines are for temperatures of the bath 0.01, 0.1, 1.0 and 2.0 respectively. Parameters used in this simulation: $m = 1.0$, $K = 1.25$, and $\xi = 0.007$.

4.4 Coupled oscillators attached to a NHC and harmonic oscillator

Using a bath of $N = 200$ harmonic oscillators to represent an environment, requires the simulation of many degrees of freedom. By introducing the NHC thermostat following non-Hamiltonian dynamics, we have shown that it is possible to simulate an environment with fewer degrees of freedom. This alternative way of representing an environment drastically reduces the time taken to perform the full simulation. The results of this study will be presented. For these simulations, we used $\eta_1 = 0$, $\eta_2 = 0$, $P_{\eta_1} = 0$ and $P_{\eta_2} = 1.0$
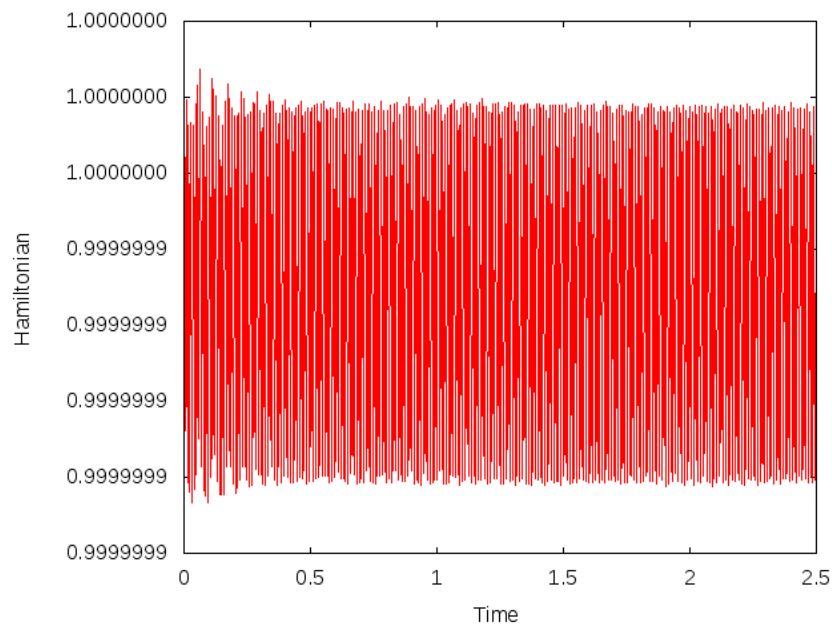
Figure 4.9: Normalized Hamiltonian of coupled oscillators, in the absence of driving, attached to NHC thermostat. Parameters used in this simulation: $m = 1.0$, $K = 1.25$, $T_1 = T_2 = 1.0$ $T_b = 1.0$ and $\xi = 0.007$.

It was first important to verify that the numerical algorithm, used to solve the system, is stable. This algorithm is not a simple generalization of the Velocity-Verlet. We have used a Yoshida weight scheme and multiple time-step procedure. In the Yoshida scheme, we used 3 weights where the weights are given by $w_1 = \frac{1}{2-2^{1/3}}$, $w_2 = 1 - 2w_1$ and $w_3 = w_1$. For the multiple time-step procedure, we used a 3 fold time step. Thus the time discretization used in the algorithm changes from Δt to $w_i \Delta t/3$. In fig. 4.9, the conserved Hamiltonian indicates that the algorithm implemented is stable.

The results shown in figs. 4.10a and 4.10b are in agreement with the results presented in figs 4.7a and 4.7b. As a result of the time-dependent interaction between the oscillators, we obtain squeezing in the position of normal mode two. This occurs at the expense of an increase in the fluctuations of the momentum of normal mode two. The influence of the temperature of the bath on the squeezing was studied using four different values which differ by an order of magnitude ($T_{ext} = 0.01, 0.1, 1.0, 2.0$) in fig. 4.11. A decrease in temperature increased the strength of squeezing. However, there is a limit to which we can squeeze the system, since temperatures 0.01 and 0.1 produced exactly the same amount of squeezing. An increase in temperature limits the amount of squeezing which eventually removes it completely.
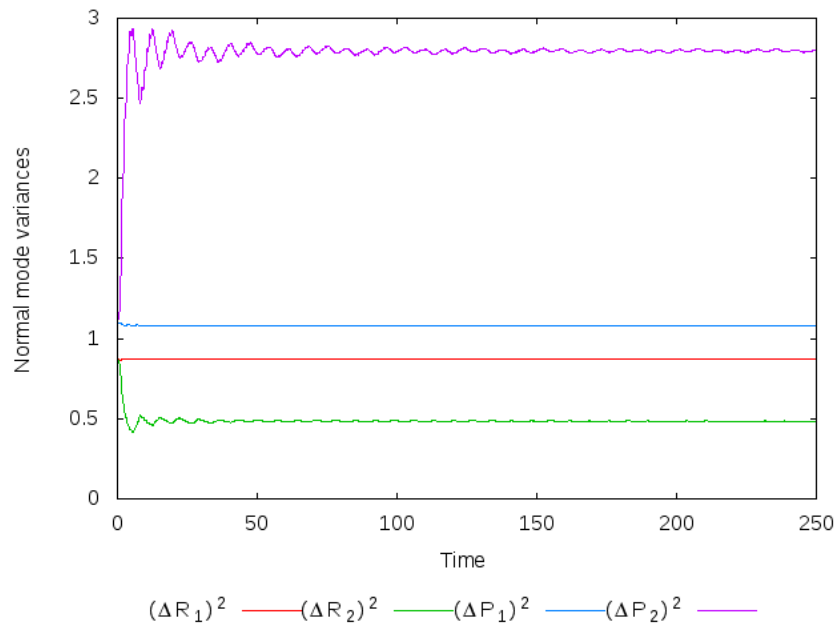
(a) Variance of each normal mode coordinate. The red, green, blue and purple lines represent the variances of R_1, R_2, P_1 and P_2 respectively.
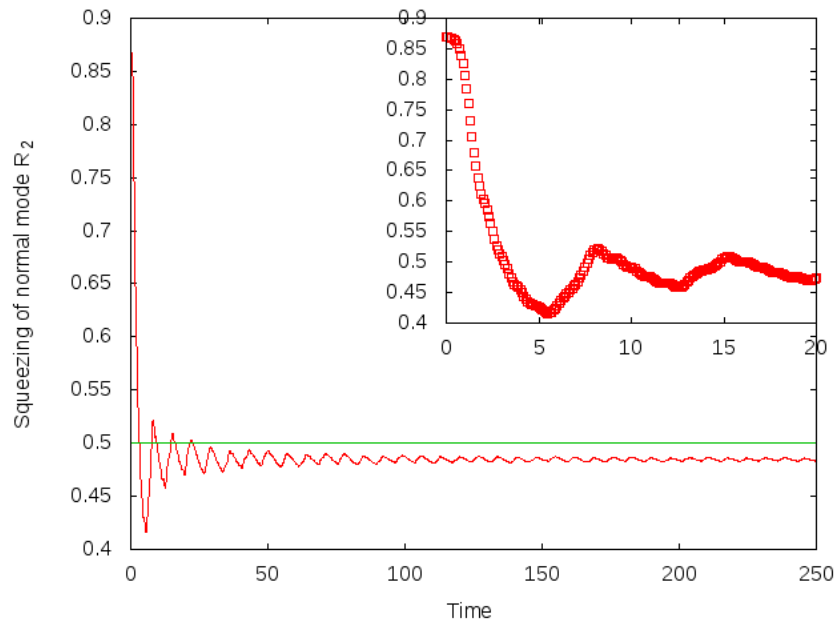
(b) Variance of normal mode coordinate R_2, indicated by the red line, below the threshold for squeezing, indicated by the green line. The inset shows the short time simulation of the variance of R_2, represented by red points.

Figure 4.10: Variance of all normal mode coordinates (a) and variance of R_2 below the threshold for squeezing together with an inset of the short time simulation (b). Parameters used in this simulation: $m = 1.0$, $K = 1.25$, $T_1 = T_2 = 1.0$, $\omega_0 = 2.50$, $\omega_d = 0.45$, $T_b = 1.0$ and $\xi = 0.007$.
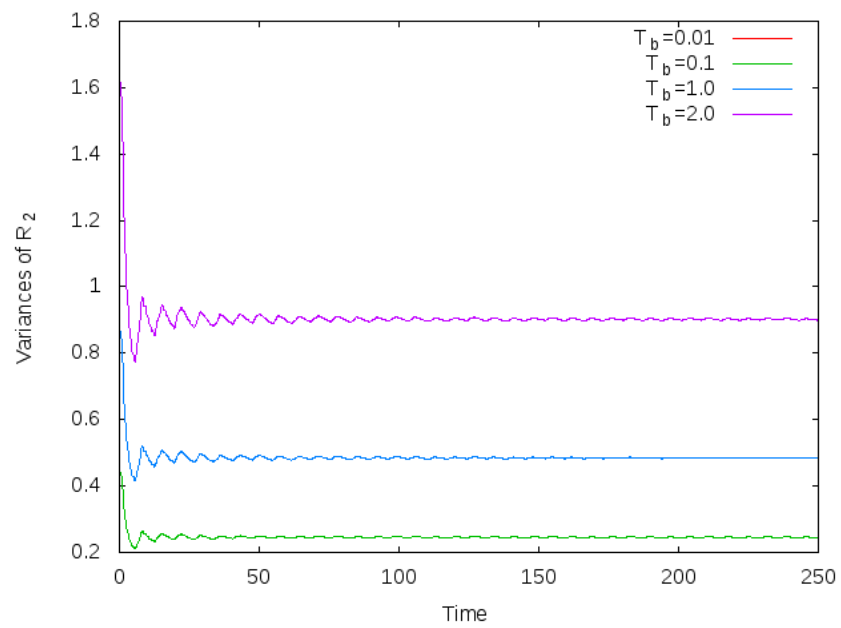
Figure 4.11: Variance of normal mode coordinate R_2, with four different temperatures of the bath. The red, green, blue and purple lines are for temperatures of the bath 0.01, 0.1, 1.0 and 2.0 respectively. Parameters used in this simulation: $m = 1.0$, $K = 1.25$, and $\xi = 0.007$.

Chapter 5

Conclusions and perspectives

This chapter contains a summary of the work presented in this dissertation. The formalism used to perform the calculations and main results of this study are highlighted. Next, concluding remarks and perspectives are elucidated. Finally, future studies extending from this work are discussed.

Recently, there have been many papers designated to understanding a variety of time-dependent processes in quantum systems. Such processes include charge transfer, transfer of energy in light harvesting complexes, transport in quantum systems, protein reactions and driven systems [6, 7, 8, 9, 10, 11, 12]. The importance of time-dependent processes in systems which are in a condensed phase was highlighted in Chapter 1. If a process is time-dependent, then the system of interest is in a non-equilibrium state. Non-equilibrium quantum dynamics are much more interesting to study compared to equilibrium dynamics, since it is possible to have many processes in a non-equilibrium system.

A subset of these time-dependent processes, which we were interested in studying, is the generation of squeezed states. Since systems which are in a condensed phase are of interest to us, we wanted to investigate the influence of temperature on the process. In particular, we wanted to understand what effect temperature has on the amount of squeezing which can be generated. To understand the usefulness of squeezing in condensed matter systems, we considered a speculative model of the motion of a proton as it passes an ion channel. It was shown that if the proton's position was squeezed in space, then it would increase the probability of the proton passing through the channel. The squeezing of the proton's position occurs at the expense of increasing the proton's momentum. However, we were not interested in the speed at which the proton moved through the channel. It may be possible that increasing the proton's speed aids in allowing it to pass through the channel. A possible source of generating a state in which the proton's position is squeezed, is the time-dependent interaction between the proton and the channel. Squeezed states were also shown to have applications in the control of quantum fluctuations, as well as in experiments which

are sensitive to quantum noise.

Having in mind that we were interested in studying temperature dependence in the generation of a squeezed state, we chose to study a model comprising two quantum harmonic oscillators with a time-dependent, non-linear coupling between them. The influence of the thermal bath on the non-equilibrium dynamics of the model was represented in terms of non-Hamiltonian thermostats and a collection of independent harmonic oscillators with Ohmic spectral density. Initially, the oscillators are decoupled and are in a thermal state. The coupling is switched on after time $t = 0$, at which point the oscillators are driven out of equilibrium as a result of the interaction. By introducing normal mode coordinates, it was shown that there is no simple analytical solution to the equations of motion of the system. Our model differs from those recently studied in [1] and [2], where analytical solutions have been found. The difference occurs in the form of the coupling used between the oscillators. The coupling we used is both non-linear and time-dependent.

The quantum equations of motion were studied in the Wigner representation, and integrated numerically by means of computer simulation. The Wigner representation proved to be advantageous in numerically solving our system since it allowed us to avoid complex matrix calculations, and use techniques and algorithms from molecular dynamics simulations. To calculate the quantum dynamics of the system, we used the Heisenberg equation of motion. Using normal mode coordinates, we were able to represent the Hamiltonian of our system as a sum of individual modes. The Wigner representation of the Heisenberg equation of motion then allowed us to reduce the quantum dynamics our system to classical evolution, since the Hamiltonian contained only quadratic terms in position and and momentum. This implied that all quantum effects were in the initial conditions. We were able to derive the analytical form of the Wigner function in the initial thermal state, which allowed us to sample the quantum initial conditions of each normal mode. In the limit of high temperature, the Wigner function was shown to reduce to the classical canonical distribution function. This distribution function was used to sample the classical initial conditions, and allowed us to make comparisons between the initial classical and quantum thermal state.

To reduce the computational effort required in simulating an environment, we used the partial Wigner transform over the bath degrees of freedom. This allowed us to give the bath a classical treatment while the system of driven oscillators were still given a full quantum treatment. Since the quantum dynamics of harmonic oscillators looks classical, we were able to perform a full quantum simulation using the partial Wigner transform, on the collection of independent harmonic oscillators. However, this method of representing an environment required the simulation of many degrees of freedom. To improve the efficiency of the computer simulation of the environment, we introduced a thermostat scheme called the Nosé-Hoover Chain thermostat. In this scheme, the

environment was simulated by forming an extended system, comprising few degrees of freedom, which follows non-Hamiltonian theory. The extended system comprised of a single harmonic oscillator and chain of two thermostats which control the temperature of the bath.

To simulate the dynamics of the Wigner function, we mapped the Wigner function as a cloud of points and used Monte-Carlo sampling of the initial conditions. We then propagated these points as classical trajectories and calculated the average of any desired observable over the time evolved Wigner function. Averages of the normal mode coordinates were then calculated and compared to the threshold condition for squeezing, to verify if a squeezed state had been generated. To visualize the squeezing effect in our system, we constructed histograms of the marginal distribution functions of each normal mode.

In investigating the differences between the initial classical and quantum state, we found the classical coordinates to be localised at the origin while the quantum initial values were more spread out, see figs. 4.1a and 4.1b. This is to be expected, as the quantum initial conditions are subject to the Heisenberg uncertainty relation. They have probabilities associated with their values, and as a results will be defined over a larger range. However, the classical initial conditions are known with unlimited accuracy. Therefore, they are expected to be well defined within a small region.

Using the symmetric Trotter factorization of the Liouville operator, we derived time reversible algorithms for each model to numerically integrate the equations of motion. To check that the algorithms are stable, we plotted the total normalized Hamiltonian for the closed system and with the two different types of environments, when there is no driving between the oscillators. In the absence of driving, the Hamiltonian is a conserved quantity. This was shown, in figs. 4.2a, 4.6 and 4.9. In each system, the Hamiltonian was conserved up to the sixth decimal place. The driving was then switched on between the oscillators. We found that the amplitude of the frequency and driving frequency were proportional to the size of the fluctuations and period of oscillations, respectively. See fig. 4.2b.

Having verified that the numerical algorithm was stable, we proceeded to check if generating a squeezed state was possible. This was done by plotting the variance of each normal mode coordinate, and comparing them to the threshold for squeezing. See figs. 4.3a, 4.7a and 4.10a. It was found that, as a result of the time-dependent interaction between the oscillators, the position of normal mode 2 was squeezed. The squeezing of the position occurred at the expense of an increase in the fluctuations of the momentum of normal mode 2. Normal mode 1 did not experience fluctuations in its coordinates because the time dependence only appears in the frequency of normal mode 2. The frequency of normal mode 1 is a constant value. In figs. 4.3b, 4.7b and 4.10b the short

time simulation of the dynamics is shown. These plots illustrate that the process of generating a squeezed state is a fast one, however not an instantaneous one, since there are initially points above the threshold for squeezing after the time dependent interaction is switched on. Also, we notice that the speed at which the system is driven into a squeezed state does not change when the system is in contact with a thermal bath.

To obtain a better visualization of squeezing with our system, and thus gain an intuitive understanding, the marginal distributions of each normal mode are shown in figs. 4.4a, 4.4b, 4.5a and 4.5b. A comparison for each normal mode is made, from the initial time when the oscillators are decoupled, to a later time after the interaction has been switched on. The marginal distribution is constructed via the formation of histograms. Initially, both normal mode 1 and 2 are in a thermal state and their distributions are circular. However, at a later time, the distribution of normal mode 1 remains the same while for normal mode 2 it becomes elliptical. This indicates that the position of normal mode 2 has been squeezed and consequently, its momentum is elongated. This behaviour was consistent with results obtained by comparing the variances of the normal modes to the threshold for squeezing. The marginal distributions were only shown for the closed system. However, when the system was in contact with the bath, the same results were obtained.

Having verified that the time-dependent interaction does generate a squeezed state, we investigated the influence of the temperature of the environment on the amount of squeezing which can be generated. Using different temperatures, we plotted the variance of the position of normal mode 2 in figs. 4.8 and 4.11. It was found that as the temperature decreased, we obtained stronger squeezing. However, we reached a point where the amount of squeezing would not change regardless of whether the temperature was decreased. This indicated that there is a limit to which we can squeeze the position of normal mode 2. As we increased the temperature of the bath, we found that the strength of squeezing decreased. It eventually resulted in removing all squeezing effects from the system. Thus, the level of squeezing can be controlled by changing the temperature of the bath, but there is a lower limit to which we can squeeze the system.

In future work I will continue my study of the generation of squeezed states, and investigate the limits of quantum to classical transitions. Additionally, I plan on quantifying entanglement in our system.

Appendix A

Derivation of the Wigner function in the initial thermal state for an ensemble of N independent harmonic oscillators

This appendix contains the derivations of the Wigner function in the initial thermal state for N independent harmonic oscillators in the canonical ensemble.

In order to calculate the quantum initial conditions of our system in the canonical ensemble, we require a distribution function which describes our system in its initial thermal state. This function is given by the analytical form of the Wigner function for an ensemble of N independent harmonic oscillators at temperature T. This distribution function is derived in [51], however I performed the derivation to further my understanding of the theory.

Let $\hat{\rho}$ denote the normalized density matrix, $\hat{\Omega}$ the un-normalized density matrix and the temperature parameter $\beta = 1/k_B T$. In the canonical ensemble, we can write $\hat{\rho}$ as

$$\hat{\rho} \quad = \quad \frac{1}{Z(\beta)}\hat{\Omega} \qquad\qquad (A.1)$$

$$= \quad \frac{1}{Z(\beta)}e^{-\beta\hat{H}} \qquad\qquad (A.2)$$

where $\hat{H}$ is the Hamiltonian operator of the system and $Z(\beta)$ is the canonical partition function,

$$Z(\beta) \quad = \quad Tr(e^{-\beta\hat{H}}). \tag{A.3}$$

The un-normalized density matrix $\hat{\Omega}$ then satisfies the Bloch Equation,

$$\frac{\partial\hat{\Omega}}{\partial\beta} = -\hat{H}\hat{\Omega} = -\hat{\Omega}\hat{H} , \tag{A.4}$$

provided it satisfies the initial condition $\hat{\Omega}(\beta = 0) = \hat{I}$, where $\hat{I}$ is the identity operator.

We introduce the notation of a symplectic matrix, $\mathcal{B}$, which in its canonical form reduces $\overleftarrow{\partial_a}\mathcal{B}_{ab}\overrightarrow{\partial_b}$ to the Poisson bracket [31]. The arrows above the derivatives indicate the direction in which the derivative operates, and we have used Einstein's notation of summation over repeated indices. Now, using the identity for the Wigner function of two operators, defined in eqn. (2.17), the Wigner transform of the Bloch equation is then

$$\frac{\partial\Omega_W(R_k, P_k)}{\partial\beta} \quad = \quad -H_W(R_k, P_k)e^{\frac{i\hbar}{2}\overleftarrow{\partial_a}\mathcal{B}_{ab}\overrightarrow{\partial_b}}\Omega_W(R_k, P_k) \tag{A.5}$$

$$= \quad -\Omega_W(R_k, P_k)e^{\frac{i\hbar}{2}\overleftarrow{\partial_a}\mathcal{B}_{ab}\overrightarrow{\partial_b}}H_W(R_k, P_k) . \tag{A.6}$$

Applying the identity defined in eqn. (2.17) to eqn. (A.6), we find

$$\frac{\partial\Omega_W(R_k, P_k)}{\partial\beta} \quad = \quad -H_W(R_k, P_k)e^{-\frac{i\hbar}{2}\overleftarrow{\partial_a}\mathcal{B}_{ab}\overrightarrow{\partial_b}}\Omega_W(R_k, P_k) . \tag{A.7}$$

However, this is possible if only even powers of the expansion of $e^{\frac{-i\hbar}{2}\overleftarrow{\partial_a}\mathcal{B}_{ab}\overrightarrow{\partial_b}}$ are taken into account. Therefore, the Wigner transform of the Bloch equation can be written as

$$\frac{\partial\Omega_W(R_k, P_k)}{\partial\beta} = -H_W(R_k, P_k)\cos\left(\frac{\hbar}{2}\overleftarrow{\partial_a}\mathcal{B}_{ab}\overrightarrow{\partial_b}\right)\Omega_W(R_k, P_k). \tag{A.8}$$

The Hamiltonian of our system consists of 2 independent harmonic oscillators, however we derive the Wigner transform of the density matrix for the general case of N independent harmonic oscillators. Consider the Hamiltonian of a system of N independent harmonic oscillators, in the Wigner representation,

$$H_W = \sum_{n=1}^{N} \left(\frac{1}{2m_n}P_n^2 + \frac{1}{2}m_n\omega_n^2 R_n^2\right). \tag{A.9}$$

The Wigner-Bloch equation is then

$$\frac{\partial\Omega_W}{\partial\beta} = \left[\left(\frac{1}{2m_n}P_n^2 + \frac{1}{2}m_n\omega_n^2 R_n^2\right)\cos\left(\frac{\hbar}{2}\left[\frac{\overleftarrow{\partial}}{\partial R_k}\frac{\overrightarrow{\partial}}{\partial P_k} - \frac{\overleftarrow{\partial}}{\partial P_k}\frac{\overrightarrow{\partial}}{\partial R_k}\right]\right)\right]\Omega_W . \tag{A.10}$$

We now perform a Taylor series expansion of $\cos(x)$ up to second order, since higher order terms

will yield zero when acting on the Hamiltonian,

$$\cos\left(\frac{\hbar}{2}\left[\frac{\overleftarrow{\partial}}{\partial R_k}\frac{\overrightarrow{\partial}}{\partial P_k} - \frac{\overleftarrow{\partial}}{\partial P_k}\frac{\overrightarrow{\partial}}{\partial R_k}\right]\right) = 1 - \frac{1}{2}\left(\frac{\hbar}{2}\right)^2\left[\frac{\overleftarrow{\partial}}{\partial R_k}\frac{\overrightarrow{\partial}}{\partial P_k} - \frac{\overleftarrow{\partial}}{\partial P_k}\frac{\overrightarrow{\partial}}{\partial R_k}\right]^2 . \quad (A.11)$$

We now write the explicit form of the square of the derivatives appearing in the equation above

$$\left(\frac{\overleftarrow{\partial}}{\partial R_k}\frac{\overrightarrow{\partial}}{\partial P_k} - \frac{\overleftarrow{\partial}}{\partial P_k}\frac{\overrightarrow{\partial}}{\partial R_k}\right)^2 = \left(\frac{\overleftarrow{\partial}}{\partial R_k}\frac{\overrightarrow{\partial}}{\partial P_k} - \frac{\overleftarrow{\partial}}{\partial P_k}\frac{\overrightarrow{\partial}}{\partial R_k}\right) \times \left(\frac{\overleftarrow{\partial}}{\partial R_l}\frac{\overrightarrow{\partial}}{\partial P_l} - \frac{\overleftarrow{\partial}}{\partial P_l}\frac{\overrightarrow{\partial}}{\partial R_l}\right)$$

$$= \frac{\overleftarrow{\partial}}{\partial R_k}\frac{\overrightarrow{\partial}}{\partial P_k}\frac{\overleftarrow{\partial}}{\partial R_l}\frac{\overrightarrow{\partial}}{\partial P_l} - \frac{\overleftarrow{\partial}}{\partial R_k}\frac{\overrightarrow{\partial}}{\partial P_k}\frac{\overleftarrow{\partial}}{\partial P_l}\frac{\overrightarrow{\partial}}{\partial R_l}$$

$$- \frac{\overleftarrow{\partial}}{\partial P_k}\frac{\overrightarrow{\partial}}{\partial R_k}\frac{\overleftarrow{\partial}}{\partial R_l}\frac{\overrightarrow{\partial}}{\partial P_l} + \frac{\overleftarrow{\partial}}{\partial P_k}\frac{\overrightarrow{\partial}}{\partial R_k}\frac{\overleftarrow{\partial}}{\partial P_l}\frac{\overrightarrow{\partial}}{\partial R_l}$$

$$= \frac{\overleftarrow{\partial^2}}{\partial R_k\partial R_l}\frac{\overrightarrow{\partial^2}}{\partial P_k\partial P_l} - \frac{\overleftarrow{\partial^2}}{\partial R_k\partial P_l}\frac{\overrightarrow{\partial^2}}{\partial P_k\partial R_l}$$

$$- \frac{\overleftarrow{\partial^2}}{\partial P_k\partial R_l}\frac{\overrightarrow{\partial^2}}{\partial R_k\partial P_l}\frac{\overleftarrow{\partial^2}}{\partial P_k\partial P_l}\frac{\overrightarrow{\partial^2}}{\partial R_k\partial R_l} . \quad (A.12)$$

Substituting eqn. (A.12) into eqn. (A.10), the Wigner-Bloch equation becomes

$$\frac{\partial\Omega_W}{\partial\beta} = -\left(\frac{P_n^2}{2m_n} + \frac{1}{2}m_n\omega_n^2 R_n^2\right)\Omega_W + \frac{\hbar^2}{8}\left(\frac{P_n^2}{2m_n} + \frac{1}{2}m_n\omega_n^2 R_n^2\right)$$

$$\times\left(\frac{\overleftarrow{\partial^2}}{\partial R_k\partial R_l}\frac{\overrightarrow{\partial^2}}{\partial P_k\partial P_l} - \frac{\overleftarrow{\partial^2}}{\partial R_k\partial P_l}\frac{\overrightarrow{\partial^2}}{\partial P_k\partial R_l} - \frac{\overleftarrow{\partial^2}}{\partial P_k\partial R_l}\frac{\overrightarrow{\partial^2}}{\partial R_k\partial P_l} + \frac{\overleftarrow{\partial^2}}{\partial P_k\partial P_l}\frac{\overrightarrow{\partial^2}}{\partial R_k\partial R_l}\right)\Omega_W$$

$$= -\left(\frac{P_n^2}{2m_n} + \frac{1}{2}m_n\omega_n^2 R_n^2\right)\Omega_W + \left(\frac{P_n^2}{2m_n}\frac{\overleftarrow{\partial^2}}{\partial P_k\partial P_l}\frac{\overrightarrow{\partial^2}}{\partial R_k\partial R_l} + \frac{1}{2}m_n\omega_n^2 R_n^2\frac{\overleftarrow{\partial^2}}{\partial R_k\partial R_l}\frac{\overrightarrow{\partial^2}}{\partial P_k\partial P_l}\right)\Omega_W .$$

The Wigner transformed Bloch equation for N independent harmonic oscillators becomes

$$\frac{\partial\Omega_W}{\partial\beta} = -\left(\frac{P_n^2}{2m_n} + \frac{1}{2}m_n\omega_n^2 R_n^2\right)\Omega_W + \frac{\hbar^2}{8}\left(\frac{1}{m_k}\frac{\overrightarrow{\partial^2}}{\partial R_k\partial R_l} + m_k\omega_k^2\frac{\overrightarrow{\partial^2}}{\partial P_k\partial P_l}\right)\Omega_W$$

$$= -\left(\frac{P_n^2}{2m_n} + \frac{1}{2}m_n\omega_n^2 R_n^2\right)\Omega_W + \frac{\hbar^2}{8}\left(\frac{1}{m_k}\frac{\partial^2\Omega_W}{\partial R_k\partial R_l} + m_k\omega_k^2\frac{\partial^2\Omega_W}{\partial P_k\partial P_l}\right) . \quad (A.13)$$

To solve this equation, we make the ansatz

$$\Omega_W(R_k, P_k) = e^{-A(\beta)H_W + B(\beta)} \quad (A.14)$$

where A and B are subject to the initial conditions, $A(0) = B(0) = 0$.

We now find the second order spatial derivatives with respect to Ω_W and substitute them into eqn.

(A.13)

$$\frac{\partial \Omega_W}{\partial R_k} = \Omega_W \left(-A\frac{\partial H}{\partial R_k}\right)$$

$$= \Omega_W \left(-Am_k\omega_k^2 R_k\right)$$

$$\frac{\partial^2 \Omega_W}{\partial R_k \partial R_l} = \frac{\partial \Omega_W}{\partial R_l} \left[-Am_k\omega_k^2 R_k\right] - A\Omega_W m_l\omega_l^2$$

$$= \left(-Am_k\omega_k^2 R_k\right)^2 \Omega_W - A\Omega_W m_k\omega_k^2$$

$$= \left[A^2 \left(m_k\omega_k^2 R_k\right)^2 - Am_k\omega_k^2\right]\Omega_W \qquad (A.15)$$

$$\frac{\partial \Omega_W}{\partial P_k} = \Omega_W \left(-A\frac{\partial H}{\partial P_k}\right)$$

$$= -\Omega_W A \left(\frac{P_k}{m_k}\right)$$

$$\frac{\partial^2 \Omega_W}{\partial P_k \partial P_l} = -A\frac{\partial^2 H}{\partial P_k \partial P_l}\Omega_W - A\frac{\partial H}{\partial P_k}\frac{\partial \Omega_W}{\partial P_l}$$

$$= -A\left(\frac{1}{m_k}\right)\Omega_W + A^2\left(\frac{P_k}{m_k}\right)\left(\frac{P_l}{m_l}\right)\Omega_W$$

$$= -A\left(\frac{1}{m_k}\right)\Omega_W + A^2\left(\frac{P_k}{m_k}\right)^2\Omega_W . \qquad (A.16)$$

Upon substituting the calculated derivatives, eqns. (A.15) and (A.16), into eqn. (A.13), the Wigner transformed Bloch equation becomes

$$\frac{\partial \Omega_W}{\partial \beta} = -H\Omega_W(P_k, R_k) + \frac{\hbar^2}{8}\left(\frac{1}{m_k}\frac{\partial^2 \Omega_W}{\partial R_k \partial R_l} + m_k\omega_k^2\frac{\partial^2 \Omega_W}{\partial P_k \partial P_l}\right)$$

$$\Omega_W\left[-\frac{\partial A}{\partial \beta}H + \frac{\partial B}{\partial \beta}\right] = -H\Omega_W(P_k, R_k) + \frac{\hbar^2}{8}\left(\frac{1}{m_k}\frac{\partial^2 \Omega_W}{\partial R_k \partial R_l} + m_k\omega_k^2\frac{\partial^2 \Omega_W}{\partial P_k \partial P_l}\right) . \quad (A.17)$$

Consider the second term on the right hand side of eqn. (A.17)

$$\frac{\hbar^2}{8}\left(\frac{1}{m_k}\frac{\partial^2 \Omega_W}{\partial R_k \partial R_l}\right) = \frac{\hbar^2}{8}\left\{\frac{1}{m_k}\left[A^2\left(m_k\omega_k^2 R_k\right)^2 - Am_k\omega_k^2\right]\right\}\Omega_W$$

$$= \frac{\hbar^2}{8}\left[A^2 m_k\left(\omega_k^2 R_k\right)^2 - A\omega_k^2\right]\Omega_W . \qquad (A.18)$$

Now consider the third term on the right hand side of eqn. (A.17)

$$\frac{\hbar^2}{8}m_k\omega_k^2\left(\frac{\partial^2 \Omega_W}{\partial P_k \partial P_l}\right) = \frac{\hbar^2}{8}m_k\omega_k^2\left[-A\frac{1}{m_k}\Omega_W + A^2\left(\frac{P_k}{m_k}\right)^2\right]\Omega_W$$

$$= \frac{\hbar^2}{8}\left[-A\omega_k^2 + A^2\frac{1}{m_k}\left(P_k\omega_k\right)^2\right]\Omega_W . \qquad (A.19)$$

We now simplify eqn. (A.17)

$$-\frac{\partial A}{\partial \beta} H_W + \frac{\partial B}{\partial \beta} = -H_W + \frac{\hbar^2}{8} \left[A^2 m_k \left(\omega_k^2 R_k \right)^2 - A\omega_k^2 - A\omega_k^2 + A^2 \frac{1}{m_k} \left(P_k \omega_k \right)^2 \right]$$

$$-\frac{\partial A}{\partial \beta} H_W + \frac{\partial B}{\partial \beta} = -H_W + \frac{\hbar^2}{4} \left[-\omega_k^2 A + A^2 \omega_k^2 H_W \right]$$

$$-\frac{\partial A}{\partial \beta} H_W + H_W = -\frac{\partial B}{\partial \beta} + \frac{\hbar^2}{4} \left[-\omega_k^2 A + A^2 \omega_k^2 H_W \right]$$

$$\left[-\frac{\partial A}{\partial \beta} + 1 - \left(\frac{\hbar \omega_k A}{2} \right)^2 \right] H_W = -\frac{\partial B}{\partial \beta} - \left[\left(\frac{\hbar \omega_k}{2} \right)^2 A \right] .$$

This equation must hold for every value of R_k and P_k. Since all terms in the square bracket are independent of R_k and P_k, each bracket must equal 0 independent of each other

$$\frac{dA}{d\beta} - 1 + \frac{(\hbar \omega_k)^2}{4} A^2 = 0 \tag{A.20}$$

$$\frac{\partial B}{\partial \beta} + \left(\frac{\hbar \omega_k}{2} \right)^2 A = 0 \tag{A.21}$$

$$\frac{dA}{d\beta} = 1 - \left(\frac{\hbar \omega_k}{2} \right)^2 A^2 \tag{A.22}$$

$$\frac{dA}{1 - \left(\frac{\hbar \omega_k}{2} \right)^2 A^2} = d\beta \tag{A.23}$$

Consider the derivative of $\ln\left(\frac{1+x}{1-x} \right)$

$$\frac{d}{dx} \ln \left(\frac{1+x}{1-x} \right) = \frac{1-x}{1+x} \frac{d}{dx} \left(\frac{1+x}{1-x} \right) \tag{A.24}$$

$$= \frac{1}{1+x} + \frac{1}{1-x} \tag{A.25}$$

$$= \frac{1-x+1+x}{1-x^2} \tag{A.26}$$

$$= \frac{2}{1-x^2} . \tag{A.27}$$

Therefore, we have the identity

$$\frac{1}{2} \frac{d}{dx} \ln \left(\frac{1+x}{1-x} \right) = \frac{1}{1-x^2} . \tag{A.28}$$

Now, identifying

$$x = \frac{\hbar \omega_k}{2} A \tag{A.29}$$

$$dA = \frac{2}{\hbar \omega_k} dx , \tag{A.30}$$

we can integrate equation (A.23)

$$\int \frac{dA}{1 - \left(\frac{\hbar\omega_k}{2}\right)^2 A^2} = \int d\beta \tag{A.31}$$

$$\frac{2}{\hbar\omega_k} \int \frac{1}{1 - x^2} = \beta + C \tag{A.32}$$

$$\frac{2}{2\hbar\omega_k} \int dx \frac{d}{dx} \ln\left(\frac{1+x}{1-x}\right) = \beta + C \tag{A.33}$$

$$\frac{1}{\hbar\omega_k} \ln\left(\frac{1+x}{1-x}\right) = \beta \tag{A.34}$$

$$\beta = \frac{1}{\hbar\omega_k} \ln\left[\frac{1 + \frac{\hbar\omega_k}{2} A}{1 - \frac{\hbar\omega_k}{2} A}\right] . \tag{A.35}$$

Inverting this equation gives

$$\hbar\omega_k\beta = \ln\left[\frac{1 + \frac{\hbar\omega_k}{2} A}{1 - \frac{\hbar\omega_k}{2} A}\right] \tag{A.36}$$

$$e^{\hbar\omega_k\beta} = \frac{1 + \frac{\hbar\omega_k}{2} A}{1 - \frac{\hbar\omega_k}{2} A} \tag{A.37}$$

$$e^{\hbar\omega_k\beta}\left(1 - \frac{\hbar\omega_k}{2} A\right) = 1 + \frac{\hbar\omega_k}{2} A \tag{A.38}$$

$$e^{\hbar\omega_k\beta} - e^{\hbar\omega_k\beta}\frac{\hbar\omega_k}{2} A - 1 = \frac{\hbar\omega_k}{2} A \tag{A.39}$$

$$e^{\hbar\omega_k\beta} - 1 = \frac{\hbar\omega_k}{2}\left(e^{\hbar\omega_k\beta} A + A\right) \tag{A.40}$$

$$= \frac{\hbar\omega_k}{2}\left(e^{\hbar\omega_k\beta} + 1\right) A . \tag{A.41}$$

We can now write A as

$$A = \frac{2}{\hbar\omega_k}\left(\frac{e^{\hbar\omega_k\beta} - 1}{e^{\hbar\omega_k\beta} + 1}\right) \tag{A.42}$$

$$= \frac{2}{\hbar\omega_k}\left(\frac{e^{\frac{\hbar}{2}\omega_k\beta} - e^{\frac{\hbar}{2}\omega_k\beta}}{e^{\frac{\hbar}{2}\omega_k\beta} + e^{\frac{\hbar}{2}\omega_k\beta}}\right) \tag{A.43}$$

$$A = \frac{2}{\hbar\omega_k}\left(\frac{e^{\frac{\hbar}{2}\omega_k\beta} - e^{\frac{\hbar}{2}\omega_k\beta}}{e^{\frac{\hbar}{2}\omega_k\beta} + e^{\frac{\hbar}{2}\omega_k\beta}}\right) \tag{A.44}$$

$$= \frac{2}{\hbar\omega_k}\tanh\left(\frac{\hbar\omega_k}{2}\beta\right) . \tag{A.45}$$

We now use equation (A.21) to find B

$$0 = \frac{\partial B}{\partial \beta} + \left(\frac{\hbar\omega_k}{2}\right)^2 A \tag{A.46}$$

$$0 = \frac{\partial B}{\partial \beta} + \left(\frac{\hbar\omega_k}{2}\right)^2 \frac{2}{\hbar\omega_k}\tanh\left(\frac{\hbar\omega_k}{2}\beta\right) \tag{A.47}$$

$$B = -\frac{\hbar\omega_k}{2} \int d\beta \tanh\left(\frac{\hbar\omega_k}{2}\beta\right) \tag{A.48}$$

Using $\tanh x = \sinh x / \cosh x$, we can construct the identity

$$\tanh x \quad = \quad \frac{d}{dx} \ln\left(\cosh x\right) \ . \tag{A.49}$$

Identifying

$$x \quad = \quad \frac{\hbar\omega_k}{2}\beta \tag{A.50}$$

$$dx \quad = \quad \frac{\hbar\omega_k}{2}d\beta \tag{A.51}$$

allows us to solve for B

$$B \quad = \quad -\frac{\hbar\omega_k}{2}\frac{2}{\hbar\omega_k}\int dx \tanh x \tag{A.52}$$

$$= \quad -\int dx \frac{d}{dx}\ln(\cosh x) \tag{A.53}$$

$$= \quad -\ln(\cosh x) \tag{A.54}$$

$$B \quad = \quad -\ln\left[\cosh\left(\frac{\hbar\omega_k}{2}\beta\right)\right] \ . \tag{A.55}$$

From

$$\Omega_W = e^{-AH_W + B} = e^{-AH_W}e^{B} \ , \tag{A.56}$$

the un-normalized density matrix is

$$\Omega_W \quad = \quad \exp\left[-\ln\left[\cosh\left(\frac{\hbar\omega_k}{2}\beta\right)\right]\right]\exp\left[-\frac{2}{\hbar\omega_k}\tanh\left(\frac{\hbar\omega_k}{2}\beta\right)H_W\right] \tag{A.57}$$

$$= \quad \exp\left[\ln\left[\cosh\left(\frac{\hbar\omega_k}{2}\beta\right)\right]^{-1}\right]\exp\left[-\frac{2}{\hbar\omega_k}\tanh\left(\frac{\hbar\omega_k}{2}\beta\right)H_W\right] \tag{A.58}$$

$$= \quad \frac{1}{\cosh\left(\frac{\hbar\omega_k}{2}\beta\right)}\exp\left[-\frac{2}{\hbar\omega_k}\tanh\left(\frac{\hbar\omega_k}{2}\beta\right)H_W\right] \ . \tag{A.59}$$

To complete the derivation, we need to normalize Ω_W

$$Z(\beta) \quad = \quad \int dR_k dP_k \Omega \tag{A.60}$$

$$\hat{\rho} \quad = \quad \frac{\hat{\Omega}}{Z(\beta)} \tag{A.61}$$

Substituting the un-normalized density matrix into the form of the partition function, we get

$$Z(\beta) \quad = \quad \frac{1}{\cosh\left(\frac{\hbar\omega_k}{2}\beta\right)}\int dR_k dP_k \exp\left[-\frac{2}{\hbar\omega_k}\tanh\left(\frac{\hbar\omega_k}{2}\beta\right)\left(\frac{P_k^2}{2m_k} + \frac{1}{2}m_k\omega_k^2 R_k^2\right)\right]$$

$$= \quad \frac{1}{\cosh\left(\frac{\hbar\omega_k}{2}\beta\right)}\int dP_k \exp\left[-\frac{2}{\hbar\omega_k}\tanh\left(\frac{\hbar\omega_k}{2}\beta\right)\frac{P_k^2}{2m_k}\right]$$

$$* \int dR_k \exp\left[-\frac{2}{\hbar\omega_k}\tanh\left(\frac{\hbar\omega_k}{2}\beta\right)\frac{m_k\omega_k^2 R_k^2}{2}\right] \tag{A.62}$$

where we have split the integral over the positions and momenta. Now, using the Gaussian integral

$$\int e^{-ax^2} = \sqrt{\frac{\pi}{a}} \, , \tag{A.63}$$

we can solve for each integral

$$\int \mathrm{dp}_k \exp\left[-\frac{2}{\hbar\omega_k}\tanh\left(\frac{\hbar\omega_k}{2}\beta\right)\frac{p_k^2}{2m_k}\right] = \sqrt{\frac{\pi}{\frac{1}{\hbar\omega_k m_k}\tanh\left(\frac{\hbar\omega_k}{2}\beta\right)}} \tag{A.64}$$

$$\int \mathrm{dq}_k \exp\left[-\frac{m_k\omega_k}{\hbar}\tanh\left(\frac{\hbar\omega_k}{2}\beta\right)q_k^2\right] = \sqrt{\frac{\pi}{\frac{m_k\omega_k}{\hbar}\tanh\left(\frac{\hbar\omega_k}{2}\beta\right)}} \, . \tag{A.65}$$

Thus, the partition function is

$$Z(\beta) = \frac{1}{\cosh\left(\frac{\hbar\omega_k}{2}\beta\right)}\frac{\pi}{\tanh\left(\frac{\hbar\omega_k}{2}\beta\right)}\frac{1}{\sqrt{\frac{1}{\hbar\omega_k m_k}\frac{m_k\omega_k}{\hbar}}} \tag{A.66}$$

$$= \frac{\pi\hbar}{\cosh\left(\frac{\hbar\omega_k}{2}\beta\right)\frac{\sinh\left(\frac{\hbar\omega_k}{2}\beta\right)}{\cosh\left(\frac{\hbar\omega_k}{2}\beta\right)}} \tag{A.67}$$

$$= \frac{\pi\hbar}{\sinh\left(\frac{\hbar\omega_k}{2}\beta\right)} \tag{A.68}$$

$$Z(\beta) = \frac{\pi\hbar}{\sinh\left(\frac{\hbar\omega_k}{2}\beta\right)} \, . \tag{A.69}$$

Finally, we divide Ω_W by $Z(\beta)$, to find the Wigner function in the initial thermal state

$$\rho_W = \frac{\sinh\left(\frac{\hbar\omega_k}{2}\beta\right)}{\pi\hbar}\frac{\exp\left[-\frac{2}{\hbar\omega_k}\tanh\left(\frac{\hbar\omega_k}{2}\beta\right)H\right]}{\cosh\left(\frac{\hbar\omega_k}{2}\beta\right)}$$

$$= \frac{1}{\pi\hbar}\tanh\left(\frac{\hbar\omega_k}{2}\beta\right)\exp\left[-\frac{2}{\hbar\omega_k}\tanh\left(\frac{\hbar\omega_k}{2}\beta\right)H\right]$$

$$= \frac{1}{\pi\hbar}\tanh\left(\frac{\hbar\omega_k}{2}\beta\right)\exp\left[-\frac{2}{\hbar\omega_k}\tanh\left(\frac{\hbar\omega_k}{2}\beta\right)\sum_{k=1}^{N}\left(\frac{1}{2m_k}P_k^2 + \frac{1}{2}m_k\omega_k^2 R_k^2\right)\right]$$

$$\rho_W(R_k, P_k, \beta) = \prod_{k=1}^{N}\left\{\frac{1}{\pi\hbar}\tanh\left(\frac{\hbar\omega_k}{2}\beta\right)\exp\left[-\frac{2}{\hbar\omega_k}\tanh\left(\frac{\hbar\omega_k}{2}\beta\right)\left(\frac{1}{2m_k}P_k^2 + \frac{1}{2}m_k\omega_k^2 R_k^2\right)\right]\right\}$$

$$= \prod_{k=1}^{N}\left\{\frac{1}{\pi\hbar}\tanh\left(\frac{\hbar\omega_k}{2}\beta\right)\exp\left[-\frac{2}{\hbar\omega_k}\tanh\left(\frac{\hbar\omega_k}{2}\beta\right)H_W\right]\right\} \, .$$

Appendix B

Transformation to Normal Mode Coordinates

This appendix contains the derivation of equations used to transform the Hamiltonian of coupled oscillators to a sum of normal modes.

Consider a system of two, coupled, driven, harmonic oscillators with a time-dependent, non-linear interaction between them. The Hamiltonian of such a system is given by eqn. (3.19). In this form, the system is expressed in Cartesian coordinates. An alternative representation of the Hamiltonian can be formed which allows us to express the Hamiltonian as a sum of individual modes. This is done by introducing normal mode coordinates. We also require the Hamiltonian to have the form of decoupled modes, in order to sample the quantum initial conditions of the system from the Wigner function in the initial thermal state.

The equations used to transform between Cartesian and normal mode coordinates, can be found by solving the set of Euler-Lagrange equations [28]. To this end, we begin by writing down the Lagrangian of the system,

$$L \quad = \quad \frac{p_1^2}{2m} + \frac{p_2^2}{2m} - \frac{K}{2}q_1^2 - \frac{K}{2}q_2^2 - \frac{K(t)}{2}\left(q_2 - q_1\right)^2 \; . \tag{B.1}$$

The equations of motion are then given by

$$\frac{\partial L}{\partial q_1} - \frac{d}{dt}\frac{\partial L}{\partial \dot{q}_1} \quad = \quad -Kq_1 + K(t)(q_2 - q_1) - m\ddot{q}_1 = 0 \tag{B.2}$$

$$\frac{\partial L}{\partial q_2} - \frac{d}{dt}\frac{\partial L}{\partial \dot{q}_2} \quad = \quad -Kq_2 - K(t)(q_2 - q_1) - m\ddot{q}_2 = 0 \; . \tag{B.3}$$

These equations can be recast as a system of two coupled differential equations

$$m\ddot{q}_1 + (K + K(t))q_1 - K(t)q_2 = 0 \tag{B.4}$$

$$m\ddot{q}_2 + (K + K(t))q_2 - K(t)q_1 = 0. \tag{B.5}$$

To solve the above equations, we assume an oscillatory form of motion

$$q_1 = A_1 e^{i\omega t} \tag{B.6}$$

$$q_2 = A_2 e^{i\omega t}, \tag{B.7}$$

where ω is the frequency of oscillation, and A_1 and A_2 are the amplitudes of each coordinate. Substituting the trial solutions, eqns (B.6) and (B.7), into the set of differential equations, and dividing by $e^{i\omega t}$, we obtain

$$-mA_1\omega^2 + (K + K(t))A_1 - K(t)A_2 = 0 \tag{B.8}$$

$$-mA_2\omega^2 + (K + K(t))A_2 - K(t)A_1 = 0. \tag{B.9}$$

This set of equations can be recast in the form of matrices as

$$\begin{pmatrix} -m\omega^2 + (K + K(t)) & -K(t) \\ -K(t) & -m\omega^2 + (K + K(t)) \end{pmatrix} \cdot \begin{pmatrix} A_1 \\ A_2 \end{pmatrix} = \begin{pmatrix} 0 \\ 0 \end{pmatrix} \tag{B.10}$$

Here we notice that eqn. (B.10) has the form of an eigenvalue problem, where ω is the eigenvalue and the amplitudes form the eigenvector.

A non-trivial solution is obtained when the determinant of the matrix of co-coefficients is 0, i.e. when

$$\det \begin{vmatrix} -m\omega^2 + (K + K(t)) & -K(t) \\ -K(t) & -m\omega^2 + (K + K(t)) \end{vmatrix} = 0 \tag{B.11}$$

$$\left(-m\omega^2 + K + K(t)\right)\left(-m\omega^2 + K + K(t)\right) - K(t)^2 = 0 \tag{B.12}$$

$$\omega^4 m^2 - \omega^2 \left(2mK + 2mK(t)\right) + \left(K^2 + 2KK(t)\right) = 0. \tag{B.13}$$

The characteristic equation reduces to solving an algebraic equation of second degree for ω^2, with solution

$$\omega^2 = \frac{(K + K(t)) \pm \sqrt{K(t)^2}}{m}. \tag{B.14}$$

Thus, the frequencies of the normal modes are

$$\omega_1 = \sqrt{\frac{K}{m}} \tag{B.15}$$

$$\omega_2 = \sqrt{\frac{K + 2K(t)}{m}} \ . \tag{B.16}$$

In order to obtain the equations for the transformation from Cartesian to normal mode coordinates, we require a rotation matrix [28]. The columns of the rotation matrix consist of the eigenvectors, which in this case are the amplitudes A_1 and A_2. The eigenvectors can be found by substituting the normal mode frequencies, eqns. (B.15) and (B.16) into eqn. (B.8). For ω_1 we find $A_1 = A_2$, and for ω_2 we find $A_1 = -A_2$. To avoid arbitrary constants appearing, we subjecting the amplitudes to the normalization condition, $A_1^2 + A_2^2 = 1$. Thus, the eigenvectors are

$$(A_1, A_2) = \frac{1}{\sqrt{2}}(1, 1) \tag{B.17}$$

$$(A_1, A_2) = \frac{1}{\sqrt{2}}(1, -1) \ , \tag{B.18}$$

corresponding to ω_1 and ω_2 respectively.

Having obtained the eigenvectors, the rotation matrix is then given by

$$U = \frac{1}{\sqrt{2}} \begin{pmatrix} 1 & 1 \\ 1 & -1 \end{pmatrix} \tag{B.19}$$

The determinant of the rotation matrix is 1, and the inverse of the rotational matrix is equal to the transpose of the rotational matrix.

$$U^T = U^{-1}$$
$$= \frac{1}{\sqrt{2}} \begin{pmatrix} 1 & 1 \\ 1 & -1 \end{pmatrix} \tag{B.20}$$

To find the transformation from Cartesian to normal mode coordinates, we perform a similarity transformation. Given a matrix A in the Cartesian basis, its representation in the normal basis is A' given by

$$A' = U^T A U. \tag{B.21}$$

We then define matrix R, which is our representation of position in normal mode coordinates.

$$
\begin{aligned}
R &= U \cdot q \\
&= \frac{1}{\sqrt{2}} \begin{pmatrix} 1 & 1 \\ 1 & -1 \end{pmatrix} \cdot \begin{pmatrix} q_1 \\ q_2 \end{pmatrix} \\
&= \frac{1}{\sqrt{2}} \begin{pmatrix} q_1 + q_2 \\ q_1 - q_2 \end{pmatrix} .
\end{aligned}
\tag{B.22}
$$

Solving for q_1 and q_2, we can simply get the transformation from normal mode to Cartesian coordinates for position

$$
q = \frac{1}{\sqrt{2}} \begin{pmatrix} R_1 + R_2 \\ R_1 - R_2 \end{pmatrix} .
\tag{B.23}
$$

Similarly, we define matrix P, which is our representation of momentum in normal mode coordinates

$$
\begin{aligned}
P &= U \cdot p \\
&= \frac{1}{\sqrt{2}} \begin{pmatrix} 1 & 1 \\ 1 & -1 \end{pmatrix} \cdot \begin{pmatrix} p_1 \\ p_2 \end{pmatrix} \\
&= \frac{1}{\sqrt{2}} \begin{pmatrix} p_1 + p_2 \\ p_1 - p_2 \end{pmatrix} .
\end{aligned}
\tag{B.24}
$$

We then solve for p_1 and p_2, to obtain the transformation from normal mode coordinates for momentum

$$
p = \frac{1}{\sqrt{2}} \begin{pmatrix} P_1 + P_2 \\ P_1 - P_2 \end{pmatrix} .
\tag{B.25}
$$

Equations (B.22) and (B.24) define the transformation from Cartesian to normal mode coordinates, while eqns. B.23) (B.25) define the transformation from normal mode to Cartesian coordinates for our system.

If the matrix of coefficients, appearing in eqn. (B.10) was not symmetric, then we would be required to diagonlize it. This is done to ensure that the eigenvectors are orthogonal. However, in this case the matrix of coefficients is symmetric and we can now express the Hamiltonian in normal mode coordinates. Substituting the transformation from Cartesian to normal mode coordinates,

appearing in eqns. (B.22) and (B.24), the Hamiltonian becomes

$$
\begin{aligned}
H &= \frac{p_1^2}{2m} + \frac{p_2^2}{2m} + \frac{K}{2}q_1^2 + \frac{K}{2}q_2^2 + \frac{K(t)}{2}\left(q_2 - q_1\right)^2 & \text{(B.26)} \\
&= \frac{(P_1 + P_2)^2}{4m} + \frac{(P_1 - P_2)^2}{4m} + \frac{K}{4}\left(R_1 + R_2\right)^2 + \frac{K}{4}\left(R_1 - R_2\right)^2 \\
&\quad + \frac{K(t)}{4}\left[(R_1 - R_2) - (R_1 + R_2)\right]^2 & \text{(B.27)} \\
&= \frac{1}{2m}P_1^2 + \frac{1}{2}P_2^2 + \frac{K}{2}R_1^2 + \frac{K + K(t)}{2}R_2^2 & \text{(B.28)} \\
&= \frac{1}{2m}P_1^2 + \frac{1}{2}P_2^2 + \frac{1}{2}m\omega_1^2 R_1^2 + \frac{1}{2}m\omega_2^2 R_2^2 & \text{(B.29)} \\
&= \sum_{n=1}^{2}\left(\frac{1}{2}P_n^2 + \frac{1}{2}m\omega_n^2 R_n^2\right) \ , & \text{(B.30)}
\end{aligned}
$$

where we have substituted the normal mode frequencies ω_1 and ω_2 appearing in eqns. (B.15) and (B.16) respectively.

Appendix C

No analytical solution to system of coupled, driven oscillators

This appendix shows why there is now analytical solution to the system of coupled oscillators with a time-dependent interaction between them.

Consider the Hamiltonian given by eqn. (3.19). To show why the system can not be solved analytically, we begin by stating the Hamiltonian equations of motion

$$
\begin{align}
\dot{q}_1 &= \frac{\partial H}{\partial p_1} = \frac{p_1}{m} \tag{C.1}\\
\dot{q}_2 &= \frac{\partial H}{\partial p_2} = \frac{p_2}{m} \tag{C.2}\\
\dot{p}_1 &= -\frac{\partial H}{\partial q_1} = -Kq_1 + K(t)\left(q_2 - q_1\right) \tag{C.3}\\
\dot{p}_2 &= -\frac{\partial H}{\partial q_2} = -Kq_2 - K(t)\left(q_2 - q_1\right) \ , \tag{C.4}
\end{align}
$$

where we have introduced the coupling function

$$
K(t) = m\omega^2(t) \ . \tag{C.5}
$$

The four coupled first order differential equations can be recast into a system of two coupled second order differential equations

$$
\begin{align}
\ddot{q}_1 &= -Kq_1 + K(t)\left(q_2 - q_1\right) \tag{C.6}\\
\ddot{q}_2 &= -Kq_2 - K(t)\left(q_2 - q_1\right) \ . \tag{C.7}
\end{align}
$$

Taking the sum and difference of the second order differential equations, we obtain

$$\ddot{q}_1 + \ddot{q}_2 \;=\; -K\left(q_1 + q_2\right) \tag{C.8}$$

$$\ddot{q}_2 - \ddot{q}_1 \;=\; -K\left(q_2 - q_1\right) - 2K(t)\left(q_2 - q_1\right) . \tag{C.9}$$

Equations (C.8) and (C.9) can be interpreted as the equations of motion of the centre of mass and relative displacement coordinates, respectively. In the equations of motion, it is important to notice the centre of mass has no driving while the relative motion between the oscillators is driven. Now, using the transformation from Cartesian to normal mode coordinates, defined in Appendix B,

$$\begin{pmatrix} R_1 \\ R_2 \end{pmatrix} \;=\; \frac{1}{\sqrt{2}} \begin{pmatrix} q_1 + q_2 \\ q_2 - q_1 \end{pmatrix} , \tag{C.10}$$

equations (C.8) and (C.9) can be rewritten as

$$\ddot{R}_1 + KR_1 \;=\; 0 \tag{C.11}$$

$$\ddot{R}_2 + \left[K + 2K_0 \sin\left(\omega_d t\right)\right] R_2 \;=\; 0 . \tag{C.12}$$

Equation (C.11) is a second order differential equation with a simple, analytical solution,

$$R_1 \;=\; C_1 \exp\left(i\sqrt{K}t\right) + C_2 \exp\left(-i\sqrt{K}t\right) . \tag{C.13}$$

Equation (C.12) is known as a Mathieu differential equation. This type of differential equation does not have any analytical solutions in terms of known functions, only in terms of infinite series with recurrent coefficients. The difficulty in producing an analytical solution, arises because of the time-dependent frequency appearing in eqn. (C.12). It is possible to use Floquet theory to establish some properties of this solution, however for practical purposes some numerical approximation must be incorporated [48].

Appendix D

Algorithm derivations

This Appendix contains all the mathematical details required to generate a time-reversible algorithm. These algorithms are used to numerically integrate the equations of motion. First, we will consider a closed system of two, coupled, harmonic oscillators with a time-dependent coupling between them. Next, the coupled oscillators are attached to a collection of harmonic oscillators with Ohmic spectral density. Lastly, the coupled oscillators are attached to a single harmonic oscillator and NHC thermostat.

D.1   Coupled, driven oscillators

Consider the Hamiltonian for the system of coupled, driven oscillators in eqn. (3.19). The Liouville operators of the coupled oscillators are

$$L_1 = \frac{p_1}{m}\frac{\partial}{\partial q_1} + \frac{p_2}{m}\frac{\partial}{\partial q_2} \tag{D.1}$$

$$L_2 = F_1\frac{\partial}{\partial p_1} + F_2\frac{\partial}{\partial p_2} , \tag{D.2}$$

where we have introduced forces

$$F_1 = -Kq_1 + K(t)(q_2 - q_1) \tag{D.3}$$

$$F_2 = -Kq_2 - K(t)(q_2 - q_1) . \tag{D.4}$$

Using the symmetric Trotter factorization, the evolution operator of the system is given by

$$e^{iLh} = e^{iL_2h/2}e^{iL_1h}e^{iL_2h/2} \tag{D.5}$$

where h is time step used in the simulation. Applying the direct translation technique to the total propagator of the system,

$$U(h) \;=\; U_2\left(\frac{h}{2}\right) U_1\left(h\right) U_2\left(\frac{h}{2}\right) \;, \tag{D.6}$$

where $U_i(h) = \exp(hL_i)$, we can obtain the pseudo-code of the time reversible algorithm. The algorithm is then given by

$$
\left.
\begin{aligned}
p_2 &\;\to\; p_2 + \tfrac{h}{2}F_2 \\
p_1 &\;\to\; p_1 + \tfrac{h}{2}F_1
\end{aligned}
\right\}
\quad : \quad U_2\left(\frac{h}{2}\right)
\tag{D.7}
$$

$$
\left.
\begin{aligned}
q_2 &\;\to\; q_2 + h\tfrac{p_2}{m} \\
q_1 &\;\to\; q_1 + h\tfrac{p_1}{m}
\end{aligned}
\right\}
\quad : \quad U_1\left(\frac{h}{2}\right)
\tag{D.8}
$$

Re-calculate F_1 and F_2

$$
\left.
\begin{aligned}
p_2 &\;\to\; p_2 + \tfrac{h}{2}F_2 \\
p_1 &\;\to\; p_1 + \tfrac{h}{2}F_1
\end{aligned}
\right\}
\quad : \quad U_2\left(\frac{h}{2}\right)
\tag{D.9}
$$

where we have used the identities appearing in eqns. (3.17) and (3.18) to apply the direct translation technique to obtain the algorithm.

D.2   Coupled, driven oscillators attached to a harmonic bath

Consider the Hamiltonian given in eqn. (3.25). We can split the the total Liouville operator into a sum of four operators

$$L \;=\; \sum_{i=1}^{4} L_i \tag{D.10}$$

where the individual operators are

$$L_1 = \sum_{\alpha=1}^{2} \frac{p_\alpha}{m_\alpha} \frac{\partial}{\partial q_\alpha} \tag{D.11}$$

$$L_2 = \sum_{\alpha=1}^{2} (F_\alpha + F_{SB}) \frac{\partial}{\partial p_\alpha} \tag{D.12}$$

$$L_3 = \sum_{j=1}^{N} \frac{P_j}{m_j} \frac{\partial}{\partial R_j} \tag{D.13}$$

$$L_4 = \sum_{j=1}^{N} F_j \frac{\partial}{\partial P_j} . \tag{D.14}$$

where we have defined the forces

$$F_1 = -Kq_1 + K(t)(q_2 - q_1) \tag{D.15}$$

$$F_2 = -Kq_2 - K(t)(q_2 - q_1) \tag{D.16}$$

$$F_j = -m_j \omega_j^2 R_j + c_j \sum_{\alpha=1}^{2} q_\alpha \tag{D.17}$$

$$F_{SB} = \sum_{j=1}^{N} c_j R_j . \tag{D.18}$$

In order to obtain a numerical algorithm, we consider a small time step h and use the symmetric Trotter formula:

$$e^{hL} \approx e^{h(L_1+L_2+L_3+L_4)} \tag{D.19}$$

$$= e^{h[(L_1+L_3)+(L_2+L_4)]} \tag{D.20}$$

$$= e^{\frac{h}{2}L_B} e^{hL_A} e^{\frac{h}{2}L_B} . \tag{D.21}$$

We have combined commuting operators by introducing

$$L_A = L_1 + L_3 \tag{D.22}$$

$$L_B = L_2 + L_4 . \tag{D.23}$$

Now, using the identities defined in eqns. (3.17) and (3.18), we can apply the direct translation technique to eqn. (D.21) to the total propagator of the system,

$$U(h) = U_B\left(\frac{h}{2}\right) U_A(h) U_B\left(\frac{h}{2}\right) , \tag{D.24}$$

where $U_i(h) = \exp(hL_i)$. In doing so, we obtain the pseudo-code to implement the time-reversible algorithm

$$
\left.
\begin{array}{rcl}
p_2 & \rightarrow & p_2 + \frac{h}{2}\left(F_2 + F_{SB}\right) \\
p_1 & \rightarrow & p_1 + \frac{h}{2}\left(F_1 + F_{SB}\right) \\
P_j & \rightarrow & P_j + \frac{h}{2}F_j
\end{array}
\right\} \quad : \quad U_B\left(\frac{h}{2}\right)
\tag{D.25}
$$

$$
\left.
\begin{array}{rcl}
q_2 & \rightarrow & q_2 + h\frac{p_2}{m} \\
q_1 & \rightarrow & q_1 + h\frac{p_1}{m} \\
R_j & \rightarrow & R_j + h\frac{P_j}{M_j}
\end{array}
\right\} \quad : \quad U_A\left(\frac{h}{2}\right)
\tag{D.26}
$$

Re-calculate F_1, F_2, F_{SB} and F_j

$$
\left.
\begin{array}{rcl}
p_2 & \rightarrow & p_2 + \frac{h}{2}\left(F_2 + F_{SB}\right) \\
p_1 & \rightarrow & p_1 + \frac{h}{2}\left(F_1 + F_{SB}\right) \\
P_j & \rightarrow & P_j + \frac{h}{2}F_j
\end{array}
\right\} \quad : \quad U_B\left(\frac{h}{2}\right)
\tag{D.27}
$$

D.3 Coupled, driven oscillators attached to a NHC thermostat

Consider the Hamiltonian given in eqn. (3.44). In section 3.2.3, it was shown that by using the symmetric Trotter factorization, the evolution operator of the system is

$$\exp\left(hL\right) \;=\; \exp\left(\frac{h}{2}L^{NHC}\right)\exp\left(\frac{h}{2}L_2\right)\exp\left(hL_1\right)\exp\left(\frac{h}{2}L_2\right)\exp\left(\frac{h}{2}L^{NHC}\right)\;, \quad \text{(D.28)}$$

where

$$\exp\left(iL^{NHC}\frac{h}{2}\right) \;=\; \prod_{i=1}^{Nc}\left[\prod_{j=1}^{Nys}\exp\left(iL^{NHC}\frac{w_j h}{2Nc}\right)\right]\;. \quad \text{(D.29)}$$

Expanding the right hand side of eqn. (D.29), produces

$$
\begin{aligned}
\exp\left(iL^{NHC}\frac{w_j h}{2Nc}\right) \;=\;\;& \exp\left(\frac{w_j h}{4Nc}F_{P_{\eta_2}}m_{\eta_2}\frac{\partial}{\partial P_{\eta_2}}\right)\exp\left(-\frac{w_j h}{8Nc}\frac{P_{\eta_2}}{m_{\eta_2}}P_{\eta_1}\frac{\partial}{\partial P_{\eta_1}}\right)\times \\
&\times\exp\left(\frac{w_j h}{4Nc}F_{P_{\eta_1}}m_{\eta_1}\frac{\partial}{\partial P_{\eta_1}}\right)\exp\left(-\frac{w_j h}{8Nc}\frac{P_{\eta_2}}{m_{\eta_2}}P_{\eta_1}\frac{\partial}{\partial P_{\eta_1}}\right)\times \\
&\times\exp\left(-\frac{w_j h}{2Nc}\left[\frac{P_{\eta_1}}{m_{\eta_1}}P_Q\frac{\partial}{\partial P_Q}\right]\right)\times \\
&\times\exp\left(\frac{w_j h}{2Nc}\left[\frac{P_{\eta_1}}{m_{\eta_1}}\frac{\partial}{\partial\eta_1}+\frac{P_{\eta_2}}{m_{\eta_2}}\frac{\partial}{\partial\eta_2}\right]\right)\times \\
&\times\exp\left(-\frac{w_j h}{8Nc}\frac{P_{\eta_2}}{m_{\eta_2}}P_{\eta_1}\frac{\partial}{\partial P_{\eta_1}}\right)\exp\left(\frac{w_j h}{4Nc}F_{P_{\eta_1}}m_{\eta_1}\frac{\partial}{\partial P_{\eta_1}}\right)\times \\
&\times\exp\left(-\frac{w_j h}{8Nc}\frac{P_{\eta_2}}{m_{\eta_2}}P_{\eta_1}\frac{\partial}{\partial P_{\eta_1}}\right) \\
&\times\exp\left(\frac{w_j h}{4Nc}F_{P_{\eta_2}}m_{\eta_2}\frac{\partial}{\partial P_{\eta_2}}\right)\;. \quad \text{(D.30)}
\end{aligned}
$$

The Liouville operators are given by

$$L_1 \;=\; \frac{p_1}{m_1}\frac{\partial}{\partial q_1}+\frac{p_2}{m_2}\frac{\partial}{\partial q_2}+\frac{P_0}{M_0}\frac{\partial}{\partial R_0} \quad \text{(D.31)}$$

$$L_2 \;=\; \left(F_1+c_0 R_0\right)\frac{\partial}{\partial p_1}+\left(F_2+c_0 R_0\right)\frac{\partial}{\partial p_2}+F_0\frac{\partial}{\partial P_0} \quad \text{(D.32)}$$

and

$$
\begin{aligned}
L_{NHC} \;=\;\;& -P_0\frac{P_{\eta_1}}{m_{\eta_1}}\frac{\partial}{\partial P_0}+\frac{P_{\eta_1}}{m_{\eta_1}}\frac{\partial}{\partial\eta_1}+\frac{P_{\eta_2}}{m_{\eta_2}}\frac{\partial}{\partial\eta_2} \\
&+\left(F_{P_{\eta_1}}-P_{\eta_1}\frac{P_{\eta_2}}{m_{\eta_2}}\right)\frac{\partial}{\partial P_{\eta_1}}+F_{P_{\eta_2}}\frac{\partial}{\partial P_{\eta_2}}\;, \quad \text{(D.33)}
\end{aligned}
$$

where the following forces have been introduced

$$F_1 \;=\; -Kq_1 + K(t)\,(q_2 - q_1) \tag{D.34}$$

$$F_2 \;=\; -Kq_2 - K(t)\,(q_2 - q_1) \tag{D.35}$$

$$F_0 \;=\; -M\omega_0^2 R_0 + c_0\,(q_1 + q_2) \tag{D.36}$$

$$F_{P_{\eta_1}} \;=\; \left(\frac{P_0^2}{M_0} - gk_B T_{ext}\right) \tag{D.37}$$

$$F_{P_{\eta_2}} \;=\; \frac{P_{\eta_1}^2}{m_{\eta_1}} - k_B T_{ext}\,. \tag{D.38}$$

By using the identities defined in eqns. (3.17) and (3.18), we can apply the direct translation technique to the evolution propagator of the system. In doing so, we obtain the pseudo code to implement the time-reversible algorithm

$$
\left.
\begin{aligned}
h &\to h \times \tfrac{\omega_j}{N_c} \\
F_{P_{\eta_2}} &\to (1/m_{\eta_2}) \times \left(\frac{P_{\eta_1}^2}{m_{\eta_1}} - k_B \times T_{ext}\right) \\
P_{\eta_2} &\to P_{\eta_2} + 0.25 \times h \times F_{P_{\eta_2}} \times m_{\eta_2} \\
P_{\eta_1} &\to P_{\eta_1} \times \exp(-0.125 \times h \times P_{\eta_2}/m_{\eta_2}) \\
F_{P_{\eta_1}} &\to (1/m_{\eta_1}) \times (P_0^2/M - g \times k_B \times T_{ext}) \\
P_{\eta_1} &\to P_{\eta_1} + 0.25 \times h \times F_{P_{\eta_1}} \times m_{\eta_1} \\
P_{\eta_1} &\to P_{\eta_1} \times \exp(-0.125 \times h \times P_{\eta_2}/m_{\eta_2}) \\
\eta_1 &\to \eta_1 + 0.5 \times h \times (P_{\eta_1}/m_{\eta_1}) \\
\eta_2 &\to \eta_2 + 0.5 \times h \times (P_{\eta_2}/m_{\eta_2}) \\
P_0 &\to P_0 \times \exp(-0.5 \times h \times P_{\eta_1}/m_{\eta_1}) \\
P_{\eta_1} &\to P_{\eta_1} \times \exp(-0.125 \times h \times P_{\eta_2}/m_{\eta_2}) \\
F_{P_{\eta_1}} &\to (1/m_{\eta_1}) \times (P_0^2/M - g \times k_B \times T_{ext}) \\
P_{\eta_1} &\to P_{\eta_1} + 0.25 \times h \times F_{P_{\eta_1}} \times m_{\eta_1} \\
P_{\eta_1} &\to P_{\eta_1} \times \exp(-0.125 \times h \times P_{\eta_2}/m_{\eta_2}) \\
F_{P_{\eta_2}} &\to (1/m_{\eta_2}) \times \left(\frac{P_{\eta_1}^2}{m_{\eta_1}} - k_B \times T_{ext}\right) \\
P_{\eta_2} &\to P_{\eta_2} + 0.25 \times h \times F_{P_{\eta_2}} \times m_{\eta_2}
\end{aligned}
\right\} \;:\; \exp\left(\frac{ih}{2} L_{NHC}\right) \tag{D.39}
$$

$$
\left.
\begin{aligned}
p_1 &\to p_1 + 0.25 \times h \times (F_1 + c_0 R_0) \\
p_2 &\to p_2 + 0.25 \times h \times (F_2 + c_0 R_0) \\
P_0 &\to P_0 + 0.5 \times h \times F_0
\end{aligned}
\right\} \;:\; \exp\left(\frac{h}{2} L_2\right) \tag{D.40}
$$

$$
\left.
\begin{array}{rcl}
q_1 & \rightarrow & q_1 + 0.5 \times h \times p_1/m \\
q_2 & \rightarrow & q_2 + 0.5 \times h \times p_2/m \\
R_0 & \rightarrow & R_0 + h \times \frac{P_0}{M}
\end{array}
\right\} \quad : \quad \exp\left(hL_1\right) \tag{D.41}
$$

Re-calculate F_1, F_2 and F_0

$$
\left.
\begin{array}{rcl}
p_1 & \rightarrow & p_1 + 0.25 \times h \times (F_1 + c_0 R_0) \\
p_2 & \rightarrow & p_2 + 0.25 \times h \times (F_2 + c_0 R_0) \\
P_0 & \rightarrow & P_0 + 0.5 \times h \times F_0
\end{array}
\right\} \quad : \quad \exp\left(\frac{h}{2} L_2\right) \tag{D.42}
$$

$$
\left.
\begin{array}{rcl}
h & \rightarrow & h \times \frac{\omega_j}{N_c} \\[4pt]
F_{P_{\eta_2}} & \rightarrow & (1/m_{\eta_2}) \times \left(\frac{P_{\eta_1}^2}{m_{\eta_1}} - k_B \times T_{ext}\right) \\[4pt]
P_{\eta_2} & \rightarrow & P_{\eta_2} + 0.25 \times h \times F_{P_{\eta_2}} \times m_{\eta_2} \\[4pt]
P_{\eta_1} & \rightarrow & P_{\eta_1} \times \exp(-0.125 \times h \times P_{\eta_2}/m_{\eta_2}) \\[4pt]
F_{P_{\eta_1}} & \rightarrow & (1/m_{\eta_1}) \times (P_0^2/M - g \times k_B \times T_{ext}) \\[4pt]
P_{\eta_1} & \rightarrow & P_{\eta_1} + 0.25 \times h \times F_{P_{\eta_1}} \times m_{\eta_1} \\[4pt]
P_{\eta_1} & \rightarrow & P_{\eta_1} \times \exp(-0.125 \times h \times P_{\eta_2}/m_{\eta_2}) \\[4pt]
\eta_1 & \rightarrow & \eta_1 + 0.5 \times h \times (P_{\eta_1}/m_{\eta_1}) \\[4pt]
\eta_2 & \rightarrow & \eta_2 + 0.5 \times h \times (P_{\eta_2}/m_{\eta_2}) \\[4pt]
P_0 & \rightarrow & P_0 \times \exp(-0.5 \times h \times P_{\eta_1}/m_{\eta_1}) \\[4pt]
P_{\eta_1} & \rightarrow & P_{\eta_1} \times \exp(-0.125 \times h \times P_{\eta_2}/m_{\eta_2}) \\[4pt]
F_{P_{\eta_1}} & \rightarrow & (1/m_{\eta_1}) \times (P_0^2/M - g \times k_B \times T_{ext}) \\[4pt]
P_{\eta_1} & \rightarrow & P_{\eta_1} + 0.25 \times h \times F_{P_{\eta_1}} \times m_{\eta_1} \\[4pt]
P_{\eta_1} & \rightarrow & P_{\eta_1} \times \exp(-0.125 \times h \times P_{\eta_2}/m_{\eta_2}) \\[4pt]
F_{P_{\eta_2}} & \rightarrow & (1/m_{\eta_2}) \times \left(\frac{P_{\eta_1}^2}{m_{\eta_1}} - k_B \times T_{ext}\right) \\[4pt]
P_{\eta_2} & \rightarrow & P_{\eta_2} + 0.25 \times h \times F_{P_{\eta_2}} \times m_{\eta_2}
\end{array}
\right\} \quad : \quad \exp\left(\frac{h}{2} L_{NHC}\right) \tag{D.43}
$$

Bibliography

[1] F. Galve, L. A. Pachón, and D. Zueco, "Bringing entanglement to the high temperature limit," *Phys. Rev. Lett.*, vol. 105, pp. 180501–1 – 180501–4, 2010.

[2] E. A. Martinez and J. P. Paz, "Dynamics and thermodynamics of linear quantum open systems," *Phys. Rev. Lett.*, vol. 110, pp. 130406–1 – 130406–4, 2013.

[3] M. P. Allen and D. J. Tildesley, *Computer Simulation of Liquids.* Oxford: Clarendon Press, 1989.

[4] G. S. Engel, T. R. Calhoun, E. L. Read, T. K. Ahn, T. Manal, Y. C. Cheng, R. E. Blankenship, and G. R. Fleming, "Evidence for wavelike energy transfer through quantum coherence in photosynthetic systems," *Nature*, vol. 446, pp. 782–786, 2007.

[5] G. D. Scholes, "Quantum biology: Coherence in photosynthesis," *Nat. Phys.*, vol. 7, pp. 448–449, 2011.

[6] J. I. Fuks, P. Elliott, A. Rubio, and N. T. Maitra, "Dynamics of charge-transfer processes with time-dependent density functional theory," *J. Phys. Chem. Lett*, vol. 4, pp. 735–739, 2013.

[7] E. Rivera, D. Montemayor, M. Masia, and D. F. Coker, "Influence of site-dependent pigment-protein interactions on excitation energy transfer in photosynthetic light harvesting," *J. Phys. Chem. B*, vol. 117, pp. 5510–5521, 2013.

[8] P. Myöhänen, R. Tuovinen, T. Korhonen, G. Stefanucci, and R. van Leeuwen, "Image charge dynamics in time-dependent quantum transport," *Phys. Rev. B*, vol. 85, p. 075105, 2012.

[9] A.-P. Jauho, N. S. Wingreen, and Y. Meir, "Time-dependent transport in interacting and noninteracting resonant-tunneling systems," *Phys. Rev. B*, vol. 50, pp. 5528–5544, 1994.

[10] M. Terazima, "Time-dependent intermolecular interaction during protein reactions," *Phys. Chem. Chem. Phys.*, vol. 13, pp. 16928–16940, 2011.

[11] R.-P. Riwar, J. Splettstoesser, and J. König, "Zero-frequency noise in adiabatically driven interacting quantum systems," *Phys. Rev. B*, vol. 87, p. 195407, 2013.

[12] X. Hu and F. Nori, "Phonon squeezed states: quantum noise reduction in solids," *Physica B*, vol. 263, pp. 16 – 29, 1999.

[13] G. Odriozola and M. Lozada-Cassou, "Statistical mechanics approach to lock-key supramolecular chemistry interactions," *Phys. Rev. Lett.*, vol. 110, p. 105701, 2013.

[14] S. L. Johnson, P. Beaud, E. Vorobeva, C. J. Milne, E. D. Murray, S. Fahy, and G. Ingold, "Directly observing squeezed phonon states with femtosecond x-ray diffraction," *Phys. Rev. Lett.*, vol. 102, no. 17, p. 175503, 2009.

[15] S.-l. Ma, P.-b. Li, A.-p. Fang, S.-y. Gao, and F.-l. Li, "Dissipation-assisted generation of steady-state single-mode squeezing of collective excitations in a solid-state spin ensemble," *Phys. Rev. A*, vol. 88, p. 013837, 2013.

[16] T. Altanhan and B. S. Kandemir, "A squeezed state approach for the large polarons," *J. Phys.: Condens. Matter*, vol. 5, no. 36, p. 6729, 1993.

[17] D. J. Wineland, J. J. Bollinger, W. M. Itano, and D. J. Heinzen, "Squeezed atomic states and projection noise in spectroscopy," *Phys. Rev. A*, vol. 50, pp. 67–88, 1994.

[18] V. C. Usenko and R. Filip, "Squeezed-state quantum key distribution upon imperfect reconciliation," *New J. Phys.*, vol. 13, no. 11, p. 113007, 2011.

[19] S. Dwyer, L. Barsotti, S. S. Y. Chua, M. Evans, M. Factourovich, D. Gustafson, T. Isogai, K. Kawabe, A. Khalaidovski, P. K. Lam, M. Landry, N. Mavalvala, D. E. McClelland, G. D. Meadors, C. M. Mow-Lowry, R. Schnabel, R. M. S. Schofield, N. Smith-Lefebvre, M. Stefszky, C. Vorvick, and D. Sigg, "Squeezed quadrature fluctuations in a gravitational wave detector using squeezed light," *Opt. Express*, vol. 21, no. 16, pp. 19047–19060, 2013.

[20] M. Razavy, *Heisenberg's Quantum Mechanics.* Singapore: World Scientific, 2011.

[21] K. Camilleri, *Heisenberg and the Interpretation of Quantum Mechanics: The Physicist as Philosopher.* New York: Cambridge University Press, 2009.

[22] M. Evans and S. Kielich, *Modern Nonlinear Optics: Part 1.* New York: John Wiley and Sons, 1993.

[23] C. C. Gerry and P. L. Knight, *Introductory quantum optics.* Cambridge: Cambridge University Press, 2005.

[24] L. E. Ballentine, *Quantum mechanics: a modern development*, ch. 15. Amsterdam: World Scientific, 2005.

[25] D. F. Styer, M. S. Balkin, K. M. Becker, M. R. Burns, C. E. Dudley, S. T. Forth, J. S. Gaumer, M. A. Kramer, D. C. Oertel, L. H. Park, M. T. Rinkoski, C. T. Smith, and T. D. Witherspoon, "Nine formulations of quantum mechanics," *Am. J. Phys.*, vol. 70, pp. 288–297, 2002.

[26] W. B. Case, "Wigner functions and weyl transforms for pedestrians," *Am. J. Phys.*, vol. 76, pp. 937–946, 2008.

[27] M. Hillery, R. F. O'Connell, M. O. Scully, and E. P. Wigner, "Distribution functions in physics: Fundamentals," *Phys. Rep.*, vol. 106, pp. 121–167, 1984.

[28] H. Goldstein, *Classical Mechanics.* Reading, MA: Addison-Wesley Publishing Company, 2nd ed., 1980.

[29] V. Zelevinsky, *Quantum Physics, Volume 1: From Basics to Symmetries and Perturbations.* Weinhein, Germany: Wiley-VCH, 2011.

[30] R. Kapral and G. Ciccotti, "Transport coefficients of quantum-classical systems," in *Computer Simulations in Condensed Matter Systems: From Materials to Chemical Biology Volume 1* (M. Ferrario, G. Ciccotti, and K. Binder, eds.), vol. 703 of *Lecture Notes in Physics*, pp. 519–551, Springer Berlin Heidelberg, 2006.

[31] A. Sergi, "Generalized bracket formulation of constrained dynamics in phase space," *Phys. Rev. E.*, vol. 69, no. 021109, pp. 021109:1–021109:9, 2004.

[32] D. Mac Kernan, G. Ciccotti, and R. Kapral, "Surface-hopping dynamics of a spin-boson system," *J. Chem. Phys.*, vol. 116, no. 6, pp. 2346–2353, 2002.

[33] R. Kapral and G. Ciccotti, "Mixed quantum-classical dynamics," *J. Chem. Phys.*, vol. 110, no. 18, pp. 8919–8929, 1999.

[34] A. Sergi, I. Sinayskiy, and F. Petruccione, "Numerical and analytical approach to the quantum dynamics of two coupled spins in bosonic baths," *Phys. Rev. A.*, vol. 80, no. 012108, pp. 012108:1–012108:7, 2009.

[35] J. E. Moyal, "Quantum mechanics as a statistical theory," *Mathematical Proceedings of the Cambridge Philosophical Society*, vol. 45, pp. 99–124, 1 1949.

[36] D. Frenkel and B. Smit, *Understanding Molecular Simulation from algorithms to applications.* San Diego, California: Academic Press, 2002.

[37] A. Sergi and M. Ferrario, "Non-hamiltonian equations of motion with a conserved energy," *Phys. Rev. E.*, vol. 64, no. 056125, pp. 056125:1–056125:9, 2001.

[38] A. Sergi, "Non-hamiltonian equilibrium statistical mechanics," *Phys. Rev. E.*, vol. 67, no. 021101, pp. 021101:1–021101:7, 2003.

[39] S. Nosé, "A unified formulation of the constant temperature molecular dynamics methods," *J. Chem. Phys.*, vol. 81, no. 1, pp. 511–519, 1984.

[40] A. Sergi and F. Petruccione, "Nosé-hoover dynamics in quantum phase space," *J. Phys. A: Math. Theor.*, vol. 41, p. 355304, 2008.

[41] G. J. Martyna, M. L. Klein, and M. Tuckerman, "Nosé-hoover chains: The canonical ensemble via continuous dynamics," *J. Chem. Phys.*, vol. 97, no. 4, pp. 2635–2643, 1992.

[42] G. J. Martyna, M. E. Tuckerman, D. J. Tobias, and M. L. Klein, "Explicit reversible integrators for extended systems dynamics," *Molec. Phys.*, vol. 87, no. 5, pp. 1117–1157, 1996.

[43] S. Nielsen, R. Kapral, and G. Ciccotti, "Statistical mechanics of quantum-classical systems," *J. Phys. Chem.*, vol. 115, no. 13, pp. 5805–5815, 2000.

[44] A. Sergi and P. V. Giaquinta, "On the geometry and entropy of non-hamiltonian phase space," *J. Stat. Mech.*, vol. 2007, no. 02, p. P02013, 2007.

[45] M. E. Tuckerman and G. J. Martyna, "Understanding modern molecular dynamics: techniques and applications," *J. Phys. Chem. B.*, vol. 104, no. 2, pp. 159–178, 2000.

[46] A. Sergi, M. Ferrario, and D. Costa, "Reversible integrators for basic extended system molecular dynamics," *Molec. Phys.*, vol. 97, no. 7, pp. 825–832, 1999.

[47] M. E. Tuckerman, *Statistical mechanics: theory and molecular simulation.* Oxford: Oxford University Press, 2002.

[48] A. Lindner and H. Freese, "A new method to compute mathieu functions," *J. Phys. A: Math. Gen.*, vol. 27, pp. 5565–5571, 1994.

[49] K. Thompson and N. Makri, "Influence functionals with semiclassical propagators in combined forward-backward time," *J. Chem. Phys.*, vol. 110, pp. 1343 – 1353, 1999.

[50] N. Makri, "The linear response approximation and its lowest order corrections: an influence functional approach," *J. Phys. Chem. B*, vol. 103, pp. 2823 – 2829, 1999.

[51] M. Hillery, R. F. O'Connell, M. O. Scully, and E. P. Wigner, "Distribution functions in physics: Fundamentals," *Phys. Rep.*, vol. 106, pp. 121–167, 1984.